U.PORTO

MESTRADO
CIÊNCIAS DO MAR - RECURSOS MARINHOS

Bioactive secondary metabolites from the culture of the marine sponge-associated fungus *Talaromyces stipitatus* KUFA 0207

Jidapa Noinart

M

2017

U.PORTO

Jidapa Noinart. Bioactive secondary metabolites from the culture of the marine sponge-associated fungus *Talaromyces stipitatus* KUFA 0207

M.ICBAS **2017**

Bioactive secondary metabolites from the culture of the marine sponge-associated fungus *Talaromyces stipitatus* KUFA 0207

Jidapa Noinart

INSTITUTO DE CIÊNCIAS BIOMÉDICAS ABEL SALAZAR

JIDAPA NOINART

BIOACTIVE SECONDARY METABOLITES FROM THE CULTURE OF THE MARINE SPONGE – ASSOCIATED FUNGUS *TALAROMYCES STIPITATUS* KUFA 0207

Dissertation for applying to the degree of Master in Marine Sciences – Marine Resources, as submitted to the institute of Biomedical Sciences Abel Salazar of the University of Porto.

Supervisor – Professor Doutor Anake Kijjoa

Category – Full Professor

Affiliation – Institute of Biomedical Sciences Abel Salazar of the University of Porto.

Acknowledgement

First of all, I would like to express my sincere gratitude to all the people who have accompanied me during my Master study journey in the University of Porto.

To my respectful supervisor, Professor Dr. Anake Kijjoa who gave me the golden opportunity to do this project and study in the University of Porto. He does not only provide me valuable guidance and help me in studying and doing thesis, but also supports and encourages me to have the best successful work during my Master study. Also, Dr. Suradet Buttachon who always gives me help and guidance in my lab works.

To Professor Dr. Eduardo Rocha, Director of the Master's program in Marine Sciences and Marine Resources of Institute of Biomedical Sciences Abel Salazar (ICBAS) for accepting me to study in this program.

Thank you to all the technicians and colleages in my laboratory, Mrs. Júlia Bessa, Miss Sónia Santos, Mrs. Isabel Silva, War War May Zin, Decha Kumla and all friends, for their supports and friendship in my daily life.

To Associate Professor Dr. Poonpipope Kasemsap who always supports and encourages me to study in this prestigious university, University of Porto and Dr. Tida Dethoup who always supports me by providing the materials for this study.

Finally, I would like to express my special thanks to the ALFABET project of the Erasmus Mundus Action 2 Scholarship and its coordinators who give me invaluable opportunities to study in the University of Porto. This chance allows me to extend my knowledges as well as gaining good experiences. This dissertation was also partially supported through national funds provided by Foundation for Science and Technology (FCT) and European Regional Development Fund (ERDF) and COMPETE, under the projects PEst-C/MAR/LA0015/2013, PTDC/MAR-BIO/4694/2014 as well as by the project INNOVMAR – Innovation and Sustainability in the Management and Exploitation of Marine Resources (reference NORTE-01-0145-FEDER-000035, within Research Line NOVELMAR/ INSEAFOOD/ ECOSERVICES), supported by North Portugal Regional

Operational Programme (NORTE 2020), under the PORTUGAL 2020 Partnership Agreement, through the European Regional Development Fund (ERDF).

Last but not least, I would like to present my greatest gratitude to my family, especially my mother and my brother, for their encouragement and patience. I also thank my friends for their advices and contribution which are very important to my successes.

Author's Declaration

I hereby declared that the following original article/ communication were prepared in the scope of this thesis.

Scientific Communication

1. **Jidapa Noinart**, Tida Dethoup, Luís Gales, José Pereira, Ralph Urbatzka, Sara Freitas, Vitor Vasconcelos, Anake Kijjoa. Anti-obesity Activity of Anthraquinones and Other Constituents of the Marine-Derived Fungus *Talaromyces stipitatus* KUFA 0207. Poster Presentation in the 2nd International Conference of Marine Fungal Natural Products (MaFNaP_2017), 27 -29 June 2017, in Kiel, Germany.

Publication

1. **Noinart, J.**; Buttachon, S.; Dethoup, T.; Gales, L.; Pereira, J.A.; Urbatzka, R.; Freitas, S.; Lee, M.; Silva, A.M.S.; Pinto, M.M.M.; Vasconcelos, V.; Kijjoa, A. A New Ergosterol Analog, a New *Bis*-Anthraquinone and Anti-Obesity Activity of Anthraquinones from the Marine Sponge-Associated Fungus *Talaromyces stipitatus* KUFA 0207. *Mar. Drugs* 2017, *15*, 139. doi:10.3390/md15050139

Contents

Acknowledgement i

Author's Declaration ii

Figure Index vii

Table Index xi

Abstract xii

Resumo xiii

Abbreviation list xiv

CHAPTER 1 1

1. General Introduction 2

1.1. Milestone of Natural Products 2

1.2. The Marine Environments and Bioactive Natural Products 3

1.2.1. Relationship between Marine Environments and Bioactive Natural Products 3

1.2.2. Importance of Marine Natural Products 4

1.3. Fungi as a Source of Bioactive Secondary Metabolites 7

1.3.1. Fungi and Marine Ecology 8

1.3.2. Sponge - Associated Fungi as a Source of Bioactive Compounds 9

1.4. The Genus *Talaromyces* 12

1.4.1. Taxonomy 12

1.4.1.1. Section *Talaromyces* 12

1.4.1.2. Section *Emersonii* 13

1.4.1.3. Section *Thermophila* 14

1.4.1.4 Section *Purpurea* 15

1.4.2. The Importance of *Talaromyces* 16

1.4.2.1. Importance in Agricultural Applications 16

1.4.2.2. Importance in Biotechnological Applications 17

1.4.2.3. Importance in Medical Applications 19

1.5. Obesity 20

1.6. Objectives 22

CHAPTER 2 23

2. Secondary Metabolites from the Fungi of the Genus *Talaromyces* Section *Talaromyces* and Their Bioactivities 24

2.1. *Talaromyces flavus* 26

2.2. *Talaromyces helicus* 31

2.3. *Talaromyces luteus* 32

2.4. *Talaromyces stipitatus* 32

2.5. *Talaromyces trachyspermus* 35

2.6. *Talaromyces wortmannii* 36

CHAPTER 3 42

3. Materials and Methods 43

3.1. Materials 43

3.1.1. Isolation and Purification of Secondary Metabolites from the Fungal Crude Extracts 43

3.1.2. Structure Elucidation of Secondary Metabolites 44

3.2. Methods 44

3.2.1. General Experimental Procedures 44

3.2.2. Fungal Material 45

3.2.2. Isolation, Purification of the Secondary Metabolites 46

3.2.3. Physical Characteristics and Spectroscopic Data 47

3.2.4. X-ray Crystallographic Analysis of Compounds IV and V 49

3.2.4. Anti-Obesity Assay 50

CHAPTER 4 51

4. Results and Discussion 52

4.1. Secondary Metabolites Isolated from *Talaromyces stipitatus* 52

4.2. Identifications and Characterization of Secondary metabolites from the culture of *Talaromyces stipitatus* 54

4.2.1. Structure Elucidation of Fatty Acid 54

4.2.1.1. Palmitic acid (**I**) 54

4.2.2. Structure Elucidation of Ergosterol Derivatives 56

4.2.2.1. Ergosterol-5,8-endoperoxide (**II**) 56
4.2.2.2. Ergosta-4,6,8(14),22-tetraen-3-one (**III**) 60
4.2.2.3. Cyathisterone (**IV**) 65
4.2.2.4. Talarosterone (**V**) 69
4.2.3. Structure Elucidation of Anthraquinones 73
4.2.3.1. Emodin (**VI**) 73
4.2.3.2. Questinol (**VII**) 77
4.2.3.3. Citreorosein (**VIII**) 81
4.2.3.4. Fallacinol (**IX**) 84
4.2.3.5. 1,3,6,8-tetrahydroxy-9,10-anthraquinone = Rheoemodin (**X**) 88
4.2.4. Structure Elucidation of *Bis* - Xanthone and *Bis* - Anthraquinone 91
4.2.4.1. Secalonic acid A (**XI**) 91
4.2.4.2. *Bis*-(7-methyl-1,4,5-trihydroxy-anthracene-9,10-dione) (**XII**) 97
4.3. Biological Activity Tests 104
4.3.1. Anti-obesity activity on the zebrafish Nile red assay 104
CHAPTER 5 106
5. Conclusion 107
CHAPTER 6 108
6. Appendix 109
6.1 NMR Spectra of Isolated Compounds 109
6.1.1 NMR Spectrum of Palmitic acid (**I**) 109
6.1.2 NMR Spectrum of Ergosterol-5,8-endoperoxide (**II**) 110
6.1.3 NMR Spectrum of Ergosta-4,6,8(14),22-tetraen-3-one (**III**) 111
6.1.4 NMR Spectrum of Cyathisterone (**IV**) 112
6.1.5 NMR Spectrum of Talarosterone (**V**) 113
6.1.6 NMR Spectrum of Emodin (**VI**) 114
6.1.7 NMR Spectrum of Questinol (**VII**) 115
6.1.8 NMR Spectrum of Citreorosein (**VIII**) 116
6.1.9 NMR Spectrum of Fallacinol (**IX**) 117
6.1.10 NMR Spectrum of Rheoemodin (**X**) 118
6.1.11 NMR Spectrum of Secalonic Acid A (**XI**) 119

6.1.12 NMR Spectrum of *Bis*- Anthraquinone (**XII**) 120

CHAPTER 7 121

7. References 122

Figure Index

Figure 1. A: opium; **B:** structure of morphine; **C:** structure of penicillin V. 2
Figure 2. All the collection areas for marine natural products discovery in 1965-2014 3
Figure 3. New compounds from marine-derived fungi, according to year of publication 8
Figure 4. Sources of new marine-derived fungi reported in literature until mid-2010 9
Figure 5. Structures of IB-01212, epoxyphomalin A, similanamide, hypofuran A and austalide R. 11
Figure 6. *Talaromyces* Taxonomy. 12
Figure 7. Morphology of *Penicillium* of the biverticillate - symmetrical type (*T. wortmannii*; **a**. conidiogenous structures; **b**. conidia; **c**. initials; **d.** chains of asci; **e**. ascospores) 13
Figure 8. Morphology of *Penicillium cylindrosporum* (*T. byssochlamydoides*; **a.** conidiogenous structures; **b.** conidia; **c.** initials; **d.** chains of asci; **e**. ascospores; **f**. loose-textured hyphae covering the ascoma). 14
Figure 9. Morphology of *Penicillium asymmetrica* - *Divaricata* (*T. thermophilus*; **a**. conidiogenous structures; **b**. conidia; **c**. initials; **d**. primordium consisting of branching hyphae; **e**. chains of asci; **f**. ascospores; **g**. fragment of ascomatal covering; **h**. chlamydospores; **i**. vegetative hyphae) 15
Figure 10. Morphology of *Penicillium restrictum* - series (*T. purpureus*; **a**. conidiogenous structures; **b**. conidia; **c**. initial surrounded by thin hyphae; **d**. initials; **e**. chains of asci; **f**. ascospores; **g**. loosely branched hyphae covering the ascoma) 16
Figure 11. Pigments from filamentous fungi in food industry; **A**. Pigmented filamentous fungi; **B**. Pigments and colorants produced and extracted and **C**. Food formulation and processing 17
Figure 12. Screening for filamentous fungi producing pigments of interest without any co-production of mycotoxins and *Monascus*-like pigment produced by *Penicillium* 18
Figure 13. Morphological characteristics of *Talaromyces stipitatus* (CBS 236.60); **A**. Colonies from left to right (top row) CYA, MEA, DG18 and OA; (bottom row) CYA reverse, MEA reverse, YES and CREA; **B**. Colony texture and ascomata on OA after 2 weeks' incubation; **C**. Ascomata; **D**, **E**. Asci and ascospores; **F**. Ascospores. Scale bars: **B** = 1000 µm; **C** = 500 µm; **D** = 10 µm, applies to **E**, **F**. 25
Figure 14. Secondary metabolites of *Talaromyces flavus* (**1**-**16**). 27
Figure 15. Structure of 15G256ω (**17**). 28
Figure 16. Secondary metabolites of *Talaromyces flavus* (**18**-**24**). 28
Figure 17. Structures of the secondary metabolites **25-32**, isolated from *Talaromyces flavus*. 29

Figure 18. Structure of diazaphilonic acid (**33**). 30
Figure 19. Structure of compounds **34-39**. 30
Figure 20. Structures of compounds **40-43**. 31
Figure 21. Structures of helicusins A-D (**44-47**). 31
Figure 22. Structures of luteusins A-E (**48-52**). 32
Figure 23. Structures of compounds **53-63**. 33
Figure 24. Structures of talaroketals A (**64**) and B (**65**). 34
Figure 25. Structures of talaromycins A-F (**66-71**) and botryodiplodin (**72**). 35
Figure 26. Structures of spiculisporic acid (**73**), spiculisporic acid E (**74**), 3-acetyl ergosterol 5,8-endoperoxide (**75**) and trachyspic acid (**76**). 36
Figure 27. Structure of compounds **77-83**. 37
Figure 28. Structures of wortmannilactones E-H (**84-87**). 37
Figure 29. Structures of compounds **88-98**. 38
Figure 30. Structures of biemodin (**99**), emodic acid (**100**), skyrin (**101**), oxyskyrin (**102**), regulosin A (**103**) and B (**104**). 39
Figure 31. Structures of bisdihydroanthraquinones **105-110**. 40
Figure 32. Equipment in the experimental, **A**. Bock monoscope; **B**. ADP410 Polarimeter; **C**. FTIR spectrometer; **D**. Bruker AMC instrument; **E**. Varian CARY 100 spectrophotometer; **F**. Waters Aquity UPLC system; **G**. Waters Xevo QToF mass spectrometer 45
Figure 33. Colony of *Talaromyces stipitatus* C.R. Benj. (KUFA 0207) on male extract agar, 14 days, 28℃ (**A**), SEM of ascospores (**B**). 46
Figure 34. Secondary metabolites isolated from the marine-derived *Talaromyces stipitatus*. 53
Figure 35. Structure of palmitic acid (**I**). 54
Figure 36. Structure of palmitic acid with chemical shifts. 54
Figure 37. Structure of ergosterol-5,8-endoperoxide (**II**) 56
Figure 38. COSY correlations (—) of the protons of the (*3E*)-5,6-dimethylhept-3-en-2-yl side chain. 57
Figure 39. HMBC correlations (⟶) of the (*3E*)-5,6-dimethylhept-3-en-2-yl side chain. 57
Figure 40. Key HMBC correlations (⟶) of the *3β*-hydroxyandrostane 58
Figure 41. Structure of ergosta-4,6,8(14),22-tetraen-3-one (**III**). 60
Figure 42. COSY correlations (—) of the protons of the (*3E*)-5,6-dimethylhept-3-en-2-yl side chain. 61
Figure 43. Key HMBC correlations (⟶) for the (*3E*)-5,6-dimethylhept-3-en-2-yl side chain of **III.** 61

Figure 44. ^{1}H and ^{13}C assignments for **III**. 63
Figure 45. Structure of cyathisterone (**IV**)..... 65
Figure 46. Key COSY (—) and HMBC (⟶) correlations of **IV.**..... 67
Figure 47. ORTEP diagram of **IV**..... 67
Figure 48. Structure of talarosterone (**V**). 69
Figure 49. Key COSY (—) and HMBC (⟶) correlations of **V.**..... 70
Figure 50. Key ROESY correlations (⟷) of **V**..... 71
Figure 51. ORTEP diagram of **V**..... 71
Figure 52. Structure of emodin (**VI**). 73
Figure 53. Key COSY correlations (—) of **VI**. 74
Figure 54. The HMBC correlations (⟶) of **VI**. 74
Figure 55. Structure of emodin (**VI**) indicating ^{1}H and ^{13}C chemical shifts. 75
Figure 56. Structure of questinol (**VII**)..... 77
Figure 57. Key COSY correlations (—) of **VII**. 78
Figure 58. The HMBC correlations (⟶) of **VII**. 78
Figure 59. The HMBC correlations (⟶) of **VII**. 79
Figure 60. Structure of questinol indicating ^{1}H and ^{13}C chemical shifts..... 79
Figure 61. Structure of citreorosein (**VIII**). 81
Figure 62. Key COSY correlations (—) of **VIII**. 82
Figure 63. Structure of citreorosein indicating ^{1}H and ^{13}C chemical shifts. 82
Figure 64. Structure of fallacinol (**IX**) 84
Figure 65. Key COSY correlations (—) of compound **IX**. 85
Figure 66. The HMBC correlations (⟶) of **IX**. 85
Figure 67. Structure of fallacinol indicating ^{1}H and ^{13}C chemical shifts. 86
Figure 68. Structure of rheoemodin (**X**). 88
Figure 69. Key COSY correlations (—) of **X**. 88
Figure 70. The HMBC correlations (⟶) of **X.** 89
Figure 71. Structure of rheoemodin (**X**) indicating ^{1}H and ^{13}C chemical shifts. 90
Figure 72. The HMBC correlations (⟶) of **XI**. 91
Figure 73. Key COSY correlations (—) of **XI**. 92
Figure 74. The HMBC correlations (⟶) of **XI**. 93
Figure 75. The partial structure of **XI** indicating the ^{1}H and ^{13}C chemical shift values..... 93
Figure 76. The structure of **XI**. 94
Figure 77. Ortep view of **XI**. 94
Figure 78. The complete structure of **XI**. 95
Figure 79. Structure of **XII**. 97
Figure 80. Key COSY (—) and HMBC (⟶) correlations of **XII.**..... 98

Figure 81. HMBC (⟶) correlations of compound **XII.** 98
Figure 82. Partial structure of 7-methyl-1,4,5-trihydroxy-9,10-anthraquinone. 99
Figure 83. HMBC correlations of the dimer of 7-methyl-1,4,5-trihydroxy-9,10-anthraquinone..... 99
Figure 84. Comparison of the ^{1}H and ^{13}C NMR data of **XII** (**A**) and 2240A (**B**) 101
Figure 85. Atropisomers of **XII**, (**P**): right-handed helix, (**M**): left-handed helix..... 102
Figure 86. Anti-obesity activity of compounds **VI-XI** in the zebrafish larvae Nile red assay. The solvent control had 0.1% DMSO and the positive control received 50 µM resveratrol (REV). Values are presented as mean fluorescent intensity (MFI) relative to the DMSO group, and are derived from 10-12 individual larvae per treatment group. Statistical differences to the solvent control are indicated with asterisks, *** = $p < 0.001$. 104
Figure 87. Representative images of the zebrafish Nile red assay. The upper images show the overlay of the fluorescence and phase contrast; the lower images show the mean fluorescence intensity (MFI) given as black and white picture. DMSO, solvent control 0.1%. 105

Table Index

Table 1. Marine-derived compounds in clinical development 5
Table 2. Anti-obesity compounds from microorganisms and algae 21
Table 3. Summary of the structural types of the secondary metabolites and their biological activities from the genus *Talaromyces* section *Talaromyces.* 41
Table 4. ^{1}H and ^{13}C NMR (DMSO, 500.13 MHz and 125.4 MHz) and HMBC assignment for palmitic acid (**I**) 55
Table 5. ^{1}H and ^{13}C NMR ($CDCl_3$, 300.13 MHz and 75.4 MHz) and HMBC assignment for ergosterol-5,8-endoperoxide (**II**). 59
Table 6. ^{1}H and ^{13}C NMR ($CDCl_3$, 300.13 MHz and 75.4 MHz) and HMBC assignment for ergosta-4,6,8(14), 22-tetraen-3-one (**III**). 63
Table 7. ^{1}H and ^{13}C NMR ($CDCl_3$, 300.13 MHz and 75.4 MHz) and HMBC assignment for cyathisterone (**IV**). 67
Table 8. ^{1}H and ^{13}C NMR ($CDCl_3$, 300.13 MHz and 75.4 MHz) and HMBC assignment for talarosterone (**V**). 72
Table 9. ^{1}H and ^{13}C NMR (DMSO, 500.13 MHz and 125.4 MHz) and HMBC assignment for emodin (**VI**). 76
Table 10. ^{1}H and ^{13}C NMR (DMSO, 300.13 MHz and 75.4 MHz) and HMBC assignment for questinol (**VII**) 80
Table 11. ^{1}H and ^{13}C NMR (DMSO, 500.13 MHz and 125.4 MHz) and HMBC assignment for citreorosein (**VIII**). 83
Table 12. ^{1}H and ^{13}C NMR (DMSO, 500.13 MHz and 125.4 MHz) and HMBC assignment for fallacinol (**IX**). 86
Table 13. ^{1}H and ^{13}C NMR (DMSO, 300.13 MHz and 75.4 MHz) and HMBC assignment for rheoemodin (**X**) 90
Table 14. ^{1}H and ^{13}C NMR (DMSO, 300.13 MHz and 75.4 MHz) and HMBC assignment for secalonic acid A (**XI**). 96
Table 15. ^{1}H and ^{13}C NMR (DMSO, 500.13 MHz and 125.4 MHz) and HMBC assignment for *2, 2'-bis*-(7-methyl-1,4,5-trihydroxy-anthracene-9,10-dione) (**XII**). 103

Abstract

A new ergosterol analog, talarosterone (**V**) and a new *bis*-anthraquinone derivative (**XII**) were isolated, together with ten known compounds including palmitic acid (**I**), ergosterol-5,8-endoperoxide (**II**), ergosta-4,6,8(14),22-tetraen-3-one (**III**), cyathisterone (**IV**), and the anthraquinones emodin (**VI**), questinol (**VII**), citreorosein (**VIII**), fallacinol (**IX**), rheoemodin (**X**), and secalonic acid A (**XI**), from the ethyl acetate extract of the culture of the marine sponge-associated fungus *Talaromyces stipitatus* KUFA 0207. The structures of the previously undescribed compounds were established based on extensive 1D and 2D NMR spectral analysis, and in case of talarosterone (**V**), the absolute configurations of its stereogenic carbons were determined by X-ray crystallographic analysis. The structures of the previously reported compounds were elucidated by ^{1}H and ^{13}C NMR analysis as well as by comparison of their NMR data to those reported in the literature. Moreover, the stereochemistry of cyathisterone and secalonic acid A were also confirmed by X-ray analysis. The anthraquinones **VI-X** and secalonic acid A (**XI**) were tested for their anti-obesity activity using zebrafish Nile red assay. Only citreorosein (**VIII**) and questinol (**VII**) exhibited significant anti-obesity activity while fallacinol (**IX**) and rheoemodin (**X**) were not active. Emodin (**VI**) and secalonic acid A (**XI**) caused toxicity (death) for all exposed zebrafish larvae after 24h.

Keywords: *Talaromyces stipitatus*, Trichocomaceae, anthraquinones, *bis*-anthraquinone, ergosterol derivatives, secalonic acid A, anti-obesity, zebrafish Nile red assay

Resumo

Do extrato de acetato de etilo da cultura do fungo marinho *Talaromyces stipitatus* KUFA 0207 foram isolados um novo derivado de ergosterol, talarosterona (**V**), e um novo derivado de *bis*-antraquinona, composto (**XII**), juntamente com outros dez compostos conhecidos incluindo ácido palmítico (**I**), ergosterol-5,8-endoperóxido (**II**), ergosta-4,6,8(14),22-tetraen-3-ona (**III**), ciatisterona (**IV**), e as anthraquinonas: emodina (**VI**), questinol (**VII**), citreoroseina (**VIII**), fallacinol (**IX**), rheoemodina (**X**), e ácido secalónico A (**XI**). As estruturas da talarosterona (**V**) e de bis-antraquinona (**XII**) foram estabelecidas com base na análise espectral de RMN uni- e bi-dimensional, e no caso da talarosterona (**V**), as configurações absolutas dos carbonos estereogénicos foram determinadas pela análise de dados de cristalografia de raios-X. As estruturas dos outros compostos foram elucidadas através da análise dos respetivos espectros de RMN de ^{1}H e ^{13}C, bem como pela comparação com dados espectrais descritos na literatura. A estereoquímica das moléculas de ciatisterona (**IV**) e do ácido secanónico A (**XI**) foi também confirmada pela análise de dados de raios-X. Os compostos antraquinonas **VI**-**X** e o ácido secanónico A (**XI**) foram testados para avaliação da atividade anti-obesidade utilizando o ensaio de "zebrafish Nile red". Apenas a citreoroseina (**VIII**) e o questinol (**VII**) exibiram atividade anti-obesidade significativa enquanto o fallacinol (**IX**) e a rheoemodina (**X**) não mostraram nenhuma atividade. Emodina (**VI**) e o ácido secalónico A (**XI**) mostraram toxicidade para o ensaio referido.

Palavras-chave: *Talaromyces stipitatus*, Trichocomaceae, antraquinonas, *bis*-antraquinona, derivados de ergosterol, ácido secalônico A, anti-obesidade, zebrafish Nile red assay

Abbreviation list

$[\alpha]^{20}_{D}$	Specific Optical Rotation at 20 °C for D (Sodium) Line
®	Register or Trademark
1D	One-Dimension
2D	Two-Dimension
A373	Human Melanoma Cancer Cell Line
A549	Human Non-Small Lung Carcinoma Cell Line
BMI	Body Mass Index
Calcd.	Calculated
COSY	Correlation Spectroscopy
CYA	Czapek Yeast Autolysate Agar
DEPT	Distortionless Enhancement of Polarization Transfer
DMSO	Dimethyl Sulfoxide
ED_{50}	Effective Dose at 50%
EMA	European Medicines Agency
EU	European Union
FDA	Food and Drug Administration
GI_{50}	Growth Inhibition
HELA	Cervical Cancer Cell Line
HMBC	Heteronuclear Multiple Bond Coherence
HRESIMS	High-Resolution Electrospray Ionization Mass Spectrometry
HSQC	Heteronuclear Single Quantum Coherence
HT29	Human Colon Cancer Cell Line
IC_{50}	Half Maximal Inhibitory Concentration
ITS	Internal Transcribed Spacer
J	Coupling Constant in Hz
LH-60	Human Promyelocytic Leukemia Cell Line
LN-caP	Prostate Cancer Cell Line
MAO	Monoamine Oxidase
MCF-7	Human Breast Adenocarcinoma Cell Line

MDA-MB-435	Human Breast Estrogen-Independent Adenocarcinoma Cell Line
MEA	Malt Extract Agar
MFI	Mean Fluorescence Intensity
MHz	Megahertz
MIC	Minimum Inhibitory Concentration
NA	Not Available
NCI-H460	Human Non-Small Cell Lung Cancer Cell Line
NMR	Nuclear Magnetic Resonance
NOESY	Nuclear Overhauser Enhancement Spectroscopy
ORTEP	Oak Ridge Thermal Ellipsoid Plot
PC-3	Human Prostate Cancer Cell Line
ppt	Parts per thousand
REV	Resveratrol
ROESY	Rotating-Frame Overhauser Effect Spectroscopy
SK-BR3	Human Breast Cancer Cell Line
SMMC-7721	Human Hepatocellular Carcinoma Cell Line
SW480	Human Colon Cancer Cell Line

CHAPTER 1

1. General Introduction

1.1. Milestone of Natural Products

Natural Products are the small molecules produced by biological sources, some of which possess interesting chemical structures and biological activities (Rollinger *et al.*, 2008). Natural Products and their derivatives have been invaluable as a source of traditional medicines and natural poisons (Koehn and Carter, 2005; Larsen *et al.*, 2005). The ancient medicines, including cannabis, opium, alcohol and mandrake were used to relieve pain. In the 1817, Friedrich Sertürner, a German pharmacist, effectively isolated morphine, the first active secondary metabolite used as an analgesic drug, from opium, the milky latex sap produced by cut seed pods of poppy (*Papaver somniferum*) (Hamilton and Baskett, 2000). In 1928, Alexander Fleming serendipitously discovered penicillin, the first antibiotic that saved millions of lives and revolutionized the pharmaceutical research. After the Second World War, most of the pharmaceutical companies started the massive screening of microorganism for new antibiotics. In 1990, around 80% of drugs were inspired by this revelation, including antibiotics (penicillin, erythromycin and tetracycline), antimalarials (quinine and artemisinin), anticancer (taxol and doxorubicin), anti-parasitic (avermectin) and immunosuppressant for organ transplants (cyclosporine and rapamycins) (Fleming, 1944; Li and Vederas, 2009).

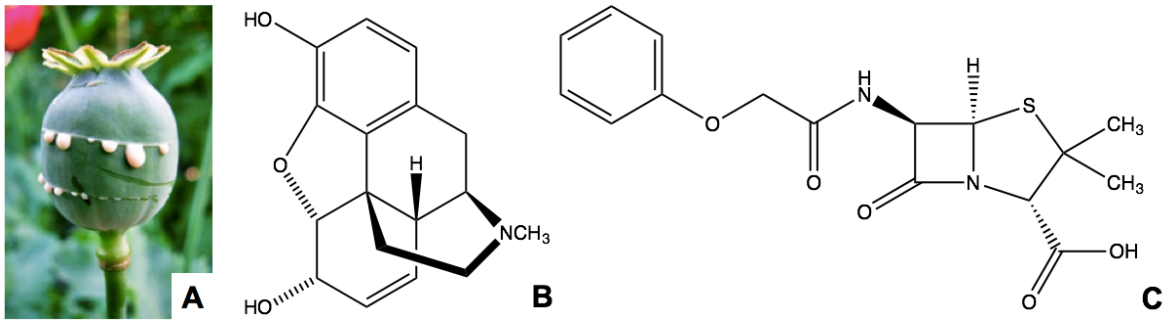

Figure 1. A: opium; **B:** structure of morphine; **C:** structure of penicillin V. (Ref: https://en.wikipedia.org/wiki/History_of_penicillin).

Natural Products have been the single most productive source of leads for drug development. More than 100 Natural Product-derived compounds are currently in preclinical and clinical development. Most of them are derived from plants and microbial sources. In the microbial area, the main sources are fungi and terrestrial actinomycetes. In the last

decade, there was a growing interest in the samples from marine environments as a source of novel bioactive metabolites (Harvey, 2008).

1.2. The Marine Environments and Bioactive Natural Products

1.2.1. Relationship between Marine Environments and Bioactive Natural Products

Even though plants continue to be a major source of new drugs with 91 compounds in clinical trials in late 2007, marine organisms and cyanobacteria have been investigated in the last few decades (Wase and Wright, 2008). Approximately 70% of the earth's surface are occupied by oceans, which are composed of enormous and complex biodiversity in the ecosystem. The marine environments are an important source for exploring bioactive natural products for pharmaceutical purposes. Due to special chemical and physical conditions in the marine environments, there are a great diversity of marine organisms which can produce a myriad of compounds with unique chemical structures. From the period of 1965-2014, about 25,700 new marine natural products have been discovered and characterized from several regions or oceans around the world (Blunt *et al.*, 2016).

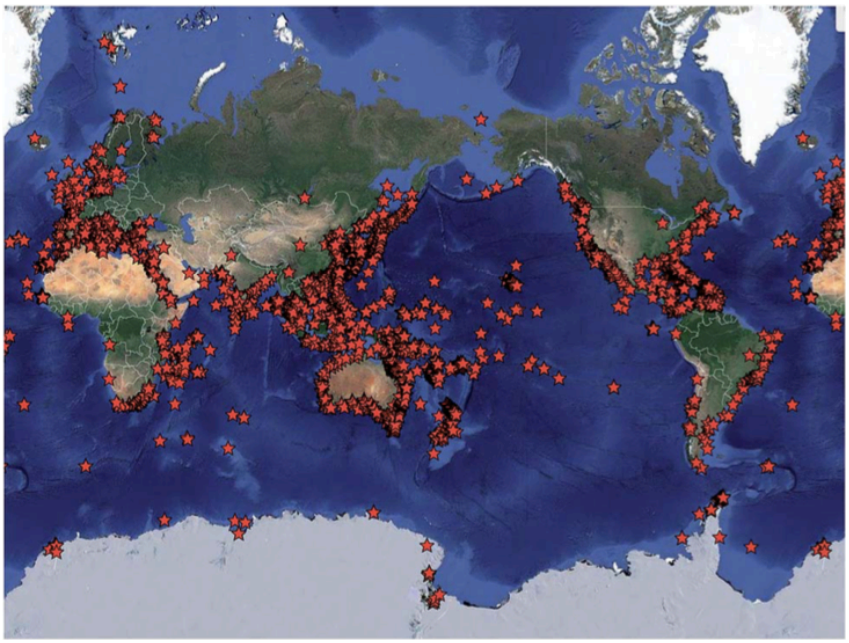

Figure 2. All the collection areas for marine natural products discovery in 1965-2014. (Blunt *et al.*, 2016).

Bioactive compounds from marine organisms might be the result of the special requirements of an organisms for surviving and adapting themselves to an extreme environment under the sea for the purpose of communication, reproduction and protection against predation, competition and infection (Firn and Jones, 2000). Interestingly, many of these compounds have not been found in terrestrial sources (Carte, 1996). Most of organisms in marine environments have been explored for their chemical compounds in potential industrial developments, including pharmaceuticals, cosmetics, nutritional supplements, fine chemicals and agrochemicals (Kijjoa and Sawangwong, 2004).

1.2.2. Importance of Marine Natural Products

Although not many compounds from marine organisms are found in pharmaceutical applications when compared to those obtained from terrestrial plants, the marine organisms continue to provide important and interesting molecules which can be considered as leads for developments of drugs for many serious diseases (Schueffler and Anke, 2014). However, as a result of several marine natural products discovering initiatives, there are some drugs from marine organisms that have been approved for pharmaceutical uses or under clinical trials nowadays.

The first marine-derived drug which is cytarabine (Cytosar-U®), was approved by the Food and Drug Administration (FDA) and European Medicines Agency (EMA) in 1969 and became available for clinical uses. Cytarabine is a synthetic pyrimidine nucleoside, which was originated from the Caribbean sponge *Tethya crypyta*. Cytarabine is a cytotoxic drug which is used for treatment of several types of leukemia (Lowenberg *et al.*, 2011; Mayer *et al.*, 2010). Later on, vidarabine (Vira-A®), a synthetic purine nucleoside that was also isolated from *Tethya crypyta*, received the FDA approval in 1976 as an antiviral drug. Vidarabine are currently obtained from *Streptomyces antibioticus* (Whitley *et al.*, 1980). Ziconotide (Prialt®), a synthetic version of peptide ω-conotoxin, was originally isolated from the venom of cone snails. This drug was approved by FDA and EMA in 2004 and 2005 respectively, for the use in chronic pain management (Schmidtko *et al.*, 2010). In 2004, the first fish oil-derived product, omega-3 acid ethyl esters (Lovaza®) was approved by FDA for the treatment of patients with severe hypertriglyceridemia (Koski, 2008). The anticancer drug trabectedin (Yondelis®), also known as ecteinascidin-743 (ET-743), is a tetrahydroisoquinoline alkaloid originally isolated from a colonial tunicate *Ecteinascidia turbinate* that collected from the Caribbean and Mediterranean seas (Rinehart *et al.*, 1990).

Trabectedin was approved in EU for patients with advanced tissue sarcoma, as well as with platinum-sensitive ovarian cancer (Newman and Cragg, 2014). Another marine-derived chemotherapeutic drug is eribulin mesylate (Halaven®) which is a synthetic derivative based on the structure of halichondrin B, a polyether macrolide isolated from the sponge *Halichondria okadai* (Hirata and Uemura, 1986). Halaven® was approved by FDA in 2010 and EMA in 2011 for the treatment of patients with metastatic breast cancer (Verdaguer *et al.*, 2013). Moreover, the antibody-drug conjugate, brentuximab vedotin (SGN-35; Adcetris®) was originally isolated from the sea hare *Dorabella auricularia*. Adcetris® was approved by FDA in 2011 for the treatment of patients with Hodgkin's lymphoma and patients with systemic anaplastic large cell lymphoma (Senter and Sievers, 2012; Younes *et al.*, 2012).

Table 1. Marine-derived compounds in clinical development [adapted from Mayer *et al.* (2010) and Martins *et al.* (2014)].

Compound name	Trademark	Original organism	Disease area	Status 2013
Cytarabine, Ara-C	Cytosar-U®	Sponge	Cancer	Approved
Vidarabine, Ara-A	Vira-A®	Sponge	Antiviral	Approved
Ziconotide	Prialt®	Cone snail	Neuropathic pain	Approved
Omega-3-acid ethyl esters	Lovaza®	Fish	Hypertriglyceridemia	Approved
Trabectedin (ET-743) (EU Registered only)	Yondelis®	Tunicate	Cancer	Approved
Eribulin mesylate (E7389)	Halaven®	Sponge	Cancer	Approved
Brentuximab vedotin (SGN-35)	Adcetris®	Sea hare	Cancer	Approved
Iota-carrageenan	Carragelose®	Red algae	Antiviral	Over-the-counter drug
Soblidotin (TZT1027)	NA	Bacterium	Cancer	Discontinued
Plitidepsin	Aplidin®	Tunicate	Cancer	Phase III
Lurbinectedin	NA	Tunicate	Cancer	Phase II

Compound name	Trademark	Original organism	Disease area	Status 2013
DMXBA (GTS-21)	NA	Worm	Cognition, Alzheimer's	Phase II
Plinabulin (NPI-2358)	NA	Fungus	Cancer	Phase II
CDX-011	NA	Sea hare	Cancer	Phase II
Elisidepsin	Irvalec®	Mollusk	Cancer	Phase II
PM00104	Zalypsis®	Sea slug	Cancer	Phase II
Tasidotin, Synthadotin (ILK-651)	NA	Bacterium	Cancer	Phase II
PM060184	NA	Sponge	Cancer	Phase I
Bryostatin 1	NA	Bryozoa	Cancer	Phase I
SGN-75	NA	Sea hare	Cancer	Phase I
Marizomib (Salinosporamide A, NPI-0052)	NA	Actinomycete	Cancer	Phase I

In the last two decades, a significant number of new compounds with several chemical structural types have been discovered from marine organisms, for example alkaloids, polyketides, peptides, lipids, proteins and glycosides, some of which present interesting biological activities such as anticancer, antibacterial, antifungal, antioxidant and antifouling properties (Rateb and Ebel, 2011). Some of the marine microorganisms, such as fungi, bacteria, actinomycetes and cyanobacteria have become an important source of pharmacologically active metabolites in the search for novel compounds for drug discovery (Bugni and Ireland, 2004a; Saleem *et al.*, 2007). Since microorganisms are renewable and reproducible sources, they can be cultured and can even be considered as a microbial factory for the natural products production (Blunt *et al.*, 2015). Moreover, marine organisms have the potential to provide new therapeutic alternatives for treating human diseases (Galeano *et al.*, 2011). These are the main reasons why marine natural products are being investigated very widely today.

1.3. Fungi as a Source of Bioactive Secondary Metabolites

Although about 1.5 million species of fungi are believed to exist all over the world, only around 72,000 fungal species have already been described worldwide (Singh and Aneja, 2012). From these numerous species, fungi have been used as a source of drug for about 80 years. The discovery of penicillin from *Penicillium notatum* by Alexander Fleming had attracted more attention of many researchers to consider fungi as a source of novel drug leads. Several structurally diverse groups of compounds, including organic acids, polyynes, polyketides (such as quinones, anthraquinones and xanthones), monoterpenes to triterpenes (volatiles and steroids), polysaccharides, lipopolysaccharides and N-, S-containing compounds have been isolated from fungi (Gill and Steglich, 1987; Quang *et al.*, 2005; Steglich *et al.*, 2000; Turner, 1971).

About 20 years after the discovery of penicillin, fungi provided many active compounds for potential modern drugs, including the antihypercholesterolemic drugs statins, antifungal agents such as cyclosporine and echinocandin, and several antibiotics such as streptomycin, chloramphenicol, chlortetracycline, cephalosporin C and vancomycin (Butler, 2004; Larsen *et al.*, 2005). Moreover, Butler (2004) reported that the fungal natural products can be used for other purposes, for examples cyclosporine is used as immunosuppressant during organ transplantation, while both natural compounds (such as lovastatin, pravastatin), and the synthetic analogs (such as crestor, lipitor) are used for treatment of cardiovascular and metabolic diseases. From 1995, the fungal-derived medicines are in the top twenty-selling prescription drugs in worldwide (Singh, 1999).

In the last decades, marine fungi are well recognized as a source of novel and biologically active natural products for drug discovery (Duarte *et al.*, 2012; Xu *et al.*, 2015). **Figure 3** shows that the number of new marine-derived fungal compounds which are published in each year is rapidly increasing, and still has not reached its climax. Currently, more than 1000 of new natural products from marine-derived fungi have been reported (Rateb and Ebel, 2011).

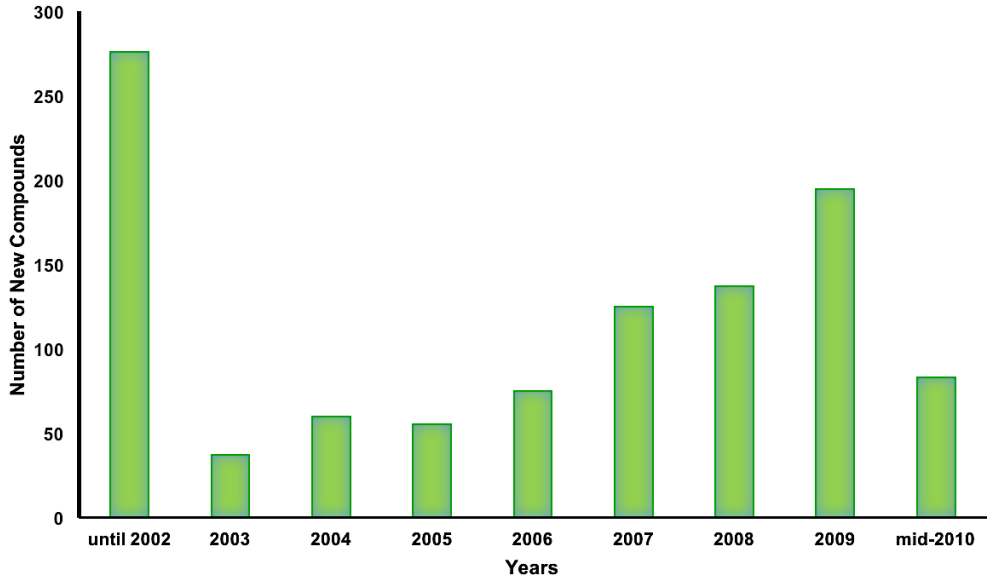

Figure 3. New compounds from marine-derived fungi, according to year of publication [Adapted from Rateb and Ebel (2011)].

1.3.1. Fungi and Marine Ecology

Marine fungi live in diverse marine environments such as oceanic, coastal, estuaries, deep-sea water and sediment habitats. Marine fungi are different from terrestrial and fresh water fungi in several ways. They can live in an extreme salinity of seawater, in average 33 to 35 ppt. They are able to adapt themselves to several factors such as increasing pH, high sodium levels, low temperature, low light and oligotrophic nutrient conditions in deep-sea environment with many challenges for survival (Jennings, 1983; Raghukumar, 2008).

Marine fungi can be divided into obligate marine fungi and facultative marine fungi. The obligate marine fungi can grow and sporulate exclusively in the marine habitat, while the facultative marine fungi are generally found in terrestrial or freshwater habitats, but they also can live and sporulate in the marine environment. (Kohlmeyer and Kohlmeyer, 1979). There are 530 filamentous marine fungi species in 321 genera and most of them are in the order Ascomycota (424 species in 251 genera), followed by Deuteromyces (anamorphic fungi) with 94 species in 61 genera and Basidiomycota with 12 species in 9 genera (Jones *et al.*, 2009).

Generally, marine fungi live as symbionts in marine organisms such as algae, mangrove plants, corals, sea anemone, starfish, seagrass, sea urchin and especially sponges (Jin *et al.*, 2016). Different sources of marine-derived fungi seem to influence the number and nature of the fungal metabolites. Fungal secondary metabolites may act specifically in interspecies interactions to protect the host against competitor or diseases (Bugni and Ireland, 2004b). Rateb and Ebel (2011) gave an overview about the sources of new chemical structures from marine-derived fungi until mid-2010 (**Figure 4**). **Figure 4** shows that most of new compounds reported from marine fungi are derived from sponges and algae.

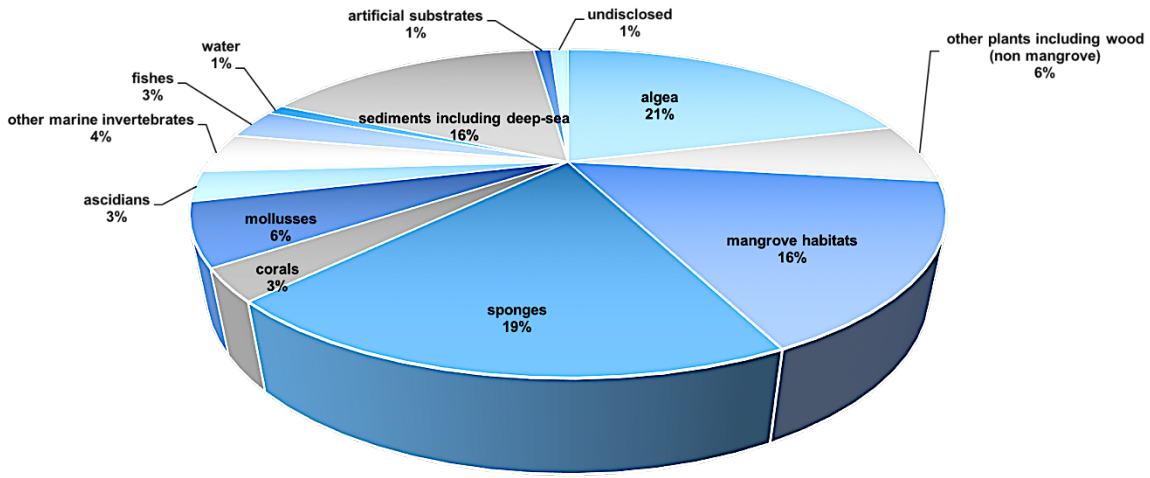

Figure 4. Sources of new marine-derived fungi reported in literature until mid-2010 [Adapted from Rateb and Ebel (2011)].

1.3.2. Sponge - Associated Fungi as a Source of Bioactive Compounds

From 1985 to 2012, more than 15,000 chemical substances, including 4,196 bioactive marine natural products were found. Approximately 75% of the novel bioactive compounds were derived from marine invertebrates, mainly from sponges (Phylum Porifera) and corals (Phylum Cnidaria). Sponges play an important role as the most productive source of new bioactive agents in preclinical development (Hu *et al.*, 2015). Moreover, sponges are also well known to be the hosts for a large community of microorganisms, including fungi and bacteria.

Microbes can compose up to 60% of the sponge tissue volume (Usher *et al.*, 2004). From the microbe symbioses, sponges may benefit from the store of nutrients, transportation of waste products, chemical defense or contribution to mechanical structure

to avoid predation and combat pathogens and competitors (Kubanek *et al.*, 2003; Unson *et al.*, 1994; Wilkinson, 1978; Wilkinson and Garrone, 1980; Wilkinson *et al.*, 1999). From these relationships, researchers have paid more attention to investigate marine sponges as a source of natural products. According to the review of Thomas *et al.* (2010), the major microorganisms which provide pharmacologically relevant secondary metabolites of sponges including fungi, cyanobacteria, actinobacteria, proteobacteria and firmicutes. However, accumulating evidence has lately showed that fungi associated with sponges are the origin of many interesting compounds (Proksch *et al.*, 2008). Interestingly, Thomas et al. (2010) have found that more than 680 fungal strains isolated from 16 sponge species mainly belong to the filamentous fungi *Penicillium* and *Aspergillus* genera.

Filamentous fungi are known to produce a wide variety of biologically active compounds and some of them are useful in drug development (Schueffler and Anke, 2014). Examples of bioactive compounds derived from sponge-associated fungi include IB-01212, a cytotoxic cyclodepsipeptide isolated from the sponge-associated fungus *Clonostachys* sp. ESNA-A009. This compound was found to be cytotoxic against 14 different human tumor cell lines, however it was most active against LN-caP (prostate cancer), SK-BR3 (breast cancer), HT29 (colon cancer) and HELA (cervix cancer) cell lines with GI_{50} (growth inhibition) values in the order of 10^{-8} M (Cruz *et al.*, 2006). Epoxyphomalin A, isolated from the fungus *Phoma* sp. which was isolated from the marine sponge *Ectyplasia perox*, exhibited a cytotoxicity at nanomolar concentrations against 12 human tumour cell lines, with IC_{50} values ranging from 0.010 µg/ml to 0.038 µg/ml (Mohamed et al., 2009). Similanamide, a new cyclohexapeptide, isolated from sponge-associated fungus *Aspergillus similanensis* KUFA 0013, exhibited a weak activity against three human cancer cell lines: breast adenocarcinoma (MCF-7), non-small cell lung cancer (NCI-H460) and melanoma (A373) (Prompanya *et al.*, 2015). Hypofuran A, a new furan derivative, was isolated from a marine fungus *Hypocrea koningii* PF04 which was associated with the marine sponge *Phakellia fusca.* This compound exhibited a moderate antibacterial activity against *Straphylococcus aureus* ATCC25923 (MIC 32 µg/mL) and moderate DPPH radical scavenging capacity with IC_{50} values of 27.4 µg/mL (Ding *et al.*, 2015b). Another example is austalide R**,** a new meroterpenoid from the fungus *Aspergillus* sp. which was isolated from the marine sponge *Tethya aurantium*, showed the antibacterial activity against a panel of marine bacteria (Zhou *et al.*, 2014). The examples of the compounds derived from filamentous fungi demonstrated that they are important sources of bioactive secondary metabolites.

One of the bioactive compound-producing genera of the filamentous fungi is *Talaromyces*. Several members of this genus have been investigated for their bioactive secondary metabolites (Nicoletti and Trincone, 2016; Zhai *et al.*, 2016). Therefore, marine-derived members of this genus are targets of the investigation of our group.

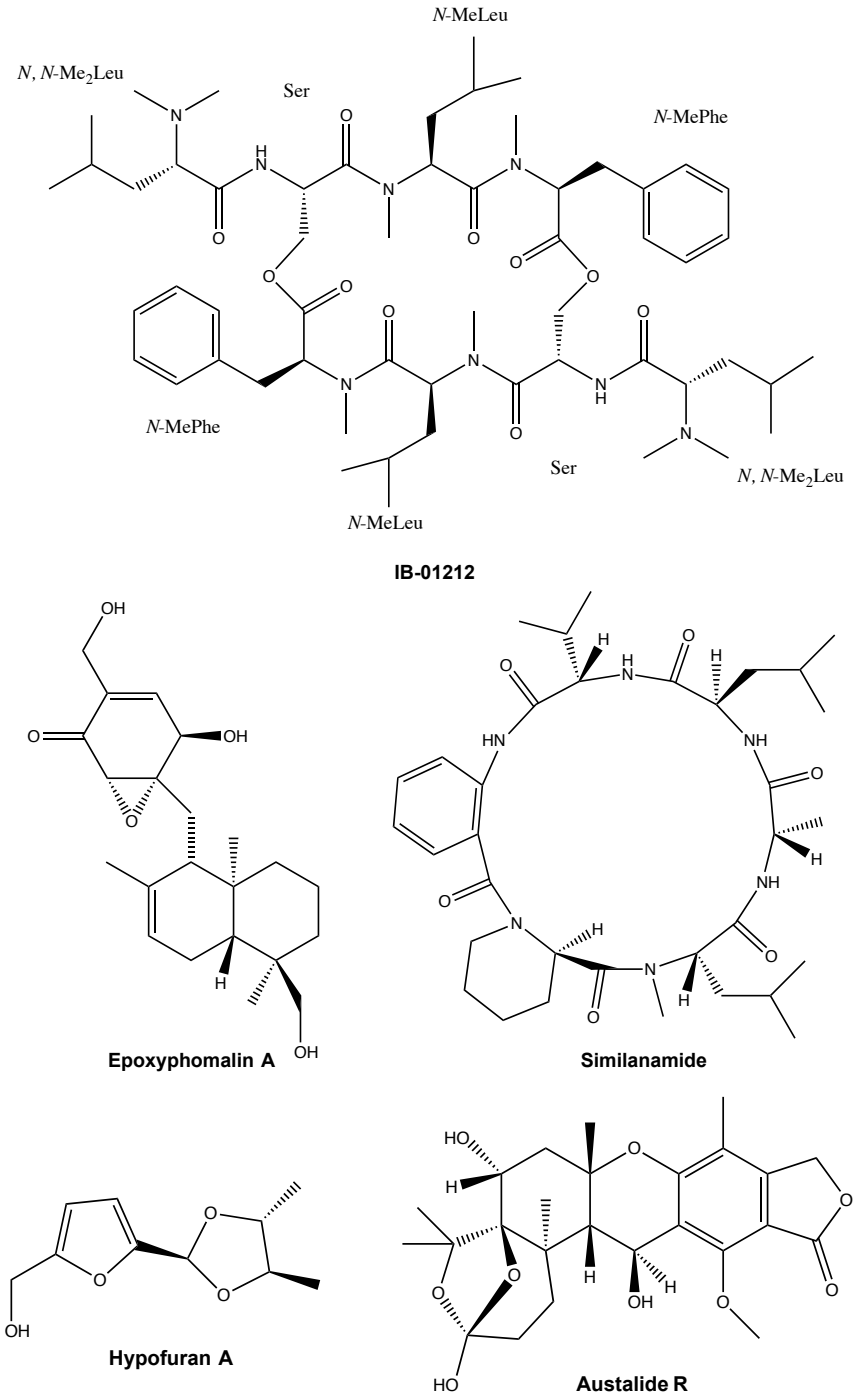

Figure 5. Structures of IB-01212, epoxyphomalin A, similanamide, hypofuran A and austalide R.

1.4. The Genus *Talaromyces*

The genus *Talaromyces* belongs to the family Trichocomaceae. The name *Talaromyces* is derived from the Greek word for 'basket', describing the shape of the ascospores which characterizes the morphology of the fungi in this genus (Zhai *et al.*, 2016). In 1995, the American mycologist Chester Ray Benjamin introduced the genus *Talaromyces* as asexual stage of *Penicillium* that produces soft walled ascomata covered with interwoven hyphae, globose and ovate asci which are produced in chains containing the spiny ascospores and showing yellowish or reddish ornamentations (Benjamin, 1955; Stolk and Samson, 1972). In 2000, 46 species and 6 varieties of the genus *Talaromyces* were found in soil, manure, dung, rubble, foods, industrial and agricultural wastes with worldwide distribution (Pitt *et al.*, 2000).

1.4.1. Taxonomy

Stolk and Samson (1972) classified *Talaromyces* into 4 sections, including section *Talaromyces, Emersonii, Thermophila* and *Purpurea,* which are primarily based on the morphological characteristics of their anamorph states (Stolk and Samson, 1972);

Figure 6. *Talaromyces* Taxonomy.

1.4.1.1. Section *Talaromyces*

The conidial state belongs to the *Penicillium* of the biverticillate - symmetrical type. They present yellow ascocarp with yellow ascospores, in some strains produce plentiful of red pigment. This section contains 10 species, 2 varieties: *Talaromyces rotundus, T. luteus, T. udagawae, T. stipitatus, T. ucrainicus, T. flavus, T. macrosporus, T. wortmannii, T. trachyspermus, T. intermedius, T. helicus* var. *helicus* and *T. helicus* var. *major*. The species belonging to this section are mesophilic with 25°C of optimum temperature and 40°C of maximum temperature. There are various types of initial ascomata, paired gametangia in 3 species; *T. flaves*, *T. helicus* and *T. stipitatus*, while in others develop as branches of hyphae. This section usually produces 8-spored asci in short coiled chains. Ascospores are normally cylindrical with their walls presenting various ornamentations.

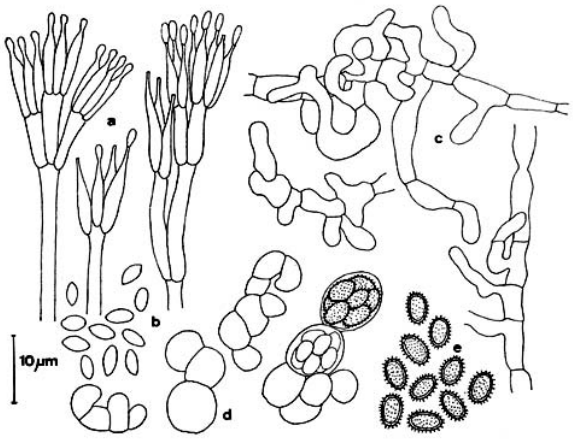

Figure 7. Morphology of *Penicillium* of the biverticillate - symmetrical type (*T. wortmannii*; **a**. conidiogenous structures; **b**. conidia; **c**. initials; **d.** chains of asci; **e**. ascospores) [Adapted from Stolk and Samson (1972)].

1.4.1.2. Section *Emersonii*

The anamorph state belongs to the *Penicillium cylindrosporum* – series or *Paecilomyces*. They have yellow ascospores and distinctly deficient the covering of ascocarp. This section consists of 4 species: *Talaromyces byssochlamydoides, T. bacillisporus, T. emersonii* and *T. leycettanus.* They are thermophilic with 35-45°C optimum temperature. No paired gametangia occur in all four species. They are short, curved asci with 8-spored. Ascospores are globose and have smooth walls.

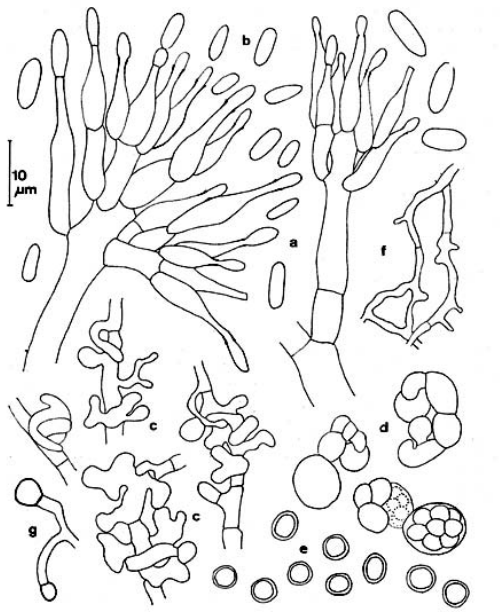

Figure 8. Morphology of *Penicillium cylindrosporum* (*T. byssochlamydoides*; **a.** conidiogenous structures; **b.** conidia; **c.** initials; **d.** chains of asci; **e**. ascospores; **f**. loose-textured hyphae covering the ascoma) [Adapted from Stolk and Samson (1972)].

1.4.1.3. Section *Thermophila*

The imperfect state is classified in the *Penicillium asymmetrica - Divaricata,* near the *P. janthinellum* - series. Ascospores are produced in branched chains and the ascocarps are well-developed walls (thick walls). There is only one species in this section: *Talaromyces thermophilus.* The section *Thermophila* differ from other sections because they are strongly thermophilic, which are able to produce ascomata at 45°C (rarely produce on agar media), and asci are produced in straight and branched chains while others of the genus *Talaromyces* are produced in helicoidal chains.

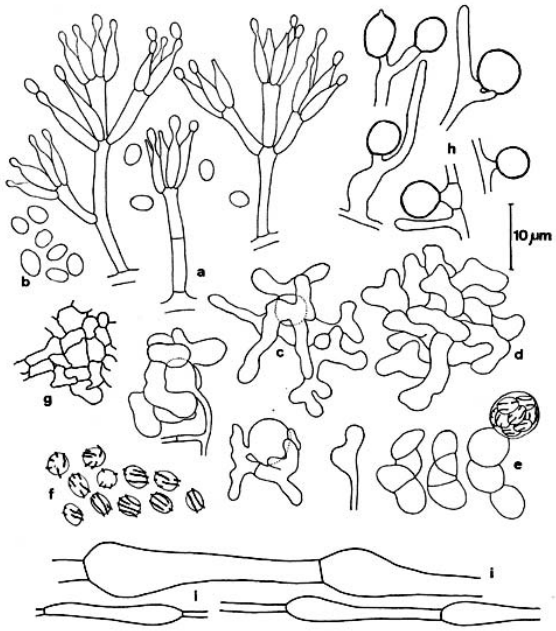

Figure 9. Morphology of *Penicillium asymmetrica* - *Divaricata* (*T. thermophilus*; **a**. conidiogenous structures; **b**. conidia; **c**. initials; **d**. primordium consisting of branching hyphae; **e**. chains of asci; **f**. ascospores; **g**. fragment of ascomatal covering; **h**. chlamydospores; **i**. vegetative hyphae) [Adapted from Stolk and Samson (1972)].

1.4.1.4 Section *Purpurea*

The anamorph state is *Penicillium restrictum* - series. They have thin, loose-textured network of hyphae and yellow ascomata (ascocarps). Ascospores are yellow and red. This section contains only one species: *Talaromyces purpureus.*

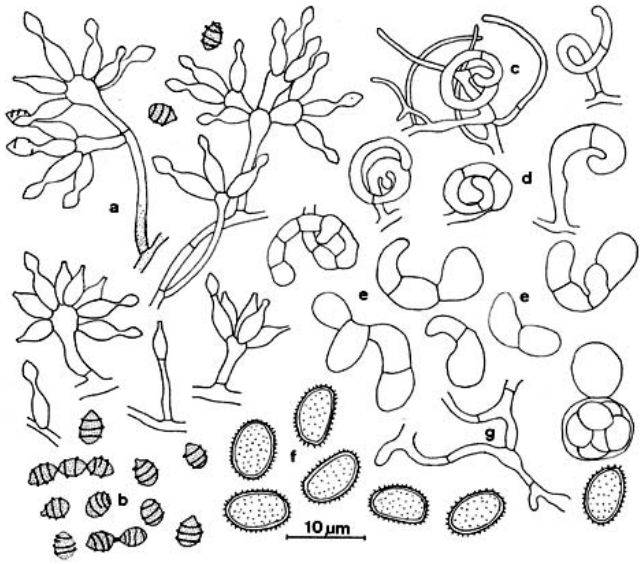

Figure 10. Morphology of *Penicillium restrictum* - series (*T. purpureus*; **a**. conidiogenous structures; **b**. conidia; **c**. initial surrounded by thin hyphae; **d**. initials; **e**. chains of asci; **f**. ascospores; **g**. loosely branched hyphae covering the ascoma) [Adapted from Stolk and Samson (1972)].

1.4.2. The Importance of *Talaromyces*

Fungi belonging to the genus *Talaromyces* are very important for human life in several ways. They provide not only various pigments which are used as natural dyes but also the compounds useful in agricultural and biotechnological applications. On the other hand, some species can cause many fatal diseases in human life and deleterious effects in food industry due to the heat resistance of their ascospores and contamination of mycotoxin in the food products (Frisvad and Filtenborg, 1988).

1.4.2.1. Importance in Agricultural Applications

The genus *Talaromyces* is a ubiquitous and important fungal genus. The members of this genus were isolated from soil, plants, foods and sponges. One of the most important fungi that was used as a bio-control agent in agriculture is *Talaromyces flavus* which is an antagonistic fungus against soil-borne pathogens such as *Verticillium dahliae, Verticillium albo-atrum, Rhizoctonia solani* and *Sclerotinia sclerotiorum* (Boosalis, 1956; Marois *et al.*, 1984; McLaren *et al.*, 1986; Naraghi *et al.*, 2010). For example, *T. flavus* can suppress and control the *Verticillium* wilt of greenhouse cucumber (Naraghi *et al.*, 2011), *V. albo-atrum*

wilt of tomato and potato (Naraghi *et al.*, 2010), *V. dahliae* wilt of cotton (Naraghi *et al.*, 2006), *Verticillium* wilt of eggplant (Marois *et al.*, 1982), white mold (*Sclerotinia sclerotiorum*) of dry bean (Huang *et al.*, 2000) and also against *Rhizoctonia solani* of sugar beet seedling damping-off disease (Kakvan *et al.*, 2013). Moreover, *T. flavus* can stimulate the growth of cotton and potato (Naraghi *et al.*, 2012). The mechanisms for bio-control activity include competition, mycoparasitism and antibiosis (Adams, 1990; Madi *et al.*, 1997; Marois *et al.*, 1984; Stosz *et al.*, 1996). In contrast, some species can cause disease in plants, for example *T. islandicus* causes yellowing of rice in Japan (Sakai *et al.*, 2005).

1.4.2.2. Importance in Biotechnological Applications

1.4.2.2.1. Biomass Degradation

Many species of the genus *Talaromyces* are used for biotechnological purposes because of their ability to produce soluble enzymes. There are many important enzyme producer species such as *T. rugulosus* which produces β-rutinosidase and phosphatase (Narikawa *et al.*, 2000; Reyes *et al.*, 1999), *T. wortmannii* (*T. variabilis*) which produces urethanase (Gu and Tian, 2013) and *T. pinophilus* (=*T. cellulolyticus*) which is used as an important cellulose-degrading enzyme producer in biomass degradation (Fujii *et al.*, 2014; Pol *et al.*, 2012).

1.4.2.2.2. Food Industry

Figure 11. Pigments from filamentous fungi in food industry; **A**. Pigmented filamentous fungi; **B**. Pigments and colorants produced and extracted and **C**. Food formulation and processing [Adapted from Dufosse *et al.* (2014)].

Filamentous fungi are being investigated as a natural source of food colorants. Normally, members of the genus *Talaromyces* produce yellow, orange and purple-red pigments. More than centuries, *Monascus* has traditionally been used as natural

food colorants and food preservative of meat and fish in Asia (Lin *et al.*, 2008). *T. aculeatus*, *T. funiculosus*, *T. purpurogenus* and *T. pinophilus* have been reported to produce *Monascus*-like polyketide azaphilone (MPA) pigments without co-production of mycotoxin citrinin (Mapari *et al.*, 2008). Also, *T. amestolkiae*, *T. stollii* and *T. ruber* have been discovered to produce this red pigments (Yilmaz *et al.*, 2012).

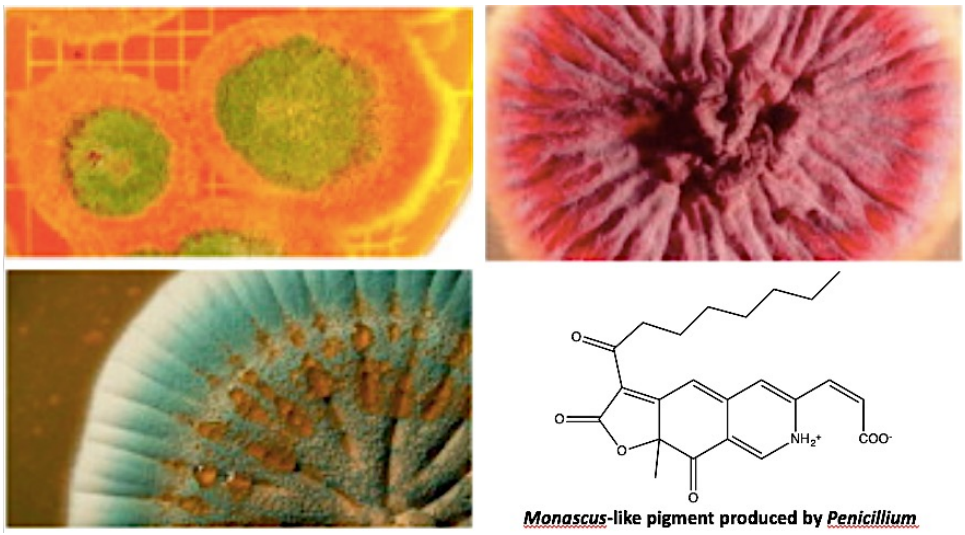

Figure 12. Screening for filamentous fungi producing pigments of interest without any co-production of mycotoxins and *Monascus*-like pigment produced by *Penicillium* [Adapted from Dufosse *et al.* (2014)].

T. atroroseus is the optimal producer of important yellow and red pigments for industrially colorants. It can produce not only the yellow pigments such as monascin, monascurubrin, xanthomonascin A and another series of yellow mitrorubrin azaphilones but also several red pigments (Frisvad *et al.*, 2013).

One of the main problems in food industry are spoilage and poisoning of food products caused by fungi (Pitt and Hocking, 2009). Some members of *Talaromyces* are very important in food industry because of their heat resistant ascospores which can cause spoilage in pasteurized food products. Many species that produce heat resistant ascospores have been reported. *T. trachyspermus*, *T. flavus, T. stipitatus, T. bacillisporus, T. wortmannii and T. helicus*, isolated from commercial fruit juices, caused spoilage in fruit products (Dijksterhuis, 2007; Enigl *et al.*, 1993; Pitt and Hocking, 2009; Scott and Bernard, 1987). *T. macrosporus* can occur in pasteurized foods (Frisvad and Filtenborg, 1988).

Mycotoxins can contaminate in a wide range of food including meats, fruits, cheeses, spices and wines. It showed acute and chronic toxicity at low concentrations and

some are mutagenic or carcinogenic causing hepatic cancer in human (Aziz *et al.*, 2006; Petzinger and Weidenbach, 2002). Some species of the genus *Talaromyces* can cause mycotoxin contamination in food products. *Talaromyces purpurogenus* produced four different kinds of mycotoxins: rubratoxins, luteoskyrin, spiculisporic acid and rugulovasins (Yilmaz *et al.*, 2012). In 1996, rubratoxin was reported to cause the critical illness, requiring immediate liver transplant in the three teenagers after drinking rhubarb wine, which contained high level of rubratoxins (Sigler *et al.*, 1996). Interestingly, rubratoxins were showed to exhibit anticancer activity (Wada *et al.*, 2010). *Talaromyces islandicus* is a harmful storage fungi which caused "yellow rice syndrome". The japanese government started foodstuff controlling for safety because this fungus produces two hepatotoxic metabolites: luteoskyrin and cyclochlorotine (Udagawa and Tatsuno, 2003). Moreover, *T. islandicus* can produce numerous industrially important extracellular enzymes such as cellulases, chitosanases, proteases, β-galactofuranosidase and polygalacturonases (Schafhauser *et al.*, 2015). Moreover, some species are beneficial for food and beverage productions such as Oak chips inoculated with *T. purpurogenum* are used for artificial aging of red wines as an alternative to wood barrel aging (Petruzzi *et al.*, 2012).

1.4.2.3. Importance in Medical Applications

Talaromyces was reported to be medically important in several publications since this genus contains species that cause many fatal diseases for human. For example, *T. marneffei* is the third most common opportunistic infection in patients with the acquired immunodeficiency syndrome (AIDS). This fungal infection is frequently found in Southeast Asian countries, China and Hong Kong (Supparatpinyo *et al.*, 1998). In 2010, *T. indigoticus* was isolated from human skin and nail lesions which were affected by onychomycosis in Panama and the American continent (Weisenborn *et al.*, 2010). *T. piceus* causes inflammation of rib bone or bone marrow in an X-linked chronic granulomatous disease (X-CGD) and fungal infection in blood (Horré *et al.*, 2001; Santos *et al.*, 2006). *T. amestolkiae* was isolated from sputum and lungs of cystic fibrosis patients (Yilmaz *et al.*, 2016). In the previous studies, *T. purpurogenus* was found to cause the human lungs infection in the 66-year-old woman patient with multiple myeloma (Atalay *et al.*, 2016). However, fungi of this genus are found to produce several bioactive secondary metabolites which can be considered useful in drug discovery. For example, talaperoxides B and D, isolated from the mangrove-derived fungus *Talaromyces flavus*, are cytotoxic against several human tumor cell lines such as HeLa, HepG2, MCF-7, PC-3 and MDA-MB-435 with IC_{50} = 2.8-9.4 μM (Li *et al.*, 2011). Moreover, the marine fungus *Talaromyces* sp. Strain LF458 produced

acetylcholinesterase inhibitors, namely talaromycesones A, B and AS-186c which showed potent acetylcholinesterase inhibitory activity with IC_{50} 7.49, 1.61 and 2.60 μM, respectively (Wu *et al.*, 2015).

1.5. Obesity

Obesity is becoming a major public worldwide health problem with inestimable social costs. The World Health Organization (WHO) reported that about 39% of adult (≥ 20 years old) world's population were overweight in 2014. The international consortium of researchers of the Institute for Health Metrics and Evaluation (IHME) at the University of Washington also stated that the global overweight (BMI range: 25-30 kg/m^2) and obesity (BMI range: > 30 kg/m^2) rates were increased in the last three decades presenting a health problem in both the developing and the developed countries. During 1980-2013, the rates of obesity among adults have increased for both men (from 29% to 37%) and women (from 30% to 38%) (Ng *et al.*, 2014).

Obesity has effects not only on personal quality of life, but numerous diseases and mortality also. It causes many diseases, including diabetes, hypertension, osteoarthritis and heart diseases. In the present, there are only two most prescribed anti-obesity drugs in global pharmaceutical market: orlistat and phentermine. Both drugs have adverse effects such as dry mouth, headache, insomnia, increased blood pressure and constipation. There is still a lack of efficient and safe drugs for curing obesity. For this reason, a wide variety of natural products have been studied for this aspect (Castro *et al.*, 2016; Yun, 2010).

Terrestrial and aquatic organisms were explored for their anti-obesity bioactive compounds. Some of them have been used in traditional medicines for centuries. Many extracts and secondary metabolites derived from plants such as extracts from *Panax japonicas*, roots of *Platycodi redix*, *Nelumbo nucifera* and *Salix matsudana* have been reported for their pancreatic lipase inhibitory activity. The phytochemicals include saponins, polyphenols, caffeine and flavonoids. Although many phenolic compound-containing plant extracts such as flavonoids have been demonstrated to have potential as anti-obesity agents, only few anthraquinones have been investigated for their anti-obesity potential (Choudhary, 2011; Yun, 2010). Tzeng *et al.* (2012) have found that the anthraquinone emodin has anti-obesity and antihyperlipidaemic effects which caused dose related

reductions in the hepatic triglyceride and cholesterol contents and lowered hepatic lipid droplets accumulation in high-fat diet-fed rats.

Microorganisms and marine algae have been also screened for anti-obesity property. However, only few of them have been explored and studied (**Table 2**).

Table 2. Anti-obesity compounds from microorganisms and algae (Yun, 2010).

Source	Active component	Experimental methods (treated dose, subjects, duration of treatment)	Major activity
Fungus, *Laetiporus sulphureus*	Mycelia extract	2 mg/ml fungal extract, lipase activity	Inhibitory effect on lipase activity = 83%
Fungus, *Tylopilus felleus*	Mycelia extract	2 mg/ml fungal extract, lipase activity	Inhibitory effect on lipase activity = 96%
Fungus, *Hygrocybe conica*	Mycelia extract	2 mg/ml fungal extract, lipase activity	Inhibitory effect on lipase activity = 97%
Basidiomycete, *Boreostereum vibran*	Vibralactone	Inhibitory activity of pancreatic lipase	IC_{50} = 0.4 ug/ml
Streptomyces toxytricini	Lipistatin	Inhibitory activity of pancreatic lipase	IC_{50} = 0.14 uM
Streptomyces sp. NR0619	Panclicins	Inhibitory activity of pancreatic lipase	IC_{50} = 0.89 uM with panclicin D
Actinomycetes sp. MG147-CF2	Valilactone Esterastin Ebelactone A Ebelactone B	Inhibitory activity of pancreatic lipase Inhibitory activity of pancreatic lipase Inhibitory activity of pancreatic lipase Inhibitory activity of pancreatic lipase	IC_{50} = 0..00014 ug/ml IC_{50} = 0.2 ug/ml IC_{50} = 0.003 ug/ml IC_{50} = 0.001 ug/ml
Marine algae, *Caulerpa taxifolia*	Caulerpenyne	Inhibitory activity of pancreatic lipase	IC_{50}=2mM

The screening of potent molecule on their anti-obesity activity has been studied in several cell lines such as murine 3T3-L1 adipocytes (Roh and Jung, 2012), 3T3-F442A preadipocytes, OP9 stromal adipocytes, porcine primary preadipocytes and feline primary preadipocytes (Choudhary, 2011; Ruiz-Ojeda *et al.*, 2016). However, the *in vitro* assays have limitations in adipogenic differentiation time, the difficulty in transfection of cells and lack of the information about the physiological conditions and complex interactions among different type of cells and tissues (Ruiz-Ojeda *et al.*, 2016).

Animal models can provide the fundamental parameters that regulate the physiological and genetic basis of obesity (Speakman *et al.*, 2008). Several animal models (commonly rodents) are used for the discovery of various treatments for obesity and for the study of factors causing obesity. Nevertheless, rat and mice have limitation about the

missing of leptin protein, which is a key part of body's system of weight regulation, or the body temperature regulating receptor problem, their low speed and high cost of animal model (Vogel, 2000). Therefore, the small size animal models have been developed including vertebrates (zebrafish), invertebrates (the nematode; *Caenorhabditis elegans* (Link *et al.*, 2000), and the fruit fly; *Drosophila melanogaster* (Shulman *et al.*, 2003)) for drug screening.

Since it is a vertebrate, the zebrafish is genetically closer to human than worms and flies. The zebrafish is accepted as the simplest animal model with full complement of vertebrate organs and their transparency bodies that can be used in the screening of the gene regulating lipid metabolism. The advantages of zebrafish are they are small whole animal model with quick generation time, low cost, amenable with large-scale screening and higher physiological relevance over cellular *in vitro* models for bioactive compound screening (Giacomotto and Ségalat, 2010; Vogel, 2000). Moreover, the zebra larvae Nile red assay is suitable to detect anti-obesogenic activities, and it exhibited similarly response to human in screening the lipid regulator drugs (Jones *et al.*, 2008). Nowadays, the potential of natural products which can be used in the treatment of obesity is still largely unexplored, especially microorganism sources. The active exploration and testing of new metabolites for anti-obesity activity may provide the hope for new drug developments.

1.6. Objectives

The main goal of this dissertation consists of two parts: i) to isolate, purify and elucidate the structure of the secondary metabolites from the sponge-associated fungus *Talaromyces stipitatus* (KUFA 0207), which was isolated from the marine sponge *Stylissa flabelliformis,* collected from the Gulf of Thailand (Samaesan Island), Chonburi province, Thailand, ii) to evaluate the bioactivities of the isolated secondary metabolites.

CHAPTER 2

2. Secondary Metabolites from the Fungi of the Genus *Talaromyces* Section *Talaromyces* and Their Bioactivities

The genus *Talaromyces* generates a wide range of compounds (used as natural colorants) and soluble enzymes that are useful in biotechnological applications. However, some species are also used as bio-control agents in agriculture, whereas other members are human pathogens. Some species can cause fatal diseases in human while others cause spoilage and poisoning in food products due to their heat-resistant ascospores. Considering their importance, this genus is widely investigated including their bioactive secondary metabolites.

Stolk and Samson (1972), have divided *Talaromyces* into 4 sections: *Talaromyces, Emersonii, Thermophila* and *Purpurea.* In this study, we focused on *Talaromyces stipitatus* which belongs to the section *Talaromyces*. The morphological characteristic of this fungus was showed in **Figure 13**. We considered secondary metabolites of the species in the section *Talaromyces* which comprise of *Talaromyces rotundus, T. luteus, T. udagawae, T. stipitatus, T. ucrainicus, T. flavus, T. macrosporus, T. wortmannii, T. trachyspermus, T. intermedius, T. helicus* var. *helicus* and *T. helicus* var. *major* (Stolk and Samson, 1972).

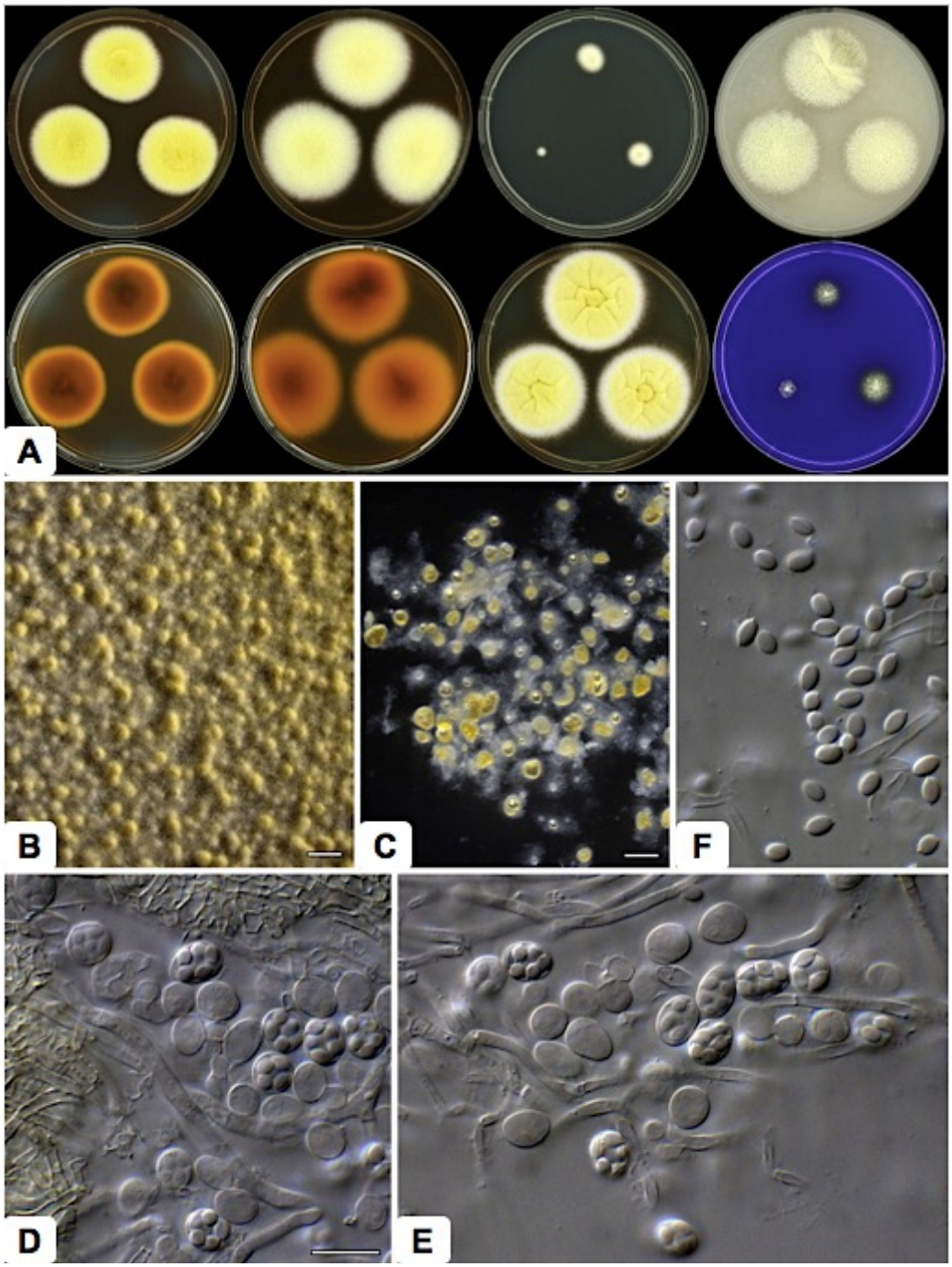

Figure 13. Morphological characteristics of *Talaromyces stipitatus* (CBS 236.60); **A**. Colonies from left to right (top row) CYA, MEA, DG18 and OA; (bottom row) CYA reverse, MEA reverse, YES and CREA; **B**. Colony texture and ascomata on OA after 2 weeks' incubation; **C**. Ascomata; **D**, **E**. Asci and ascospores; **F**. Ascospores. Scale bars: **B** = 1000 µm; **C** = 500 µm; **D** = 10 µm, applies to **E**, **F**. (Yilmaz *et al.*, 2014).

Zhai *et al.* (2016) reported that 221 secondary metabolites, including alkaloids, peptides, esters, polyketides, quinones, steroids, terpenoids and other structural type compounds, were isolated from the species of the genus *Talaromyces*. However, in this

study, only 110 compounds and their bioactivities from only six species in the section *Talaromyces* of genus *Talaromyces* are presented below.

2.1. *Talaromyces flavus*

Since *T. flavus* was used as a bio-control agent against soil-borne pathogens in agricultural application and has an ability to produce heat resistance ascospores, numerous secondary metabolites of diverse structural types such as esters, polyketides, quinones, steroids and terpenoids, among others, were isolated from this fungus. He *et al.* (2014b) reported the isolation and their bioactivities of the secondary metabolites, including six polyesters, talapolyesters A-F (**1-4, 14** and **16**) along with eleven macrolide polyesters, 15G256v (**5**), 15G256v-me (**6**), 15G256Π (**7**), 15G256β-2 (**8**), 15G256α-2 (**9**), 15G256α-2-me (**10**), 15G256ι (**11**), 15G256β (**12**), 15G256α (**13**), 15G256α-1 (**15**) and 15G256ω (**17**), from the wetland soil-derived fungus *T. flavus* BYD07-13. While compounds **12, 13** and **15** showed toxicity against mouse peritoneal macrophage, the macrocyclic polyesters **11**-**17** displayed cytotoxicity against five tumor cell lines: HL-60, SMMC-7721, A-549, MCF-7 and SW480. Interestingly, the cyclic compounds **12** and **17** exhibited significant cytotoxicity against MCF-7 cell line with IC_{50} value of 3.27 and 4.32 μM, respectively, while the linear polyesters **1**-**10** were inactive (IC_{50}>40 μM) (He *et al.*, 2014b)

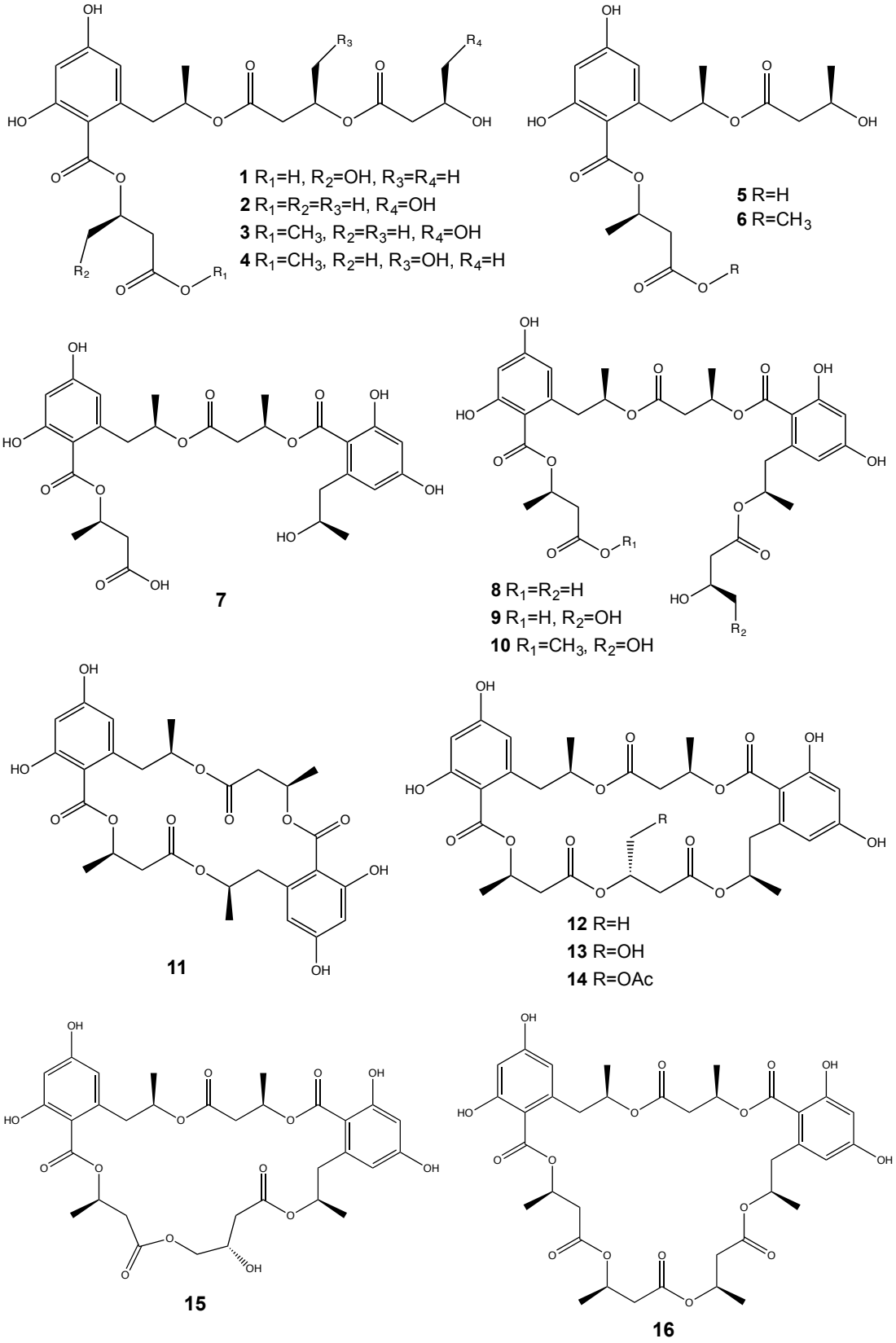

Figure 14. Secondary metabolites of *Talaromyces flavus* (**1**-**16**).

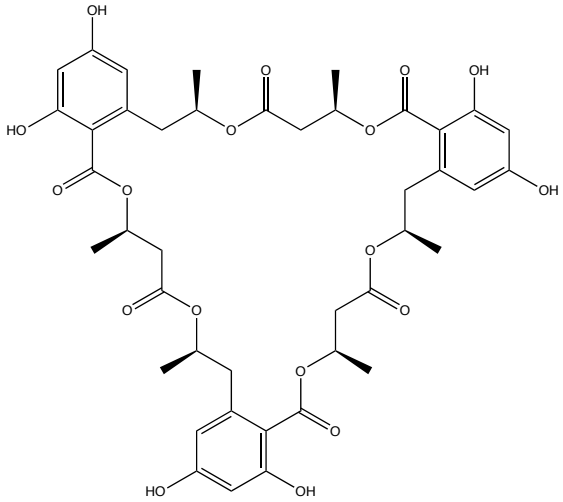

17

Figure 15. Structure of 15G256ω (**17**).

In 1990, a coumarin (**18**), two isocoumarin derivatives (**21** and **22**) and phthalide derivative (**23**) were isolated from the organic extracts of soil fungus *T. flavus* (Ayer and Racok, 1990). Later, He *et al.* (2014c) isolated two new coumarins, talacoumarins A (**19**) and B (**20**) from the ethyl acetate extract of the wetland soil-derived fungus *T. flavus* BYD07-13. The two compounds had moderate anti-$A\beta_{42}$ aggregation activity. Vermistatin (**24**) was obtained from the culture broth of *T. flavus* FKI-0076 as well as from the extract of *T. flavus* IFM52668 (Arai *et al.*, 2002).

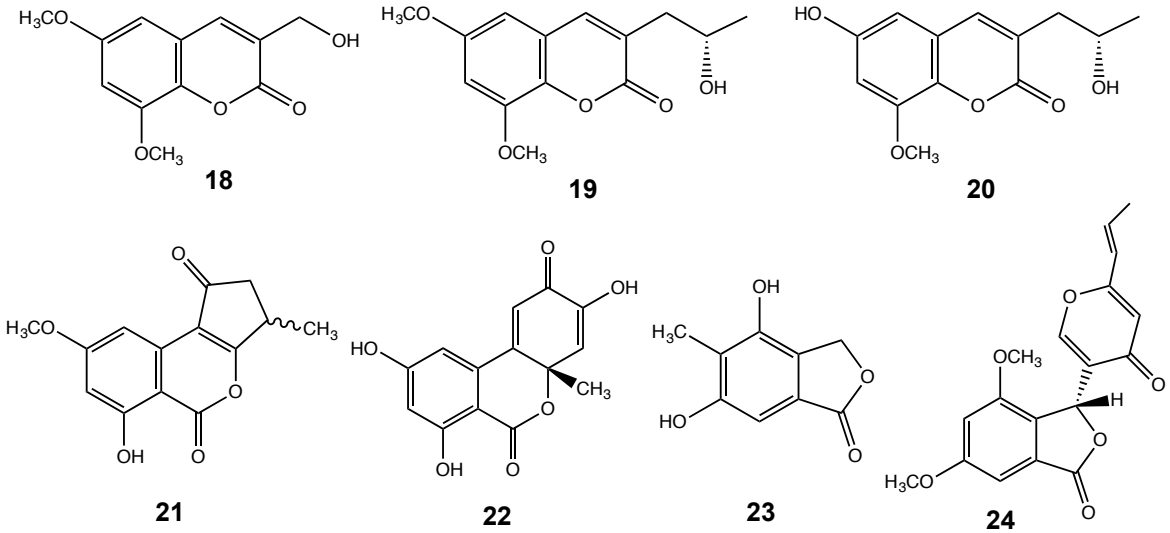

Figure 16. Secondary metabolites of *Talaromyces flavus* (**18**-**24**).

Ayer and Racok (1990) isolated many secondary metabolites from the organic extracts of this fungus, including a lactone (**25**), D-glucono-1,4-lactone (**26**),

hydroxymethylmaltol (**27**) and a benzopyrone derivative (**28**). Funicone (**29**) and funicone-related compounds i.e. 9,14-epoxy-11-deoxyfunicone (**30**), deoxyfunicone (**31**) and actofunicone (**32**), were also obtained from the strain of *T. flavus*. Funicone (**29**) showed antifungal activity against a human pathogenic filamentous fungus *Aspergillus fumigatus* (11-mm inhibition zone at 100 µg/disc), while compound **30** exhibited weak inhibition against *A. niger* (10-mm inhibition zone at 200 µg/disc) (Arai *et al.*, 2002; Nicoletti *et al.*, 2009).

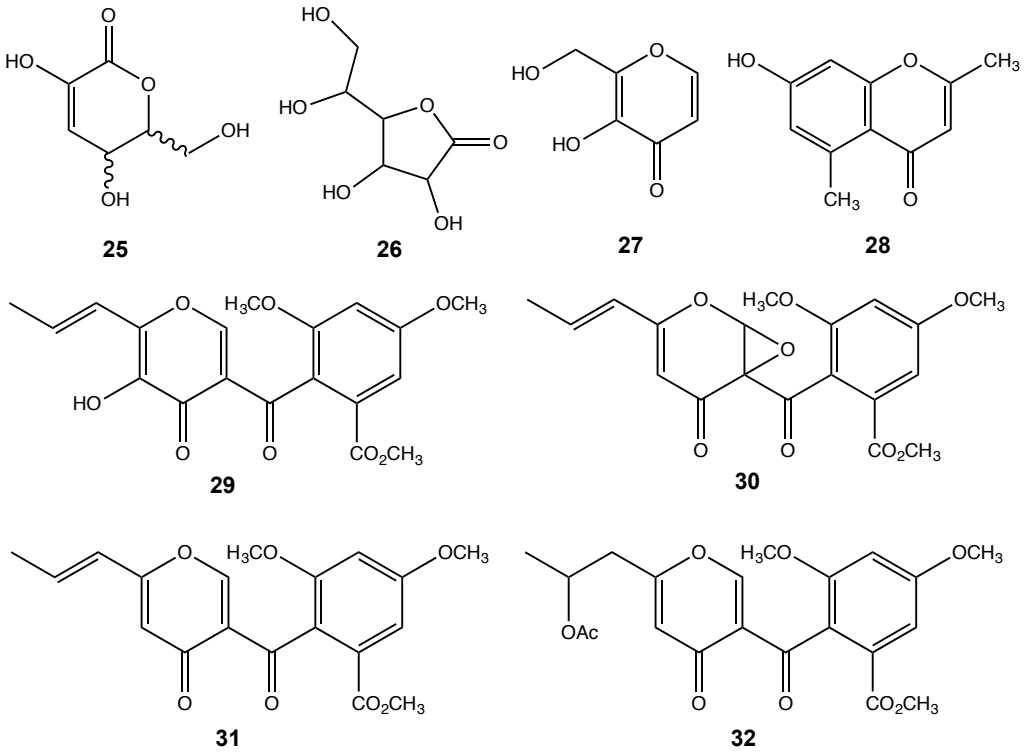

Figure 17. Structures of the secondary metabolites **25-32**, isolated from *Talaromyces flavus*.

Diazaphilonic acid (**33**), isolated from *T. flavus* PF1195, inhibited DNA amplification by polymerase chain reaction (PCR) with *Thermus thermophilus* DNA polymerase, with the IC_{50} value of 2.6 µg/mL, and almost completely inhibited telomerase activity of human leukemia at 50 µM (Tabata *et al.*, 1999).

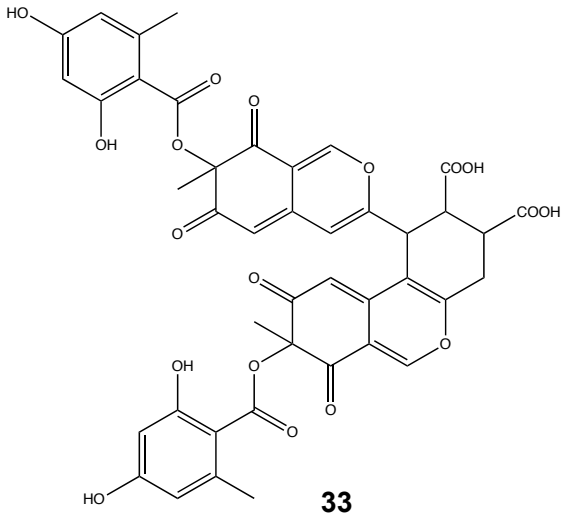

33

Figure 18. Structure of diazaphilonic acid (**33**).

Moreover, *T. flavus* can produce several terpenoid structural types. A novel nardosinane sesquiterpene, talaflavuterpenoid A (**34**), isolated from the wetland soil-derived fungus *T. flavus* BYD07-13, exhibited cytotoxic activity against five human cancer cell lines: HL-60, SMMC-7721, A-549, MCF-7 and SW480, with IC_{50} > 40 μM as well as antimicrobial activities against *Escherichia coli*, *Staphylococcus aureus*, *Candida albicans*, and *Aspergillus niger* (MIC > 1.0 mg/mL) (He *et al.*, 2014a). Four norsesquiterpene peroxides, talaperoxides A-D (**35**-**38**) and steperoxide B (**39**) were isolated from a mangrove endophytic fungus *T. flavus.* Talaperoxide B (**36**) and steperoxide B (**39**) showed cytotoxicity against five human tumor cell lines: MCF-7, MDA-MB-435, HepG2, HeLa and PC-3, with IC_{50} values between 0.70 and 2.78 μg/mL (Li *et al.*, 2011).

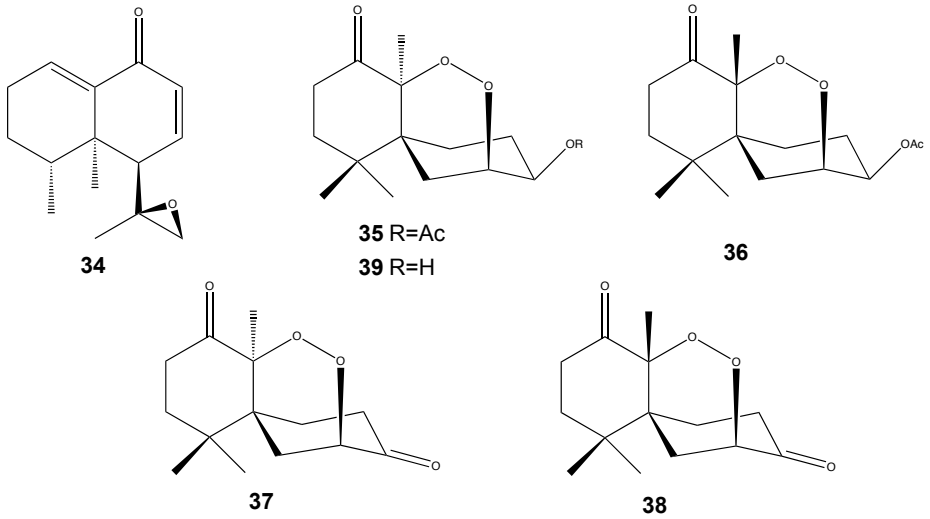

34 **35** R=Ac **39** R=H **36** **37** **38**

Figure 19. Structure of compounds **34-39**.

A benzoic acid derivative (**40**), altenusin (**41**), 5-hydroxymethylfurfural (**42**) and fosfonochlorin (**43**) were isolated from the fungus *T. flavus*. Altenusin (**41**) showed an ability to inhibit the enzyme HIV-1 integrase in the coupled and the strand-transfer assays with IC_{50} values of 19 μM and 25 μM, respectively. Compound **43** was active against *Proteus vulgaris* and *P. mirabilis* and weakly active against *Klebsiella pneumoniae, Providencia rettgeri* and *Salmonella enteritidis* (Ayer and Racok, 1990; Singh *et al.*, 2003; Takeuchi *et al.*, 1989).

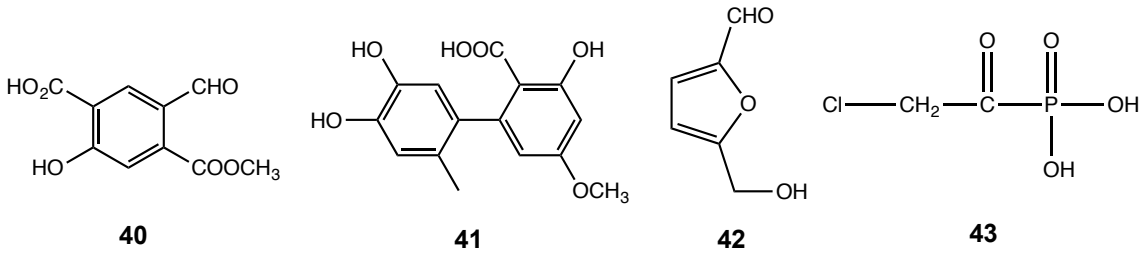

40 **41** **42** **43**

Figure 20. Structures of compounds **40**-**43**.

2.2. *Talaromyces helicus*

Osmanova *et al.* (2010) reported an isolation of four chlorinated azaphilones, helicusins A (**44**), B (**45**), C (**46**) and D (**47**) from *T. helicus.* Helicusins A-D presented weak MAO-inhibitory activity.

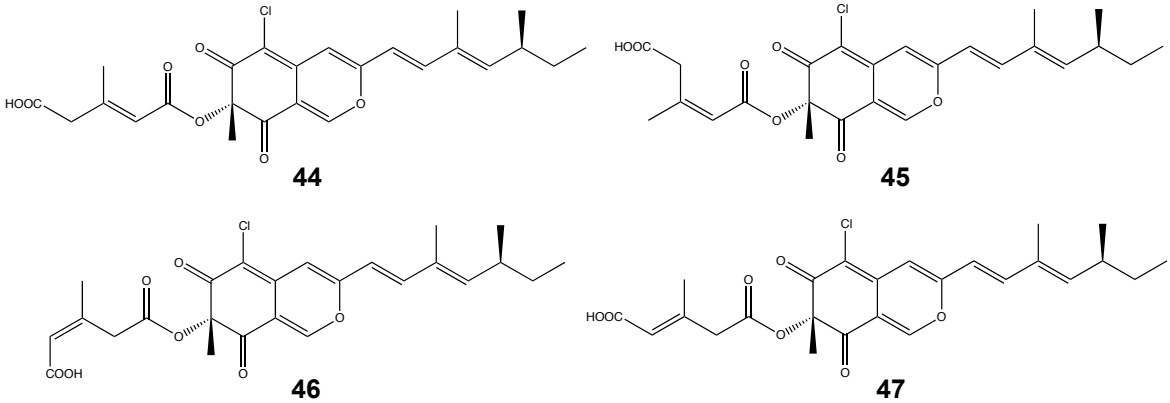

44 **45** **46** **47**

Figure 21. Structures of helicusins A-D (**44**-**47**).

2.3. *Talaromyces luteus*

Two monoamine oxidase (MAO) inhibitors, luteusins A (**48**) and B (**49**) were isolated from *T. luteus* (Fujimoto *et al.*, 1990). Later on, Yoshida *et al.* (1996) discovered luteusins C (**50**), D (**51**) and E (**52**) from this fungus but the three compounds had no MAO-inhibitory activity.

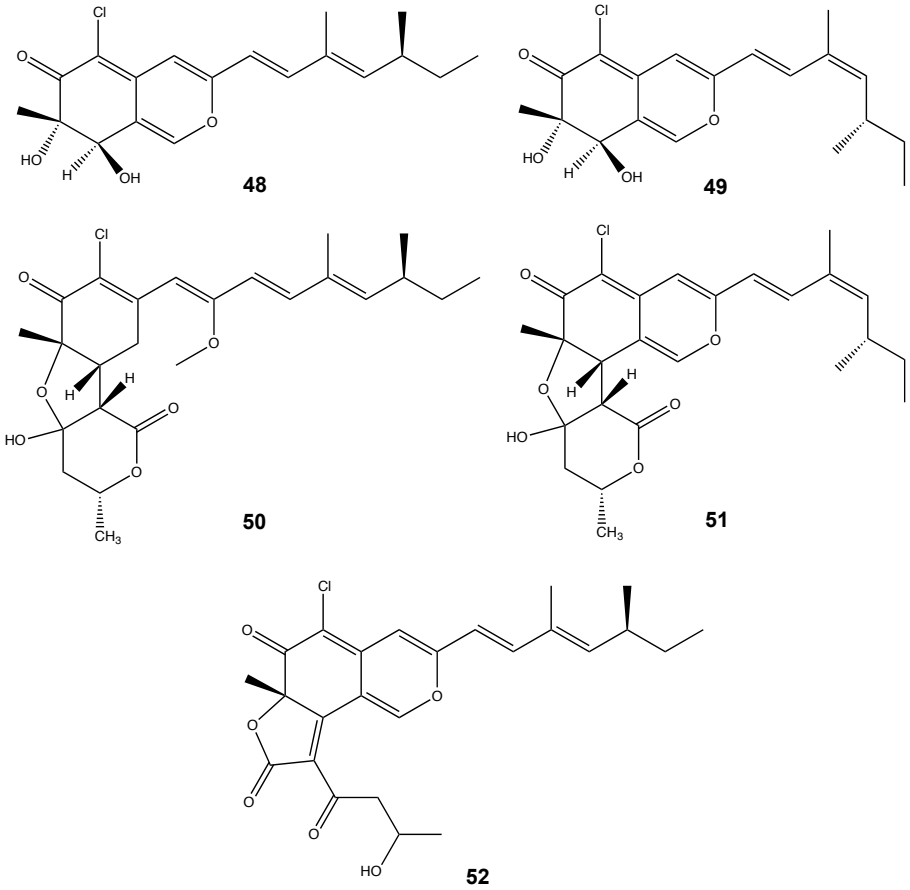

Figure 22. Structures of luteusins A-E (**48**-**52**).

2.4. *Talaromyces stipitatus*

Zang *et al.* (2015) isolated and characterized four new compounds: talaroenamines B-E (**54-57**) along with the previously reported talaroenamine A (**53**) and a new linear polyester, talapolyester G (**58**) from the fungus *T. stipitatus* ATCC 10500. Talaroenamine D (**56**) exhibited inhibition against the chloroquine-resistant *Plasmodium falciparum*, however, it showed no toxicity on HeLa and preadipose cell lines. Frisvad *et al.* (1990) reported the

isolation of emodin (**59**), catenarin (**60**), duclauxin (**61**), erythroglaucin (**62**) and stipitatic acid (**63**) from this fungus.

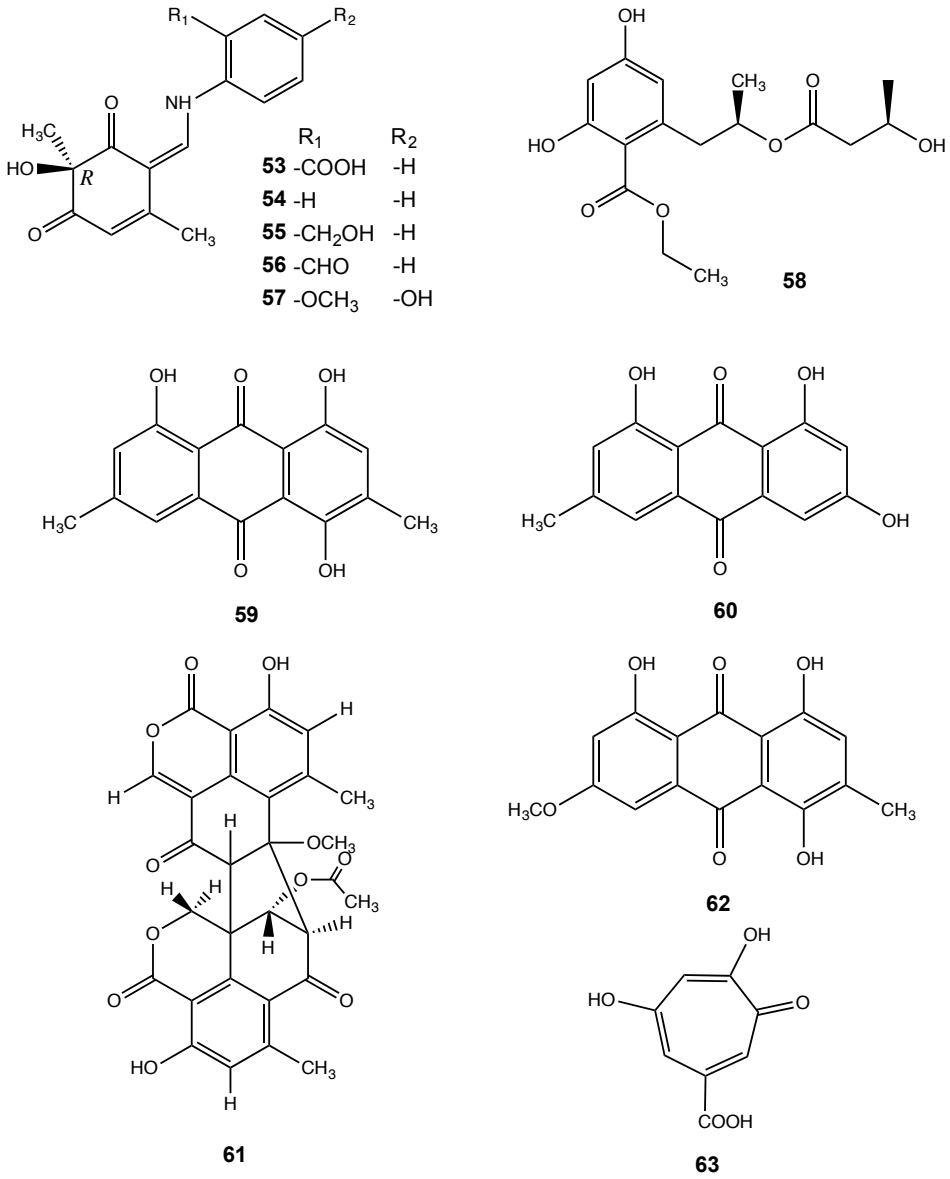

Figure 23. Structures of compounds **53**-**63**.

Two novel oxaphenalenone dimers, talaroketals A (**64**) and B (**65**) were isolated from the soil fungus *T. stipitatus.* These two compounds present moderately antimicrobial activity against *Staphylococcus aureus* (Zang *et al.*, 2016).

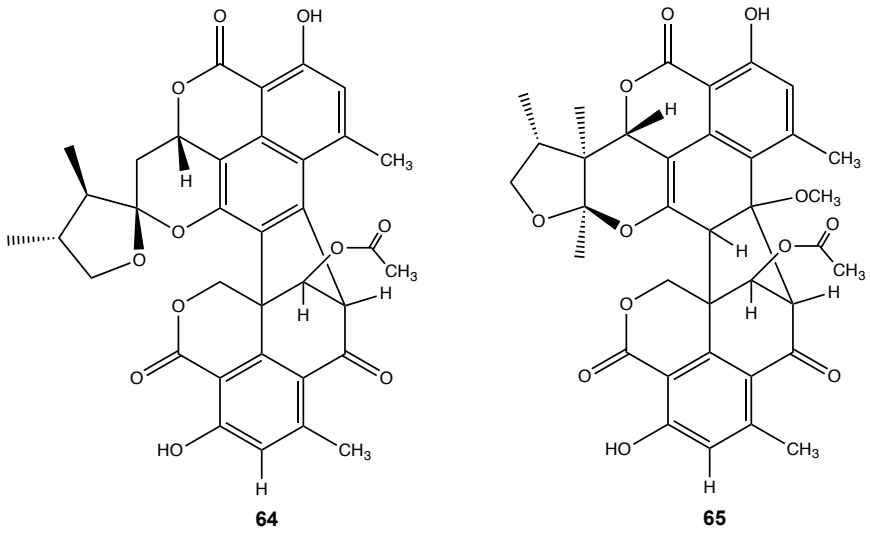

Figure 24. Structures of talaroketals A (**64**) and B (**65**).

Phillips *et al.* (1987) discovered four new spiroketal talaromycins, talaromycins C (**68**), D (**69**), E (**70**) and F (**71**) from *T. stipitatus*. This fungus produces mycotoxins such as duclauxin (**61**), botryodiplodin (**72**) and talaromycins A (**66**) and B (**67**) (Hashimoto *et al.*, 2015; Lynn *et al.*, 1982). Moulé *et al.* (1981) reported the inhibition of cell multiplication in growing cultures of mammal cells by botryodiplodin (**72**) without any toxic effect.

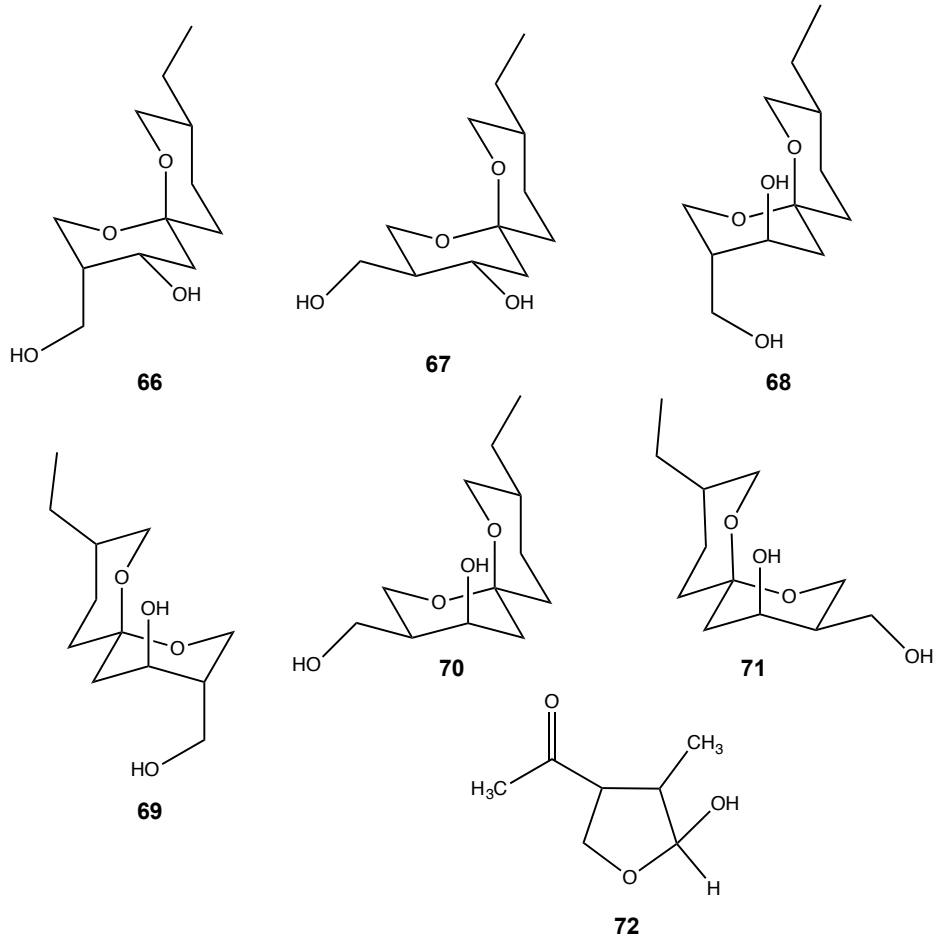

Figure 25. Structures of talaromycins A-F (**66**-**71**) and botryodiplodin (**72**).

2.5. *Talaromyces trachyspermus*

Frisvad *et al.* (1990) have identified the presence of spiculisporic acid (**73**) from the culture of *Talaromyces trachyspermus*, and later on, Kuml *et al.* (2014) isolated a new analog of spiculisporic acid, spiculisporic acid E (**74**) in addition to 3-acetyl ergosterol 5,8-endoperoxide (**75**) from the culture of the marine-sponge associated fungus *T. trachyspermus* (KUFA 0021). Trachyspic acid (**76**) was isolated from the culture broth of *T. trachyspermus* (SANK 12191). Compound **76** is also a new metabolite which inhibited the enzyme heparanase with IC_{50} value 36 μM (Shiozawa *et al.*, 1995).

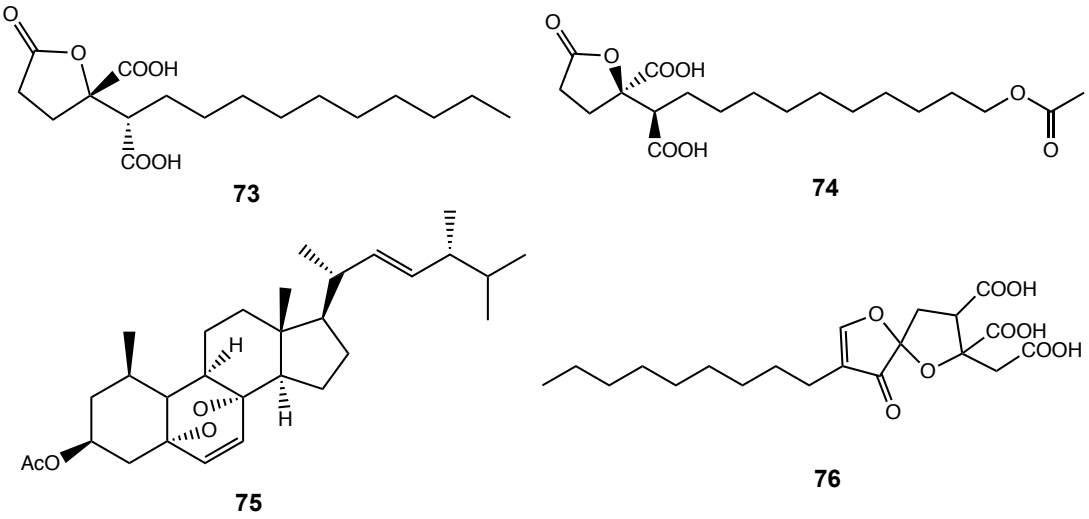

Figure 26. Structures of spiculisporic acid (**73**), spiculisporic acid E (**74**), 3-acetyl ergosterol 5,8-endoperoxide (**75**) and trachyspic acid (**76**).

2.6. *Talaromyces wortmannii*

The secondary metabolites from *Talaromyces wortmannii* comprised of diverse structural type compounds, including peptides, esters, polyketides, steroids and quinones. Two new cyclic peptides, talaromins A (**77**) and B (**78**) were isolated from the endophytic fungus *T. wortmannii* which derived from *Aloe vera*. Both cyclopeptides (**77** and **78**) showed neither cytotoxicity against L5178Y mouse lymphoma cells using the MTT assay nor antibacterial activity against a broad spectrum of bacterial strains up to a concentration at 64 µg/mL (Bara *et al.*, 2013b). A macrolide lactone antibiotic, namely, vermiculine (**79**) had been found in a crystalline form in agar and liquid media cultures of *T. wortmannii* by Jones *et al.* (1984). The fungus *T. wortmannii*, isolated from a soil sample collected in China's Yunnan province, furnished four novel macrolides, wortmannilactones A-D (**80-83**). These compounds exhibited *in vitro* cytotoxicity against several human cancer cell lines with IC_{50} values from 28.7 to 130.5 µM (Dong *et al.*, 2006).

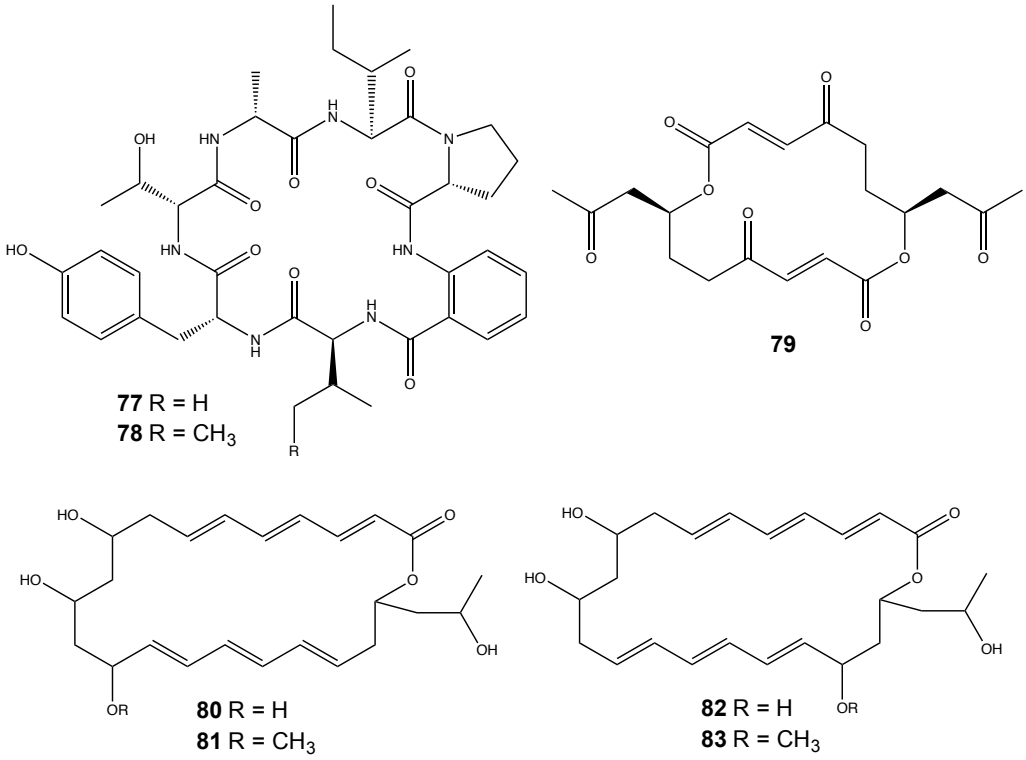

Figure 27. Structure of compounds **77-83**.

Another four new lactones, wortmannilactones E-H (**84-87**), were isolated from the culture of the soil filamentous fungus *T. wortmannii.* These compounds exhibited inhibitory activity against cathepsin B with IC_{50} values of 4.3, 6.5, 13.0 and 6.0 μM, respectively (Dong *et al.*, 2009).

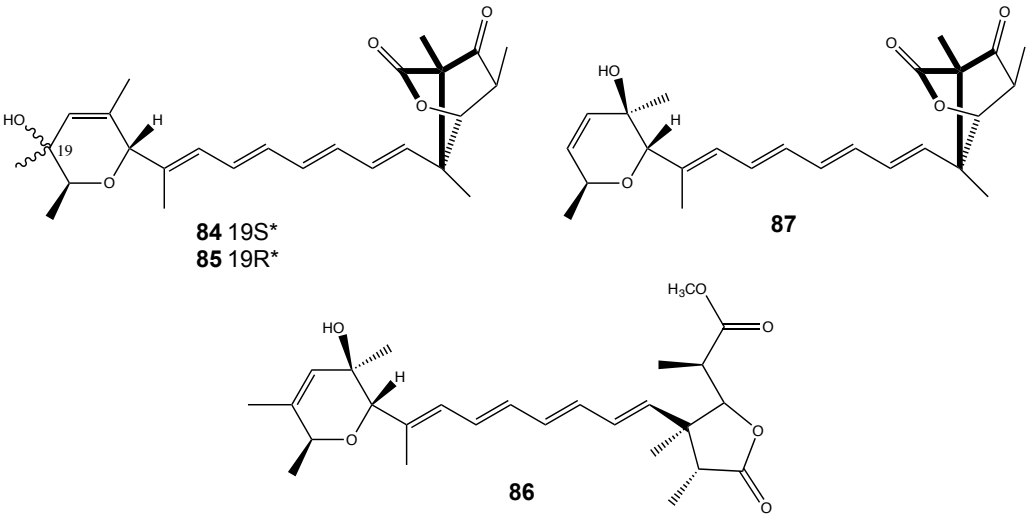

Figure 28. Structures of wortmannilactones E-H (**84-87**).

Ding *et al.* (2015a) reported isolation of secovironolide (**88**), wortmannin (**89**), 11-desacetoxywortmannin-17β-ol (**90**), 11-desacetoxywortmannin (**91**), wortmannolone (**92**),

epoxyvirone (**93**), wortmannin B (**94**), 3-dihydrovirone (**95**), wortmannin-diol (**96**), wortmin (**97**) and deacetylisowortmin (**98**) from the culture broth of endophytic fungus *T. wortmannii* LGT-4, which was isolated from the Chinese medicinal plant *Tripterygium wilfordii*. However, only compound **88** and **89** showed weak MAO inhibition with IC_{50} of 91.22 and 40.17 µg/mL, respectively (Bara *et al.*, 2013a; Ding *et al.*, 2015a).

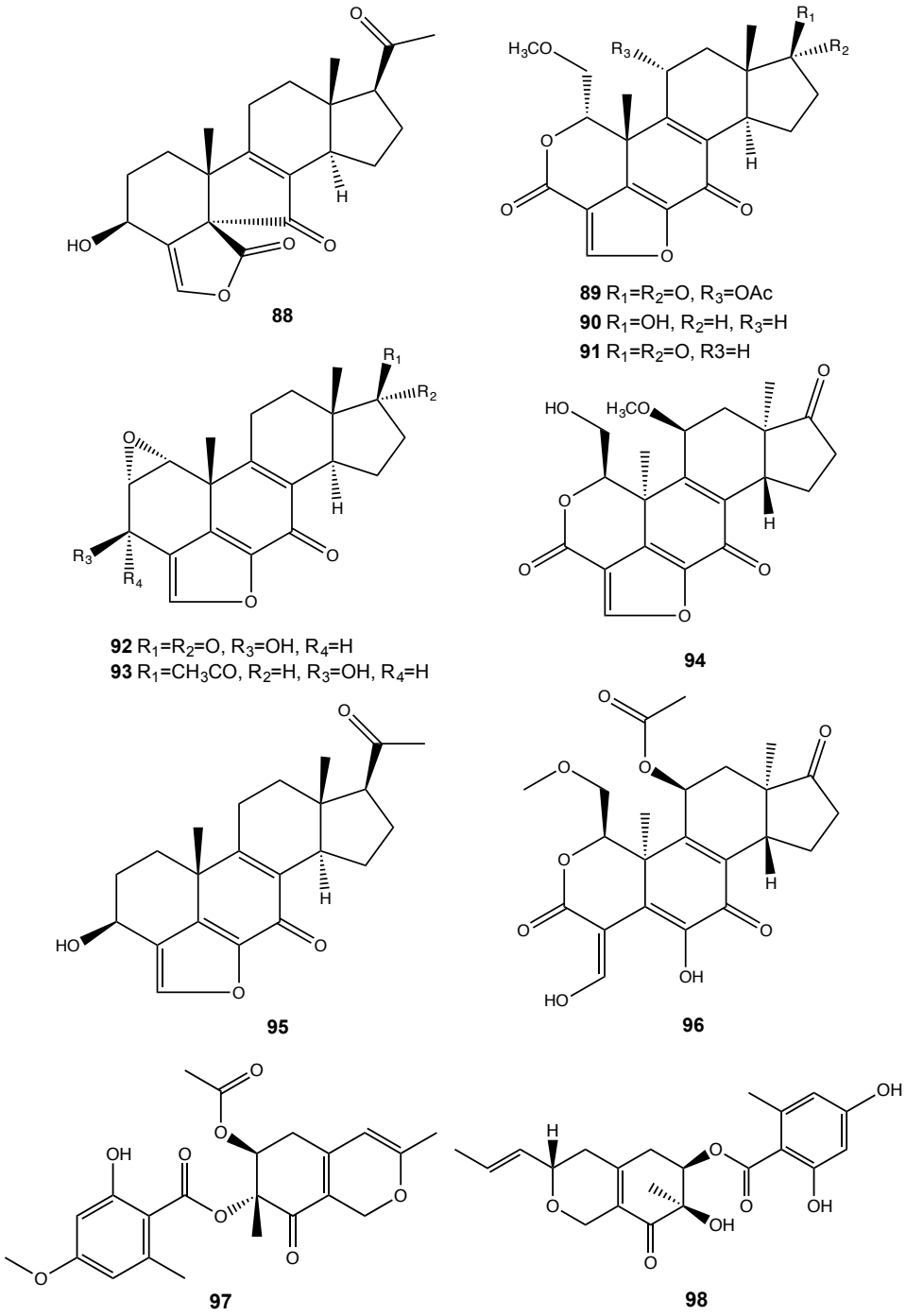

Figure 29. Structures of compounds **88-98**.

Talaromyces wortmannii which was obtained from a healthy tissue of *Aloe vera* collected in Alexandria, Egypt, provides a number of quinone pigments such as biemodin (**99**), emodic acid (**100**), skyrin (**101**), oxyskyrin (**102**), rugulosins A (**103**) and B (**104**). Skyrin (**101**) and rugulosin A (**103**) exhibited antibiotic activity against Gram positive pathogenic bacteria, especially against Methicillin-resistant *Staphylococcus aureus* (MRSA) with MIC values between 4 and 6 µg/mL. Biemodin (**99**) also showed strong antibiotic activity against Gram positive bacteria but less than skyrin (**101**) and rugulosin A (**103**) (Bara *et al.*, 2013a).

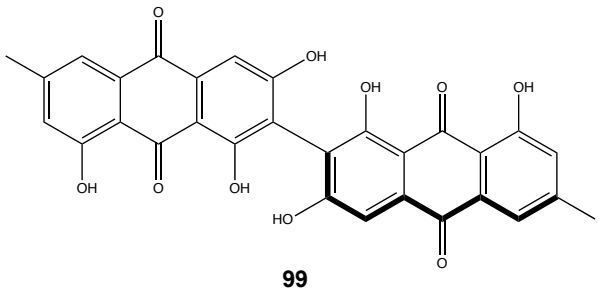

99

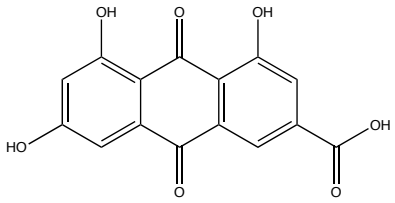

100

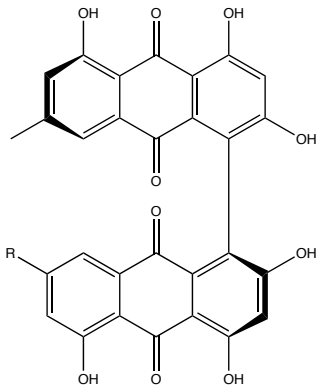

101 R = CH_3
102 R = CH_2OH

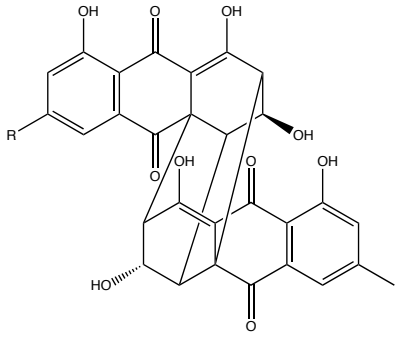

103 R = CH_3
104 R = CH_2OH

Figure 30. Structures of biemodin (**99**), emodic acid (**100**), skyrin (**101**), oxyskyrin (**102**), regulosin A (**103**) and B (**104**).

Two bisdihydroanthracenone atropodiastereomeric pairs: homodimeric flavomannins A (**105**) and B (**106**), two unsymmetrical dimers **107** and **108**, and two mixed dihydroanthraquinone dimers **109** and **110** were isolated from the endophytic fungus *T. wortmannii.* All the compounds showed antibacterial activity against *Staphylococcus aureus*, including (multi) drug-resistant clinical isolates, however they did not exhibit any cytotoxic activity (Bara *et al.*, 2013c).

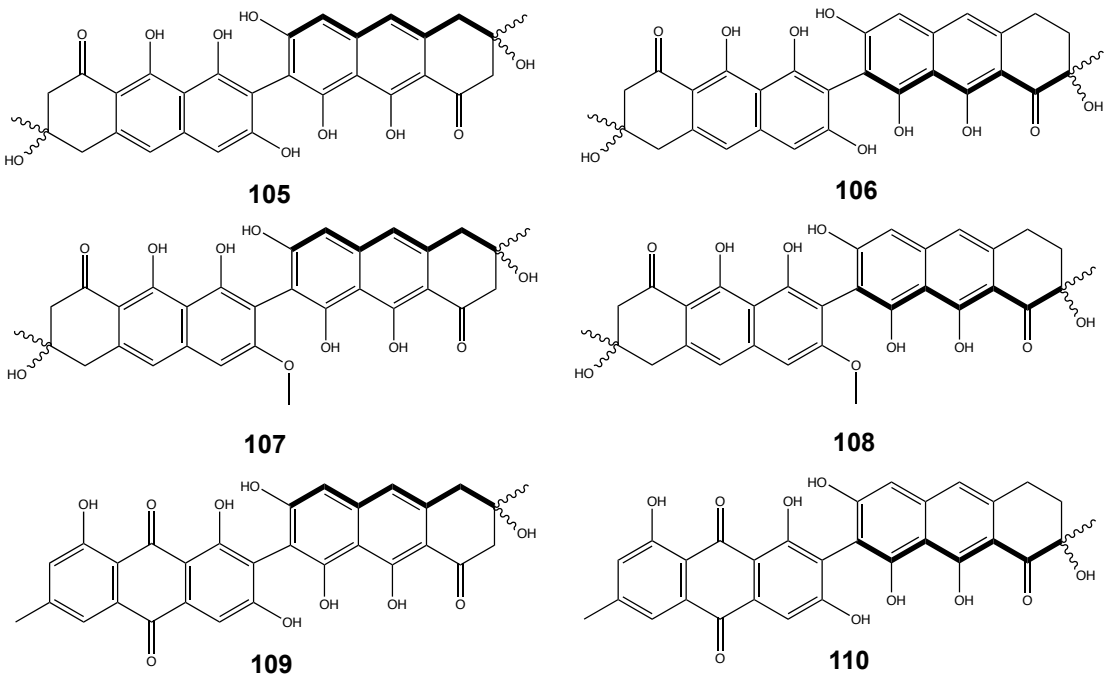

Figure 31. Structures of bisdihydroanthraquinones **105**-**110**.

A recent review by Zhai *et al.* (2016) showed that diverse types of compounds, including polyester, macrolide, benzopyrone, terpenoid, amine, anthraquinone, peptide, steroid, azaphilone, oxaphenalenone, spiroketal and others were isolated from the fungi of the genus *Talaromyces* section *Talaromyces*. Interestingly, the most common bioactivities of the secondary metabolites of these fungi are cytotoxic and antibacterial activities as showed in **Table 3**.

Table 3. Summary of the structural types of the secondary metabolites and their biological activities from the genus *Talaromyces* section *Talaromyces*.

Structural Types	Species					
	T. flavus	*T. helicus*	*T. luteus*	*T. stipitatus*	*T. trachyspermus*	*T. wortmannii*
Polyester	C (11 – 17)			(58)		
Lactone	(23, 25, 26)					C (80 – 87)
Benzopyrone	AI (19, 20)					
Terpeniod	B (34), C (34, 36, 39), F (34)					
Amine				M (56)		
Anthraquinone				(59, 60, 62)		B (99, 101, 103 – 110)
Peptide						(77, 78)
Steroid					(75)	P (88, 89)
Azaphilone	C (33)	P (44 – 47)	P (48, 49)			
Funicone	F (29, 30)					
Oxaphenalenone				B (64, 65)		
Spiroketal				(66 – 71)		
Others	B (43) F (29, 30) HIV (41)			C (72)	C (76)	

AI: immunotherapy for Alzheimer's disease; **B**: antibacterial activity; **C**: cytotoxic activity; **F**: antifungal activity; **HIV**: HIV-1 integrase inhibition; **M**: antimalarial; **P**: monoamine oxidase inhibition (treatment of Parkinson's disease) and **numbers in the parenthesis**: represent numbers of the compounds described in chapter 2.

CHAPTER 3

3. Materials and Methods

3.1. Materials

3.1.1. Isolation and Purification of Secondary Metabolites from the Fungal Crude Extracts

- Distilled water
- Erlenmeyer flask size 250, 500, 1,000 mL.
- Separating funnel
- Filtrate pump
- Paper filtrate Whatman No. 1
- Laboratory mortar and pestle
- Microcapillary pipettes, calibrated size 10 µL.
- TLC aluminium sheets 20 x 20 cm silica gel 60 GF_{254}, Merck
- Silica gel 60 GF_{254} (0.2-0.5 mm), Merck for column chromatography
- Silica gel 60 GF_{254}, Merck for thin layer chromatography
- Sephadex LH-20 for column chromatography
- 20 x 20 glass plates
- Tank chamber
- Sea sand
- Cotton
- Vials, 4 drams
- Hot plate
- UV detector (254 nm and 365 nm)
- Column chromatography
- Rotary evaporator (Buchi)
- Petroleum ether (Petrol)
- Chloroform ($CHCl_3$)
- Acetone (Me_2CO)
- Methanol (CH_3OH)
- Ethyl acetate (EtOAc)
- Formic acid (HCO_2H)

3.1.2. Structure Elucidation of Secondary Metabolites

- Proton Nuclear Magnetic Resonance (^{1}H NMR)
- Carbon-13 Nuclear Magnetic Resonance (^{13}C NMR)
- Heteronuclear Single Quantum Coherence (HSQC)
- Correlation Spectroscopy (COSY)
- Heteronuclear Multiple Bond Correlation (HMBC)
- High Resolution Mass Spectrometry (HRMS)
- Bock monoscope
- ADP410 Polarimeter
- FTIR spectrometer Nocolet iS10
- Varian CARY 100 spectrophotometer
- Bruker AMC instrument
- Waters Xevo QToF mass spectrometer
- Waters Aquity UPLC system

3.2. Methods

3.2.1. General Experimental Procedures

A Merck (Darmstadt, Germany) silica GF_{254} was used for preparative TLC, a Merck Si gel 60 (0.2-0.5 mm), LiChroPrep Si 60 (0.04-0.063) and Sephadex LH-20 were used for column chromatography.

^{1}H and ^{13}C NMR spectra were taken in $CDCl_3$ or DMSO-d_6 and were recorded at ambient temperature on a Bruker AMC instrument (Bruker Biosciences Corporation, Billerica, MA, USA) operating at 300.13 and 75.4 MHz or 500.13 and 125.4 MHz, respectively.

The solvents were evaporated at reduced pressure, using Büchi heating bath B-49, rotavapor R-210, vacuum module V-801 EasyVac and vacuum pump V-700.

High resolution mass spectra were measured with a Waters Xevo QToF mass spectrometer (Waters Corporations, Milford, MA, USA) coupled to a Waters Aquity UPLC system.

Optical rotations were measured on a ADP410 Polarimeter (Bellingham + Stanley Ltd., Tunbridge Wells, Kent, UK).

Melting points were determined on a Bock monoscope and are uncorrected.

Infrared spectra were recorded in a KBr microplate in a FTIR spectrometer Nicolet iS10 from Thermo Scientific (Waltham, MA, USA) with Smart OMNI-Transmission accessory (Software 188 OMNIC 8.3).

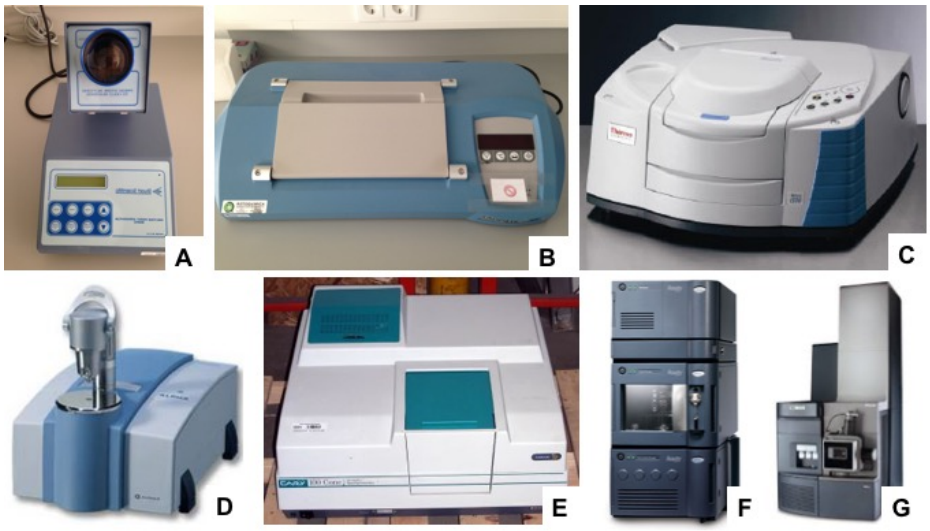

Figure 32. Equipment in the experimental, **A**. Bock monoscope; **B**. ADP410 Polarimeter; **C**. FTIR spectrometer; **D**. Bruker AMC instrument; **E**. Varian CARY 100 spectrophotometer; **F**. Waters Aquity UPLC system; **G**. Waters Xevo QToF mass spectrometer. [Adapted from http://www.selectscience.net/products/alpha-ftir-spectrometer/?prodID=80550; http://www.labequip.com/cary-100-cone-series-ii-uvvisible-scanning-spectrophotometer.html; http://www.businesswire.com/news/home/20140616005646/en/Waters-Introduces-Xevo-G2-XS-QTof-Xevo-TQ-S].

3.2.2. Fungal Material

The strain KUFA 0207 was isolated from the marine sponge *Stylissa flabelliformis* which was collected, by scuba diving at a depth of 10-15 m, from the coral reef at Samaesarn Island (12°34' 36.64" N 100°56' 59.69" E) in the Gulf of Thailand, Chonburi Province, in April 2014. The sponge was washed with 1% sodium hypochlorite solution for 1 min, followed by sterilized seawater 3 times, and then dried on sterile filter paper under a laminar flow hood, cut into small pieces (5 x 5 mm), and placed on a malt extract agar (MEA) plates containing 70% seawater and 300 mg/L of streptomycin sulfate. The plates were incubated at 28°C for 7 days, after which the hyphal tips were transferred onto a slant MEA and maintained as pure culture for further identification. The fungus was identified as *Talaromyces stipitatus* C.R. Benj., based on morphological characteristics, and was also confirmed by analysis sequence of the internal transcribed spacer (ITS) gene according the

procedure previously described (Zin *et al.*, 2015). Its gene sequences were deposited in GenBank with accession number KU500028. The pure cultures were deposited as KUFA 0207 at Kasetsart University Fungal Collection, Department of Plant Pathology, Faculty of Agriculture, Kasetsart Unversity, Bangkok, Thailand. The fungus was cultured for one week at 28°C in 10 Petri dishes (i.d. 90 mm) containing 25 mL of MEA. In order to obtain the mycelial suspension, the mycelial plugs were transferred to two 500 mL Erlenmeyer flasks containing 200 mL of potato dextrose broth, and then incubated on a rotary shaker at 120 rpm at 28°C for one week. Fifty 1000 mL Erlenmeyer flasks, each containing 300 g of cooked rice, were autoclaved at 121°C for 15 min, and then incubated with 20 mL of mycelial suspension of *T. stipitatus* and incubated at 28°C for 30 days, after which the moldy rice was macerated in ethyl acetate for 7 days, and then filtrated. The ethyl acetate solution was concentrated under reduced pressure to yield 65.5 g of crude ethyl acetate extract.

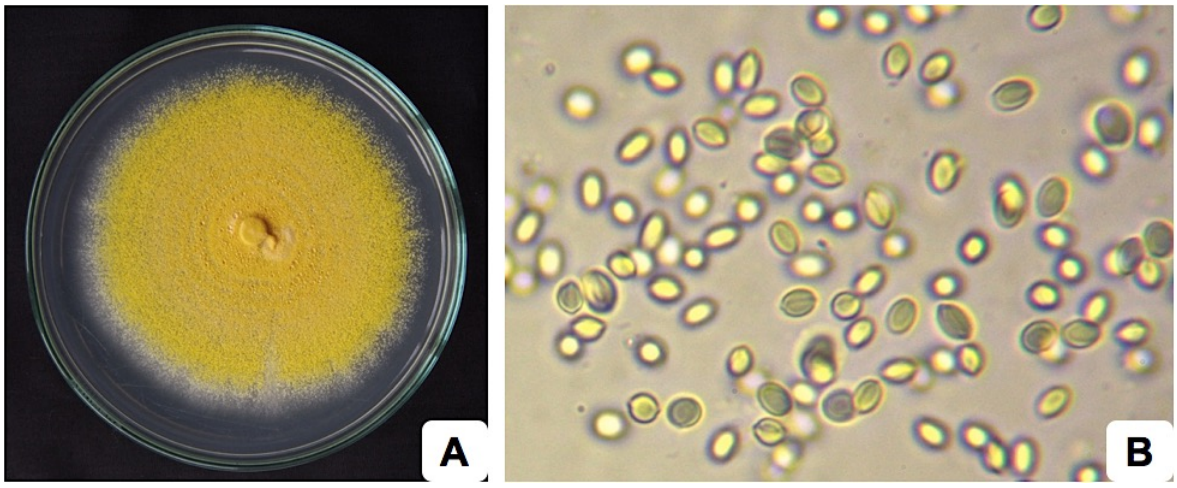

Figure 33. Colony of *Talaromyces stipitatus* C.R. Benj. (KUFA 0207) on male extract agar, 14 days, 28°C (**A**), SEM of ascospores (**B**).

3.2.2. Isolation, Purification of the Secondary Metabolites

The crude ethyl acetate (35 g) was applied on a column chromatography of silica gel (335 g) and eluted with mixtures of petrol-$CHCl_3$, $CHCl_3$-Me_2CO, Me_2CO and Methanol, 250 mL fractions were collected as follow: Frs 1-133 (petrol-$CHCl_3$, 1:1), 134-249 (petrol: $CHCl_3$, 3:7), 250-314 (petrol-$CHCl_3$, 1:9), 315-440 ($CHCl_3$-Me_2CO, 9:1), 441-511 ($CHCl_3$-Me_2CO, 7:3), 512-546 ($CHCl_3$-Me_2CO, 1:1). Frs 156-170 were combined (382.7 mg) and crystallized in methanol to give **palmitic acid** (**I**) (20 mg). Frs 171-182 were combined (370 mg) and purified by TLC (silica gel G_{254}, $CHCl_3$-petrol-EtOAc-HCO_2H, 16:3:1:0.1) to give

compound **talarosterone** (**V**) (10.5 mg), **palmitic acid** (**I**) (21.7 mg) and **ergosta-4,6,8(14),22-tetraen-3-one** (**III**) (23.3 mg). Frs 220-250 were combined (201.5 mg) and crystallized in MeOH to give **ergosta-4,6,8(14),22-tetraen-3-one** (**III**) (10.6 mg). Frs 315-317 were combined (4.53 g) and applied over a column chromatography of silica gel (35 g) and eluted with mixture of petrol- $CHCl_3$ and $CHCl_3$-Me_2CO, wherein 250 mL fractions were collected as follows: sfrs 1-101 (petrol- $CHCl_3$, 1:1), 102-170 (petrol: $CHCl_3$, 3:7), 171-296 (petrol-$CHCl_3$, 1:9), 297-311 ($CHCl_3$-Me_2CO, 9:1). Sfrs 19-38 were combined (329 mg) and applied over a column chromatography of Sephadex LH-20 (10 g) and eluted with a 1:1 mixture of $CHCl_3$: MeOH, to give forty 15 mL ssfrs. Ssfrs 8-37 were combined and purified by TLC (silica gel G_{254}, $CHCl_3$-petrol-EtOAc-HCO_2H, 80:16.5:3.5:0.1) to give **cyathisterone** (**IV**) (12.2 mg). Sfrs 229-296 were combined (179 mg) and purified by TLC (silica gel G_{254}, $CHCl_3$-petrol-EtOAc-HCO_2H, 80:15:5:0.1) to give **emodin** (**VI**) (10 mg). Frs 318-330 were combined (3.77 g) and applied over a column chromatography of silica gel (100 g) and eluted with mixture of petrol-$CHCl_3$ and $CHCl_3$-Me_2OH, wherein 100 mL fractions were collected as follows: sfrs 1-118 (petrol-$CHCl_3$, 1:1), 199-277 (petrol-$CHCl_3$, 3:7), 278-289 (petrol-$CHCl_3$, 1:9), 290-471 ($CHCl_3$), 472-589 ($CHCl_3$-Me_2CO, 9:1), 590-633 ($CHCl_3$-Me_2CO, 7:3). Sfrs 238-395 were combined (473.7 mg) and crystallized in a mixture of $CHCl_3$ and petrol to give **ergosterol-5,8-endoperoxide** (**II**) (22 mg). Sfrs 477 (146.2 mg) was crystallized in a mixture of $CHCl_3$ and petrol to give a reddish orange solid of **2, 2'-*bis*-(7-methyl-1,4,5-trihydroxy-anthracene-9,10-dione)** (**XII**) (9 mg). Sfrs 510-524 were combined (53 mg) and crystallized in $CHCl_3$ to give yellow solid of **fallacinol** (**IX**) (21 mg). Frs 332-345 were combined (60.0 mg) and crystallized in a mixture of $CHCl_3$ and MeOH to give 15.2 mg of **secalonic acid A** (**XI**). Frs 355-365 were combined (103.0 mg) and crystallized in a mixture of $CHCl_3$ and MeOH to additional 10.5 mg of **secalonic acid A** (**XI**) whereas the mother liquor was further purified by TLC (silica gel G_{254}, $CHCl_3$-Me_2CO-HCO_2H, 4:1:0.01) to give 8.5 mg of **citreorosein** (**VIII**). Frs 392-440 were combined (316 mg) and crystallized in Me_2CO to give **questinol** (**VII**) (10.7 mg). Frs 443-450 were combined and crystallized in Me_2CO to give **rheoemodin** (**X**) (6 mg).

3.2.3. Physical Characteristics and Spectroscopic Data

Palmitic acid (I): white solid; mp. 60-63°C; For ^1H and ^{13}C NMR spectra (DMSO, 500.13 and 125.4 MHz), see **Table 4**; (+)-HRESIMS *m/z* 257.2484 $(M+H)^+$, (calcd for $C_{16}H_{33}O_2$, 257.2481).

Ergosterol-5,8-endoperoxide (II); colorless crystal; mp. 180-182°C; For ^{1}H and ^{13}C NMR spectra (DMSO, 300.13 and 75.4 MHz) see **Table 5.**

Ergosta-4, 6, 8(14), 22-tetraen-3-one (III): white crystal; mp. 108-111°C; For ^{1}H and ^{13}C NMR spectra ($CDCl_3$, 300.13 and 75.4 MHz), see **Table 6**.

Cyathisterone (IV): white crystal; mp. 200-202°C; $[\alpha]^{23}_{D}$ +200 (*c* 0.03, $CHCl_3$); IR (KBr) υ_{max} 2951, 1717, 1701, 1661, 1622, 1457, 1384, 1263 cm^{-1}; For ^{1}H and ^{13}C NMR data ($CDCl_3$, 300.13 and 75.4 MHz), see **Table 7**; (+)-HRESIMS *m/z* 411.3262 $(M+H)^{+}$, (calcd for $C_{28}H_{43}O_2$, 411.3263).

Talarosterone (V): white crystal; mp. 146-148°C; $[\alpha]^{23}_{D}$ +204 (*c* 0.04, $CHCl_3$); IR (KBr) υ_{max} 2956, 2873, 1689, 1670, 1593, 1458, 1411, 1276, 1260 cm^{-1}; For ^{1}H and ^{13}C NMR data ($CDCl_3$, 300.13 and 75.4 MHz), see **Table 8**; (+)-HRESIMS *m/z* 425.3056 $(M+H)^{+}$, (calcd for $C_{28}H_{41}O_3$, 425.3056).

Emodin (VI): orange solid; mp. 105-110°C; For ^{1}H and ^{13}C NMR spectra (DMSO, 500.13 and 125.4 MHz) see **Table 9**.

Questinol (VII): orange solid; mp. 255-265°C; For ^{1}H and ^{13}C NMR spectra (DMSO, 300.13 and 75.4 MHz) see **Table 10**; (+)-HRESIMS *m/z* 301.0713 $(M+H)^{+}$, (calcd for $C_{16}H_{13}O_6$, 301.0712).

Citreorosein (VIII); yellow solid; mp. 287-289°C; For ^{1}H and ^{13}C NMR spectra (DMSO, 500.13 and 125.4 MHz) see **Table 11.**

Fallacinol (IX); yellowish orange crystal; mp. 205-208°C; For ^{1}H and ^{13}C NMR spectra (DMSO, 500.13 and 125.4 MHz) see **Table 12**; (+)-HRESIMS *m/z* 301.0705 $(M+H)^{+}$, (calcd for $C_{16}H_{13}O_6$, 301.0712).

Rheoemodin (X); brown solid; mp. 164-167°C; For ^{1}H and ^{13}C NMR spectra (DMSO, 300.13 and 75.4 MHz) see **Table 13.**

Secalonic acid A (XI); yellow crystal; mp. 268-270°C; For ^{1}H and ^{13}C NMR spectra (DMSO, 300.13 and 75.4 MHz) see **Table 14**; (+)-HRESIMS *m/z* 639.1733 $(M+H)^{+}$, (calcd for $C_{32}H_{31}O_{14}$, 639.1714).

***Bis*-(7-methyl-1,4,5-trihydroxy-9,10-anthraquinone) (XII)**; reddish orange solid; mp. 258-260°C; $[\alpha]^{20}_{D}$ -100 (*c* 0.05, MeOH) and - 40 (*c* 0.05, dioxin); IR (KBr) υ_{max} 3463, 2359, 1622, 1550, 1480, 1457, 1247, 1207 cm^{-1}; For ^{1}H and ^{13}C NMR spectra (DMSO, 500.13 and 125.4 MHz) see **Table 15**; (+)-HRESIMS *m/z* 539.0942 $(M+H)^{+}$, (calcd for $C_{30}H_{19}O_{10}$, 539.0978).

3.2.4. X-ray Crystallographic Analysis of Compounds IV and V

Diffraction data were collected at 293 K with a Gemini Ultra equipped with CuKα radiation (λ = 1.54184 Å). The structures were solved by direct methods using SHELXS-97 and refined with SHELXL-97 (Sheldrick, 2008). Carbon and oxygen atoms were refined anisotropically. Hydrogen atoms were either placed at their idealized positions using appropriate HFIX instructions in SHELXL, and included in subsequent refinement cycles, or were directly found from difference Fourier maps and were refined freely with isotropic displacement parameters. Full details of the data collection and refinement and tables of atomic coordinates, bond lengths and angles, and torsion angles have been deposited with the Cambridge Crystallographic Data Centre.

Cyathisterone (**IV**). Crystals were monoclinic, space group $P2_1$, cell volume 1278.36(8) $Å^3$ and unit cell dimensions *a* = 6.6142(2) Å, *b* = 6.46731(19) Å and *c* = 29.8941(13) Å and angle *β* = 91.419(4)º (uncertainties in parentheses). The refinement converged to *R* (all data) = 6.96% and wR_2 (all data) = 14.86%. CCDC 1527349.

Talarosterone (**V**). Crystals were orthorhombic, space group $C222_1$, cell volume 5091.3(10) $Å^3$ and unit cell dimensions *a* = 8.4602(5) Å, *b* = 12.407(2) Å and *c* = 48.504(5) Å. The refinement converged to *R* (all data) = 9.72% and wR_2 (all data) = 15.83%. CCDC 1527335.

3.2.4. Anti-Obesity Assay

Compound **VI**-**XI** were dissolved in DMSO at a concentration of 5 mM and stored at -20°C until analyses. Anti-obesity activity of the compounds were analyzed with the zebrafish Nile red assay as described in Jones *et al.* (2008) with some modifications. Zebrafish adults and larvae were maintained under standard conditions at 28°C as defined in the zebrafish book available at ZFIN database (https://zfin.org/). In brief, zebrafish embryos were raised from 1 DPF (days post fertilization) in egg water (60 µg/ml marine sea salt dissolved in distilled H_2O) with 200 µM PTU (1-phenyl-2-thiourea) to inhibit pigmentation. From 3 DPF to 5 DPF, zebrafish larvae were exposed to compounds at a final concentration of 5 µM with daily renewal of water and compounds in a 24-well plate with a density of 10-12 larvae/well. A solvent control (0.1% DMSO) and positive control (REV, resveratrol, final concentration 50 µM) were included in the assay. Lipids were stained with the Nile red overnight at the final concentration of 10 ng/ml. For imaging, the larvae were anaesthetized with the tricaine (MS-222, 0.03%) for 5 minutes and fluorescence analyzed with a fluorescence microscope (Leica DM6000B, Wetzlar, Germany). Fluorescence intensity was quantified in individual zebrafish larvae by ImageJ (https://imagej.nih.gov/ij/index.html).

CHAPTER 4

4. Results and Discussion

4.1. Secondary Metabolites Isolated from *Talaromyces stipitatus*

The crude ethyl acetate extract of the marine-derived fungus *Talaromyces stipitatus* (KUFA 0207) furnishes ten previously reported compounds including palmitic acid (**I**), ergosterol-5,8-endoperoxide (**II**), ergosta-4,6,8(14),22-tetraen-3-one (**III**), cyathisterone (**IV**), emodin (**VI**), questinol (**VII**), citreorosein (**VIII**), fallacinol (**IX**), rheoemodin (**X**), secalonic acid A (**XI**) and two previously undescribed compounds: talarosterone (**V**), and *bis*-(7-methyl-1,4,5-trihydroxy-9,10-anthraquinone) (**XII**). The structures of these compounds are showed in **Figure 34.**

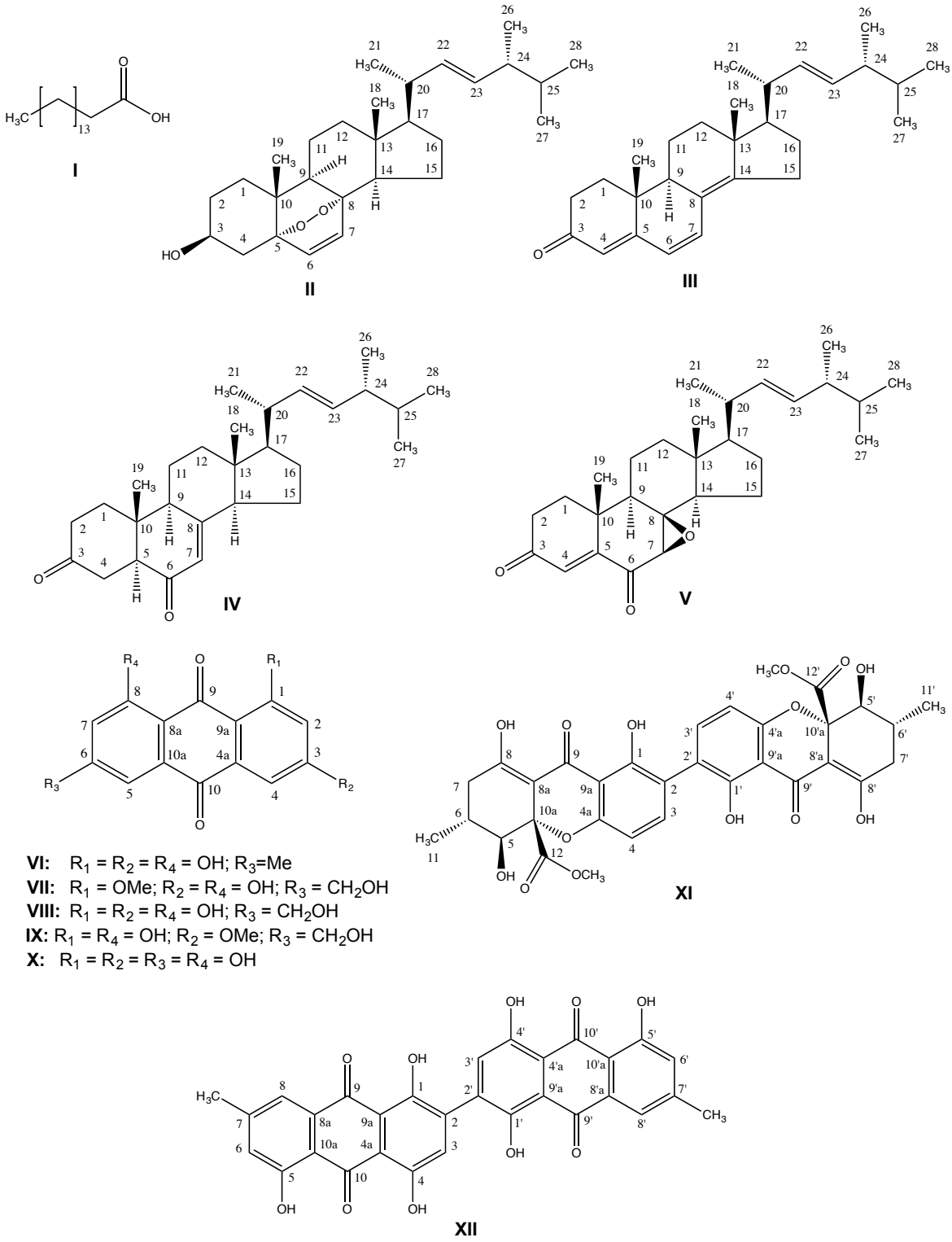

Figure 34. Secondary metabolites isolated from the marine-derived *Talaromyces stipitatus*.

4.2. Identifications and Characterization of Secondary metabolites from the culture of *Talaromyces stipitatus*

4.2.1. Structure Elucidation of Fatty Acid

4.2.1.1. Palmitic acid (I)

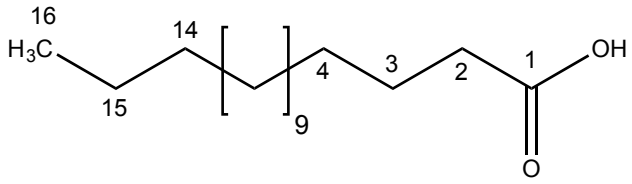

Figure 35. Structure of palmitic acid (**I**).

Compound **I** was isolated as white solid (mp.60-63°C), and its molecular formula $C_{16}H_{32}O_2$ was determined based on the (+)-HRESIMS *m/z* 257.2484 $[M+H]^+$ (calculated 257.2481), indicating one degree of unsaturation. The ^{13}C NMR spectrum (**Table 4**) exhibited, in combination with DEPT and HSQC spectra, the signals of one carboxyl carbonyl at δ_C 179.5, several methylene sp^3 at δ_C 34.0 (δ_H 2.35, t, *J* = 7.5 Hz), 31.9, 29.6, 29.4, 29.3, 29.1, 24.7 (δ_H 1.63, q, *J* = 7.2 Hz), 22.7 and a cluster of peaks centered at δ_C 29.7, as well as one terminal methyl group at δ_C 14.1 (δ_H 0.88, t, *J* = 7.0 Hz). Combination of the ^1H and ^{13}C NMR chemical shift values and multiplicities with the HRMS data revealed that compound **I** has, besides a methyl and carboxyl groups, fourteen methylene groups. Therefore, compound **I** was identified as palmitic acid which has been isolated from several fungal extracts including *Penicillium atrovenetum* (Gottlieb and Van Etten, 1964).

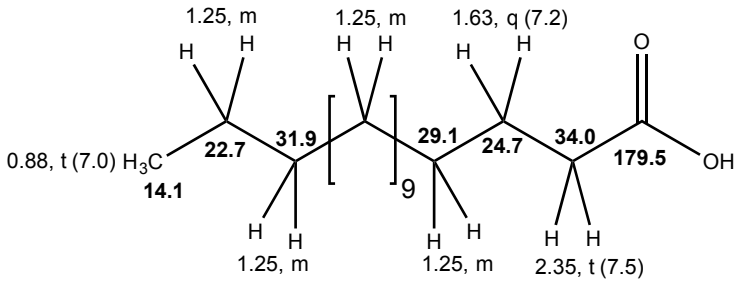

Figure 36. Structure of palmitic acid with chemical shifts.

Table 4. ^{1}H and ^{13}C NMR (DMSO, 500.13 MHz and 125.4 MHz) and HMBC assignment for palmitic acid (**I**)

Position	δ_C, type	δ_H, (*J* in Hz)	COSY	HMBC
1	179.5, CO	---	---	---
2	34.0, CH_2	2.35, t (7.5)	H_2-3	C-3,4
3	24.7, CH_2	1.63, q (7.2)	H_2-2,4	C-4
4	29.4, CH_2	1.25, m	---	---
5-13	29.69, CH_2	1.25, m	---	---
	29.66, CH_2	1.25, m	---	---
	29.65, CH_2	1.25, m	---	---
	29.6, CH_2	1.25, m	---	---
	29.37, CH_2	1.25, m	---	---
	29.3, CH_2	1.25, m	---	---
	29.1, CH_2	1.25, m	---	---
14	31.9, CH_2	1.25, m	---	---
15	22.7, CH_2	1.25, m	---	---
16	14.1, CH_3	0.88, t (7.0)	H_2-15	C-14,15
OH-1	-	7.26, s	---	---

4.2.2. Structure Elucidation of Ergosterol Derivatives

4.2.2.1. Ergosterol-5,8-endoperoxide (II)

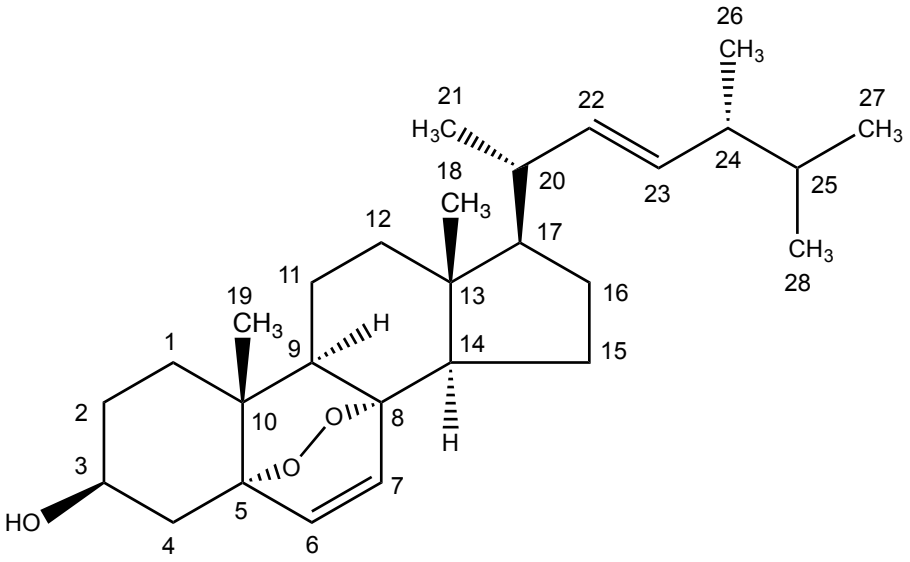

Figure 37. Structure of ergosterol-5,8-endoperoxide (**II**)

Compound **II** was isolated as colorless crystal (mp.180-182°C). The ^{13}C NMR spectrum (**Table 5**) exhibited twenty-eight carbon signals which, through DEPTs and HSQC spectra, can be categorized as four methine sp^2 (δ_C 135.4, 135.2, 132.3 and 130.7), two oxyquaternary sp^3 (δ_C 82.2, 79.4), two quaternary sp^3 (δ_C 44.6, 37.0), seven methine sp^3 (δ_C 66.5, 56.2, 51.7, 51.1, 42.8, 39.8 and 33.1), seven methylene sp^3 (δ_C 39.3, 36.9, 34.7, 30.1, 28.7, 23.4 and 20.6), four secondary methyl (δ_C 20.9, 20.0, 19.6, 17.6) and two tertiary methyl (δ_C 18.2, 12.8) groups. The ^1H NMR spectrum, in conjunction with the COSY spectrum (**Table 5**), showed a pair of doublets of a *cis* double bond at δ_H 6.51, d (*J* = 8.5 Hz; δ_C 130.7)/ δ_H 6.24, d (*J* = 8.5 Hz; δ_C 135.4), a pair of double doublets of a *trans* double bond at δ_H 5.23, dd (*J* = 15.2, 7.1 Hz; δ_C 132.3)/ 5.14, dd (*J* = 15.2, 7.9 Hz; δ_C 135.2), two methyl singlets at δ_H 0.88 (δ_C 18.2) and δ_H 0.82 (δ_C 12.8), and four methyl doublets at δ_H 1.00, d (*J* = 6.6 Hz; δ_C 20.9), δ_H 0.91, d (*J* = 6.8 Hz; δ_C 17.6), δ_H 0.82, d (*J* = 6.9 Hz; δ_C 19.6) and δ_H 0.81, d (*J* = 6.9 Hz; δ_C 20.0).

The general features of the ^1H and ^{13}C NMR spectra of **II** resembled those of ergosterol (Gao *et al.*, 2003). The presence of the (*3E*)-5,6-dimethylhept-3-en-2-yl side chain, similar to that of ergosterol, was evidenced by the COSY correlations (**Table 5**) from the double doublet at δ_H 5.23 (*J* = 15.2, 7.1, H-23; δ_C 132.3) to the multiplet at δ_H 1.85 (H-24;

δ_C 42.8), from the double doublet at δ_H 5.14 (*J* = 15.2, 7.9, H-22; δ_C 135.2) to the multiplet at δ_H 2.10 (H-20; δ_C 39.8), from the methyl doublet at δ_H 1.00 (*J* = 6.6 Hz CH_3-21; δ_C 20.9) to H-20, from the multiplet at δ_H 1.85 (H-24; δ_C 42.8) to H-23 and the methyl doublet at δ_H 0.91 (*J* = 6.8, CH_3-26; δ_C 17.6), as well as from the multiplet at δ_H 1.45 (H-25; δ_C 33.1) to the two methyl doublets at δ_H 0.82 (*J* = 6.9 Hz CH_3-27; δ_C 19.6) and δ_H 0.81 (*J* = 6.9 Hz, CH_3-28; δ_C 20.0) (**Figure 38**).

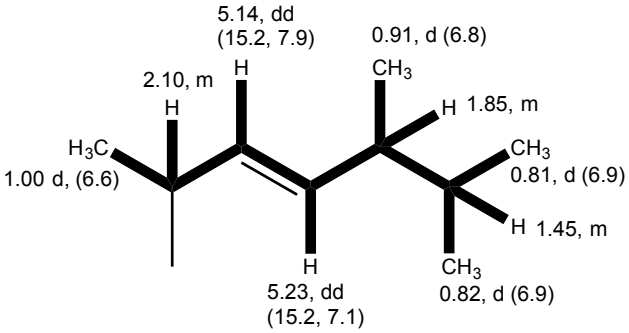

Figure 38. COSY correlations (—) of the protons of the (*3E*)-5,6-dimethylhept-3-en-2-yl side chain.

This structure was supported by the HMBC correlations from H_3-21 to C-17 (δ_C 56.2), C-20 (δ_C 39.8), C-22 (δ_C 135.2), from H-22 to C-24 (δ_C 42.8), from H-23 to C-20, from H-24 to C-22, 23 (δ_C 132.3), 25 (δ_C 31.1), 26 (δ_C 17.6), 28 (δ_C 20.0), from H_3-26 to C-23, H_3-27 to C-24, 25, 28 and from H_3-28 to C-24, 25, 27 (δ_C 19.6) (**Figure 39**).

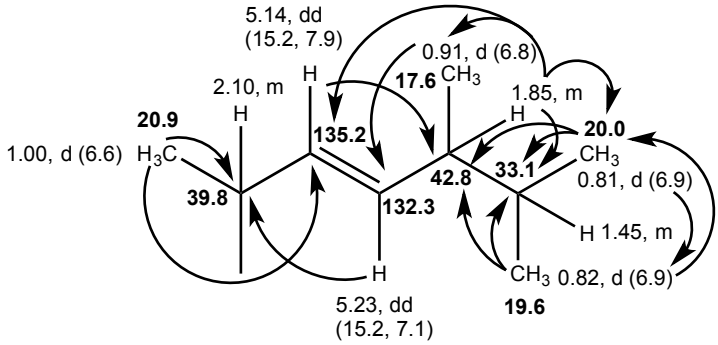

Figure 39. HMBC correlations (⟶) of the (*3E*)-5,6-dimethylhept-3-en-2-yl side chain.

The remaining 19 carbons that belong to the β-hydroxyandrostane skeleton, are similar to that of ergosterol. Since the ^{1}H and ^{13}C NMR of **II** displayed two olefinic protons of a *cis* double bond at δ_H 6.24, d (*J* = 8.5 Hz; δ_C 135.4) and δ_H 6.51, d (*J* = 8.5 Hz; δ_C 130.7), two oxygenated quaternary sp^3 carbons at δ_C 79.4 (C-8) and δ_C 82.2 (C-5) instead of two endocyclic conjugated double bonds, suggested that **II** is ergosterol-5,8-endoperoxide

(**Figure 40**). This hypothesis was supported by the HMBC correlations from H_3-19 (δ_H 0.88, s) to C-5 (δ_C 82.2) and C-10 (δ_C 37.0), H-4 (δ_H 2.11, ddd, *J* = 13.8, 5.2, 1.8 Hz; δ_C 36.9) to C-3 (δ_C 66.5) and C-5, from H-6 (δ_H 6.24, d, *J* = 8.5 Hz; δ_C 135.4) to C-5, C-7 (δ_C 130.7), C-8 (δ_C 79.4), C-10, and from H-7 (δ_H 6.51, d, *J* = 8.5 Hz; δ_C 130.7) to C-5, C-6, C-8, C-9 (δ_C 51.1) and C-14 (δ_C 51.7).

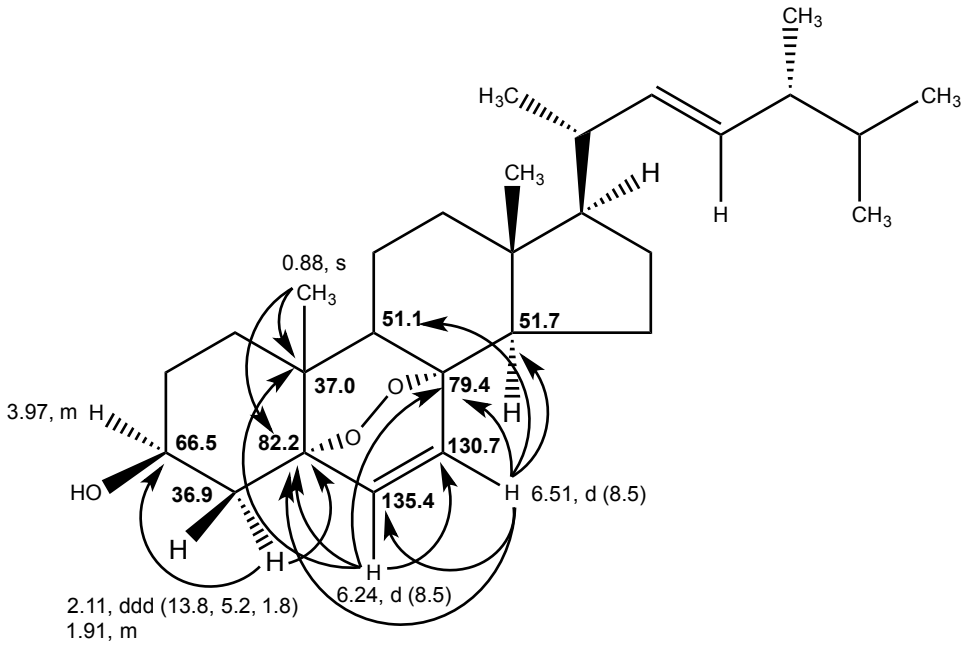

Figure 40. Key HMBC correlations (⟶) of the 3β-hydroxyandrostane.

Literature search revealed that ergosterol-5,8-endoperoxide was isolated from different parts of flowering plants such as flowers of *Erigeron annuus* L. (Kim *et al.*, 2005) and from the aerial parts of *Ajuga remota* Benth. (Cantrell *et al.*, 1999). Moreover, it has been isolated from the extract of fruiting bodies of the fungi *Armillariella mellea* (Kim *et al.*, 1999) and *Lactarius hatsudake* (Zhang *et al.*, 2007).

It is worth mentioning that the chemical shift values assigned for C-5/C-8 and C-6/C-7 of ergosterol-5,8-endoperoxide, isolated from flowers of *Erigeron annuus* L., (Kim *et al.*, 2005) were not correct. The correct assignment of the carbons and protons of ergosterol-5,8-endoperoxide, which is based on HMBC correlations, is shown in **Table 5.**

Table 5. ^{1}H and ^{13}C NMR ($CDCl_3$, 300.13 MHz and 75.4 MHz) and HMBC assignment for ergosterol-5,8-endoperoxide (**II**).

Position	δ_C, type	δ_H, mult. (*J* in Hz)	COSY	HMBC
1	39.3, CH_2	1.22, m/ 1.95, m	---	---
2	30.1, CH_2	1.53, m/ 1.83, m	H-3	---
3	66.5, CH	3.97, m	H-2, 4	---
4	36.9, CH_2	1.91, m/ 2.11, ddd (13.8, 5.2, 1.8)	H-3	C-3, 5
5	82.2, C	---	---	---
6	135.4, CH	6.24, d (8.5)	H-7	C-5, 7, 8, 10
7	130.7, CH	6.51, d (8.5)	H-6	C-5, 6, 8, 9, 14
8	79.4, C	---	---	---
9	51.1, CH	1.48, m	---	---
10	37.0, C	---	---	---
11	20.6, CH_2	1.39, m/ 1.58, m	---	---
12	34.7, CH_2	1.69, m/ 1.95, m	---	C-8, 10
13	44.6, C	---	---	---
14	51.7, CH	1.55, m	---	---
15	28.7, CH_2	1.35, m/ 1.75, m	---	---
16	23.4, CH_2	1.22, m/ 1.50, m	---	---
17	56.2, CH	1.21, m	H-20	---
18	12.8, CH_3	0.82, s	---	C-13, 14, 17, 20
19	18.2, CH_3	0.88, s	---	C-5, 10
20	39.8, CH	2.10, m	H-17, 21, 22	---
21	20.9, CH_3	1.00, d (6.6)	H-20	C-17, 20, 22
22	135.2, CH	5.14, dd (15.2, 7.9)	H-20	C-24
23	132.3, CH	5.23, dd (15.2, 7.1)	H-24	C-20
24	42.8, CH	1.85, m	H-23, 26	C-22, 23, 25, 26, 28
25	33.1, CH	1.45, m	H-27, 28	---
26	17.6, CH_3	0.91, d (6.8)	H-24	C-23
27	19.6, CH_3	0.82, d (6.9)	H-25	C-24, 25, 28
28	20.0, CH_3	0.81, d (6.9)	H-25	C-24, 25, 27

4.2.2.2. Ergosta-4,6,8(14),22-tetraen-3-one (III)

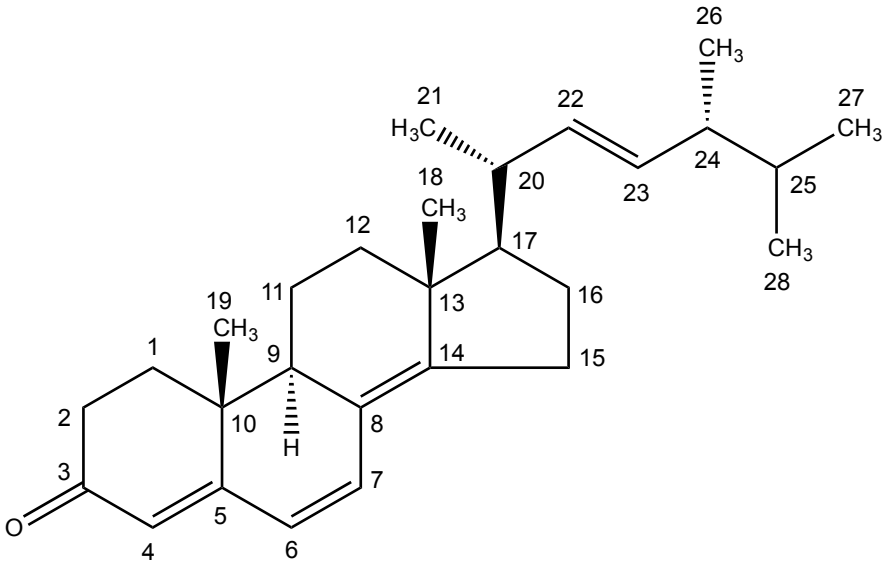

Figure 41. Structure of ergosta-4,6,8(14),22-tetraen-3-one (**III**).

Compound **III** was isolated as white crystals (mp. 108-111°C). The ^{13}C NMR spectrum (**Table 6**) exhibited the presence of 28 carbon signals which, through DEPTs and HSQC spectra, were identified as one conjugated ketone carbonyl (δ_C 199.6), three quaternary sp^2 (δ_C 164.4, 156.2 and 124.4), five methine sp^2 (δ_C 135.0, 134.0, 132.5, 124.5 and 123.0), two quaternary sp^3 (δ_C 44.0 and 36.8), five methine sp^3 (δ_C 55.7, 44.3, 42.9, 39.3 and 33.1), six methylene sp^3 [δ_C 35.6, 34.1 (2C), 27.7, 25.4 and 19.0], two tertiary methyl (δ_C 18.9 and 16.7), and four secondary methyl (δ_C 21.2, 20.0, 19.7 and 17.7) groups. The ^1H NMR spectrum (**Table 6**) showed a pair of doublets of a *cis* double bond at δ_H 6.61 (J = 9.5 Hz; δ_C 134.0)/ δ_H 6.03 (J = 9.5 Hz; δ_C 124.5), a pair of double doublets of a *trans* double bond at δ_H 5.26 (J = 15.2, 7.3 Hz; δ_C 132.5)/ δ_H 5.20 (J = 15.2, 8.1 Hz; δ_C 135.0), one singlet of a trisubstituted double bond at δ_H 5.74, s (δ_C 123.0), two methyl singlets at δ_H 1.00 (δ_C 16.7) and δ_H 0.96 (δ_C 18.9), and four methyl doublets at δ_H 1.06 (J = 6.7 Hz; δ_C 21.2), δ_H 0.93 (J = 6.8 Hz; δ_C 17.7), δ_H 0.85 (J = 6.8 Hz; δ_C 20.0) and δ_H 0.83 (J = 6.8 Hz; δ_C 19.7).

The general features of the ^1H and ^{13}C NMR spectra of compound **III** resembled those of ergosterol (Gao *et al.*, 2003). The presence of the (*3E*)-5,6-dimethylhept-3-en-2-yl side chain, similar to that of ergosterol, was evidenced by the COSY correlations from the double doublet at δ_H 5.26 (J = 15.2, 7.3 Hz, H-23) to the double doublet at δ_H 5.20 (J = 15.2, 8.1 Hz, H-22) and a multiplet at δ_H 1.85 (H-24; δ_C 42.9), from H-22 to H-23 and a multiplet at δ_H 2.13 (H-20; δ_C 39.3), from the methyl doublet at δ_H 1.06 (J = 6.7 Hz, CH_3-21; δ_C 21.2)

to H-20, from the methyl doublet at δ_H 0.93 (*J* = 6.8 Hz, CH_3-26; δ_C 17.7) to H-24, as well as from the doublets at δ_H 0.85 (*J* = 6.8 Hz, CH_3-27; δ_C 20.0) and δ_H 0.83 (*J* = 6.8 Hz, CH_3-28; δ_C 19.7) to the multiplet at δ_H 1.48 (H-25; δ_C 33.1) (**Figure 42.**).

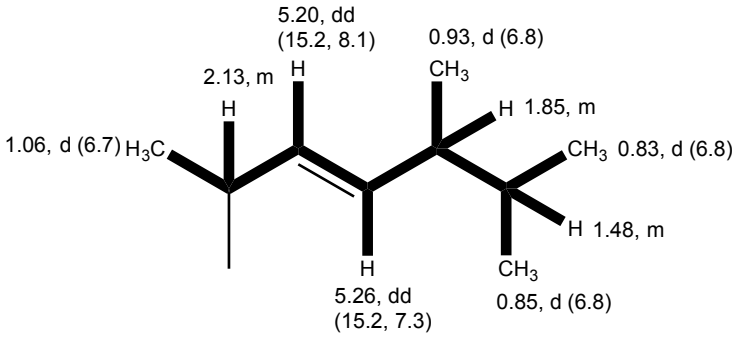

Figure 42. COSY correlations (—) of the protons of the (*3E*)-5,6-dimethylhept-3-en-2-yl side chain.

This was supported by the HMBC correlations from H_3-21 to C-20 and C-22, from H-22 to C-21, 23, 24, from H-23 to C-20, 22, 24, from H_3-26 to C-23, 24, 25, from H_3-27 to C-24, 25, 28 and from H_3-28 to C-24, 25, 27 (**Figure 43.**).

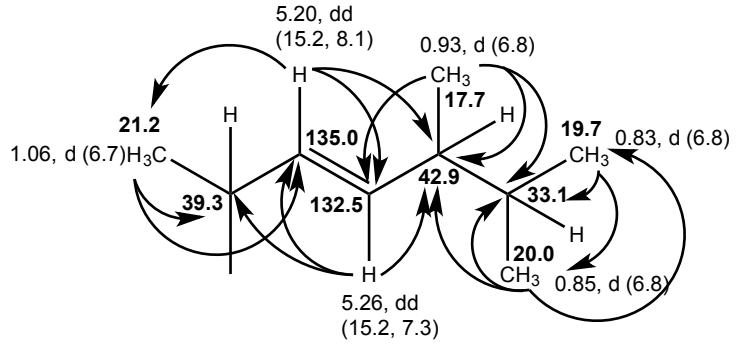

Figure 43. Key HMBC correlations (⟶) for the (*3E*)-5,6-dimethylhept-3-en-2-yl side chain of **III.**

Taking into account the presence of the *trans* double bond and four secondary methyl groups in the side chain, the *cis* double bond, the trisubstituted double bond and the two tertiary methyl groups have to be located in the cyclopentanoperhydrophenanthrene nucleus of compound **III**.

Since the HMBC spectrum exhibited correlations from both H_3-21 and the tertiary methyl singlet at δ_H 0.96 (δ_C 18.9) to the methine sp^3 carbon at δ_c 55.7, the singlet at δ_H 0.96 (δ_C 18.9) and the methine sp^3 carbon at δ_c 55.7 were assigned to CH_3-18 and CH-17,

respectively. Therefore, another tertiary methyl singlet (δ_H 1.00/ δ_C 16.7) was assigned to CH_3-19. The fact that both H_3-19 and the singlet at δ_H 5.74 (δ_C 123.0) exhibited cross peaks to the quaternary sp^3 carbon at δ_C 36.8, while the H_3-19 also showed HMBC cross peak to the quaternary sp^2 carbon at δ_C 164.4 (C-5), the trisubstituted double bond was placed between C-4 and C-5. Therefore, the singlet at δ_H 5.74 was assigned to H-4, whereas the carbons at δ_C 36.8, δ_C 123.0 and δ_C 164.4 were assigned to C-10, C-4 and C-5, respectively. Moreover, the HMBC spectrum (**Table 6**) also exhibited correlations from the proton of the *cis* double bond at δ_H 6.03 d (J = 9.5 Hz; δ_C 124.5) to C-10, C-4, C-5 and the quaternary sp^2 carbon at δ_C 124.4 as well as from another proton of the *cis* double bond at δ_H 6.61 d (J = 9.5 Hz; δ_C 134.0) to C-5, the quaternary sp^2 carbon at δ_C 156.2 (C-14) and methine sp^3 carbon at δ_C 44.3 (C-9). Therefore, the *cis* double bond was placed between C-6 (δ_C 124.5) and C-7 (134.0), while the tetrasubstituted double bond was located between C-8 (δ_C 124.4) and C-14 (δ_C 156.2). This was supported also by the HMBC correlations from H_3-19 to C-9 and from H_3-18 to C-14.

Taking into account the number of carbon atoms, the ^1H and ^{13}C chemical shift values and the COSY and HMBC correlations, the structure of compound **III** was identified as ergosta-4,6,8(14), 22-tetraen-3-one. Ergosta-4,6,8(14), 22-tetraen-3-one has been isolated from several fungi including *Polyporus umbellatus,* an edible species of a mushroom, which is a widely used as anti-aldosteronic diuretic in Traditional Chinese Medicine (Zhao *et al.*, 2009). This compound was also reported from the marine sponge associated fungus *Talaromyces trachyspermus* from the Gulf of Thailand (Kuml *et al.*, 2014) as well as from the marine sponge *Dysidea herbacea* which was collected from the Lakshadweep Islands, Indian Ocean (Kobayashi *et al.*, 1992).

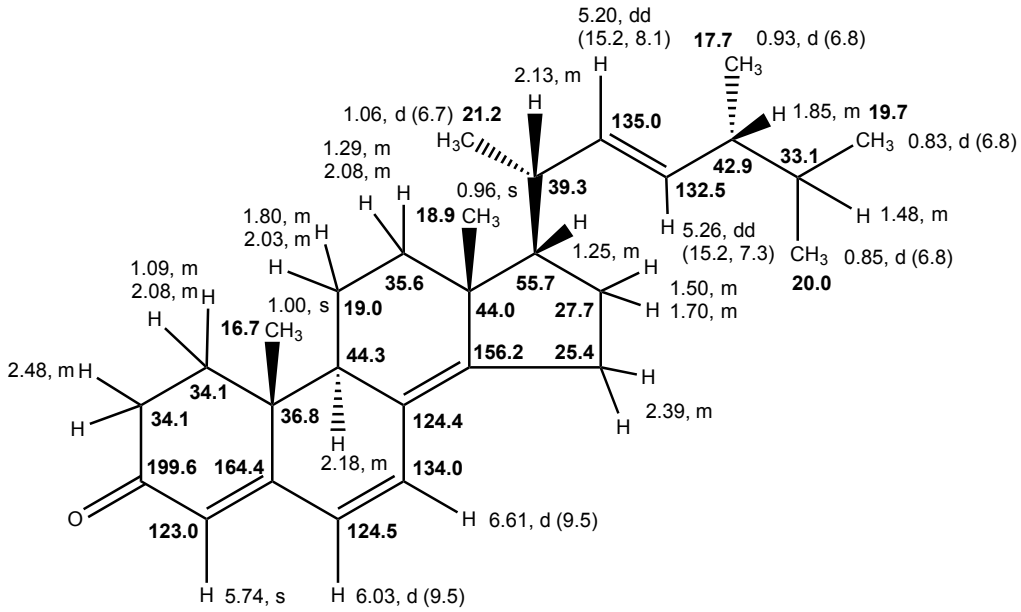

Figure 44. ^{1}H and ^{13}C assignments for **III**.

Table 6. ^{1}H and ^{13}C NMR ($CDCl_3$, 300.13 MHz and 75.4 MHz) and HMBC assignment for ergosta-4,6,8(14), 22-tetraen-3-one (**III**).

Position	δ_C, type	δ_H, mult. (*J* in Hz)	COSY	HMBC
1	34.1, CH_2	1.09, m 2.08, m	---	---
2	34.1, CH_2	2.48, m	---	C-3
3	199.6, CO	---	---	---
4	123.0, CH	5.74, s	---	C-2, 5, 6, 10, 19
5	164.4, C	---	---	---
6	124.5, CH	6.03, d (9.5)	H-7	C-4, 5, 8, 10
7	134.0, CH	6.61, d (9.5)	H-6	C-5, 8, 9, 14
8	124.4, C	---	---	---
9	44.3, CH	2.18, m	---	C-14
10	36.8, C	---	---	---
11	19.0, CH_2	1.80, m 2.03, m	--- ---	C-8 ---
12	35.6, CH_2	1.29, m 2.08, m	--- ---	C-9, 13 ---
13	44.0, C	---	---	---
14	156.2, C	---	---	---
15	25.4, CH_2	2.39, m	---	C-14
16	27.7, CH_2	1.50, m	---	---

Position	δ_C, type	δ_H, mult. (*J* in Hz)	COSY	HMBC
		1.70, m	---	C-13
17	55.7, CH	1.25, m	---	---
18	18.9, CH_3	0.96, s	---	C-13, 14, 17
19	16.7, CH_3	1.00, s	---	C-1, 5, 9, 10
20	39.3, CH	2.13, m	H-22	C-22, 23
21	21.2, CH_3	1.06, d (6.7)	H-20	C-17, 20, 22
22	135.0, CH	5.20, dd (15.2, 8.1)	H-20, 23	C-21, 23, 24
23	132.5, CH	5.26, dd (15.2, 7.3)	H-22, 24	C-20, 22, 24
24	42.9, CH	1.85, m	H-23,25,26	C-23, 25, 26, 28
25	33.1, CH	1.48, m	H-27, 28	---
26	17.7, CH_3	0.93, d (6.8)	H-24	C-23, 24, 25
27	20.0, CH_3	0.85, d (6.8)	H-25	C-24, 25, 28
28	19.7, CH_3	0.83, d (6.8)	H-25	C-24, 25, 27

4.2.2.3. Cyathisterone (IV)

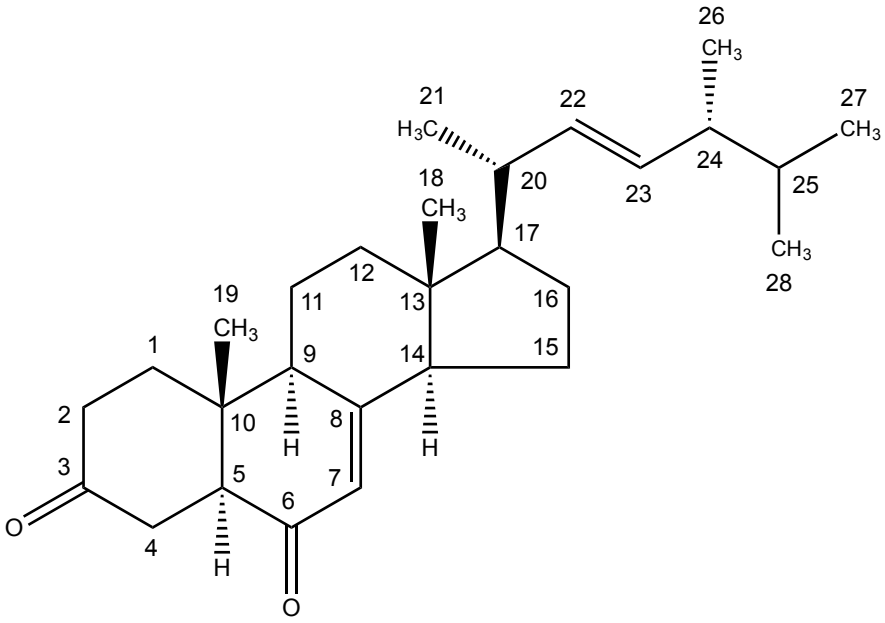

Figure 45. Structure of cyathisterone (**IV**)

Compound **IV** was isolated as white crystals (mp. 200-202 °C), and its molecular formula $C_{28}H_{42}O_2$ was determined based on the (+)-HRESIMS *m/z* 411.3262 $[M+H]^+$ (calculated 411.3263), indicating eight degrees of unsaturation. The IR spectrum showed absorption bands for ketone carbonyl (1717 cm^{-1}), conjugated ketone carbonyl (1661 cm^{-1}) and olefin (1622 cm^{-1}) groups. The general feature of the ^1H and ^{13}C NMR spectra of compound **IV** revealed that it was an ergosterol derivative.

The ^{13}C NMR spectrum (**Table 7**) exhibited twenty-eight carbon signals which, in conjunction with DEPTs and HSQC spectra, can be categorized as one ketone carbonyl (δ_C 211.0), one conjugated ketone carbonyl (δ_C 198.3), one quaternary sp^2 (δ_C 163.8), three methine sp^2 (δ_C 134.9, 132.6 and 122.8), two quaternary sp^3 (δ_C 44.5 and 38.3), seven methine sp^3 (δ_C 56.1, 55.7, 54.6, 49.6, 42.8, 40.3 and 33.1), seven methylene sp^3 (δ_C 38.6, 38.2, 37.3, 37.0, 27.9, 22.6 and 22.0), two tertiary methyl (δ_C 12.8 and 12.7) and four secondary methyl (δ_C 21.1, 20.0, 19.7 and 17.6) groups.

The ^1H NMR spectrum (**Table 7**) showed a broad triplet of the olefinic proton of the trisubstituted double bond at δ_H 5.78 (*J* = 2.3 Hz), two doublets of the *trans* double bond at δ_H 5.25 (*J* = 15.2, 7.2 Hz) and 5.16 (*J* = 15.2, 7.9 Hz), two singlets of tertiary methyls at δ_H 1.08 and 0.65, and four doublets of secondary methyls at δ_H 1.50 (*J* = 6.6 Hz), δ_H 0.92 (*J* =

6.8 Hz), δ_H 0.82 (*J* = 6.8 Hz) and δ_H 0.84 (*J* = 6.8 Hz). That **IV** had the same (*3E*)-5,6-dimethylhept-3-en-2-yl side chain as ergosterol (Martinez, 2016) and ergosta-4,6,8(14),22-tetraen-3-one (**III**) (Kuml *et al.*, 2014), was evidenced by COSY correlations from CH_3-21 (δ_H 1.05, d, *J* = 6.6 Hz) to H-20 (δ_H 2.04, m), from H-22 (δ_H 5.16, dd, *J* = 15.2, 7.9 Hz) to H-20 and H-23 (δ_H 5.25, dd, *J* = 15.2, 7.2 Hz), from H-23 to H-22 and H-24 (δ_H 1.85, m), from H_3-26 (δ_H 0.92, d, *J* = 6.8 Hz) to H-24, and from H_3-27 (δ_H 0.82, d, *J* = 6.8 Hz), H_3-28 (δ_H 0.84, d, *J* = 6.8 Hz) and H-24 to H-25 (δ_H 1.48, m), as well as by HMBC correlations from H_3-27 and H_3-28 to C-24 (δ_C 42.8), C-25 (δ_C 33.1) and CH_3-26 (δ_C 17.6), from H_3-26 to C-23 (δ_C 132.5), C-24 and C-25, and from H_3-21 to C-20 (δ_C 40.3), C-22 (δ_C 134.9) and C-17 (δ_C 56.1) (**Table 7 and Figure 46**).

The trisubstituted double bond was located between C-7 and C-8, and the conjugated ketone carbonyl was on C-6 of the cyclopentanoperhydrophenanthrene moiety was supported by the COSY correlations from H-7 (δ_H 5.78, brt, *J* = 2.3 Hz) to H-9 (δ_H 2.26, m) and H-14 (δ_H 2.09, m), as well as by the HMBC correlations from H-7 to C-9 (δ_C 49.6), from H_3-19 to C-5 (δ_C 54.6), C-9 and C-10 (δ_C 38.3), from H-5 (δ_H 2.64, dd, *J* = 12.8, 4.5 Hz) to C-6 (δ_C 198.3). Since H-2 (δ_H 2.33, m and 2.38, m; δ_C 37.3) and H-4 (δ_H 2.59, m; δ_C 37.0) exhibited cross peaks to the carbonyl carbon at δ_C 211.0, another ketone function was placed on C-3 (**Table 7 and Figure 46**).

Consequently, the structure of **IV** was elucidated as ergosta-7, 22-dien-3,6-dione. The structure and the stereochemistry of **IV** were confirmed by X-ray analysis (**Figure 47**), and since the diffraction data were collected with the Gemini PX Ultra equipped with CuKα radiation, it was possible to establish the absolute configurations of C-5, C-9, C-10, C-13, C-14, C-17, C-20 and C-24, respectively, as 5*S*, 9*R*, 10*R*, 13*R*, 14*R*, 17*R*, 20*S*, 24*R*. From all data, **IV** was elucidated as cyathisterone which has been isolated from *Calvatia cyathiformis* (Kawahara *et al.*, 1994).

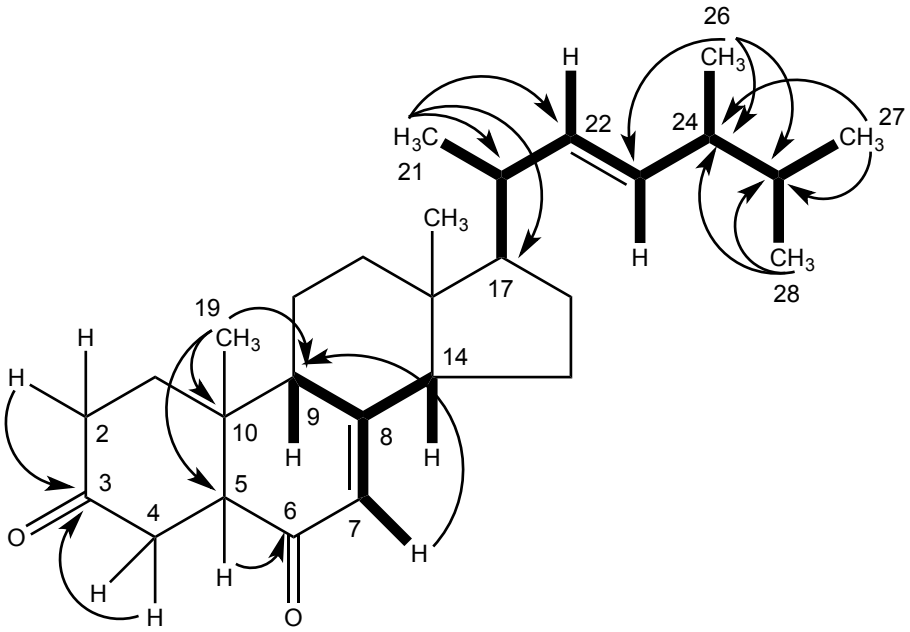

Figure 46. Key COSY (—) and HMBC (⟶) correlations of **IV.**

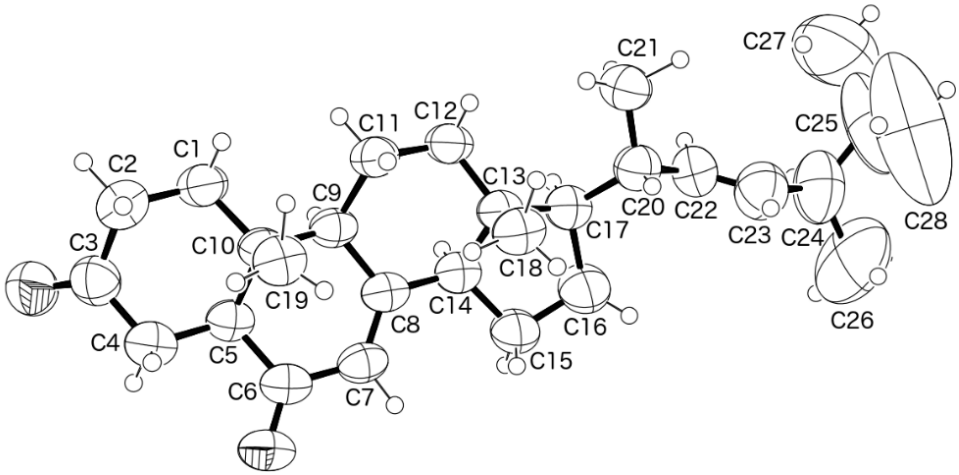

Figure 47. ORTEP diagram of **IV**.

Table 7. ^{1}H and ^{13}C NMR ($CDCl_3$, 300.13 MHz and 75.4 MHz) and HMBC assignment for cyathisterone (**IV**).

Position	δ_C, type	δ_H, mult. (J in Hz)	COSY	HMBC
1	38.2, CH_2	1.70, m 2.14, m	---	---
2	37.3, CH_2	2.33, m 2.38, m	---	CO-3
3	211.0, CO	---	---	---
4	37.0, CH_2	2.59, m	H-5	CO-3
5	54.6, CH	2.64, dd (12.8, 4.5)	H-4	CO-6

Position	δ_C, type	δ_H, mult. (J in Hz)	COSY	HMBC
6	198.3, CO	---	---	---
7	122.8, CH	5.78, brt (2.3)	H-9, 14	C-9
8	163.8, C	---	---	---
9	49.6, CH	2.26, m	H-7, 11	---
10	38.3, C	---	---	---
11	22.0, CH_2	1.72, m	---	---
		1.85, m	---	---
12	38.6, CH_2	1.45, m	---	---
		2.14, m	---	---
13	44.5, C	---	---	---
14	55.7, CH	2.09, m	H-9, 15	---
15	22.6, CH_2	1.50, m	---	---
		1.60, m	---	---
16	27.9, CH_2	1.37, m	---	---
		1.79, m	---	---
17	56.1, CH	1.36, m	H-16, 20	---
18	12.7, CH_3	0.65, s	---	---
19	12.8, CH_3	1.08, s	---	C-5, 9, 10
20	40.3, CH	2.04, m	H-21, 22	---
21	21.1, CH_3	1.05, d (6.6)	H-20	C-17, 20, 22
22	134.9, CH	5.16, dd (15.2, 7.9)	H-20, 23	C-20, 25
23	132.6, CH	5.25, dd (15.2, 7.2)	H-22, 24	C-20, 24
24	42.8, CH	1.85, m	H-22, 25, 26	C-22, 23
25	33.1, CH	1.48, m	H-24, 27, 28	C-23
26	17.6, CH_3	0.92, d (6.8)	H-24	C-23, 24, 25
27	20.0, CH_3	0.82, d (6.8)	H-25	C-24, 25, 26, 28
28	19.7, CH_3	0.84, d (6.8)	H-25	C-24, 25, 26, 27

4.2.2.4. Talarosterone (V)

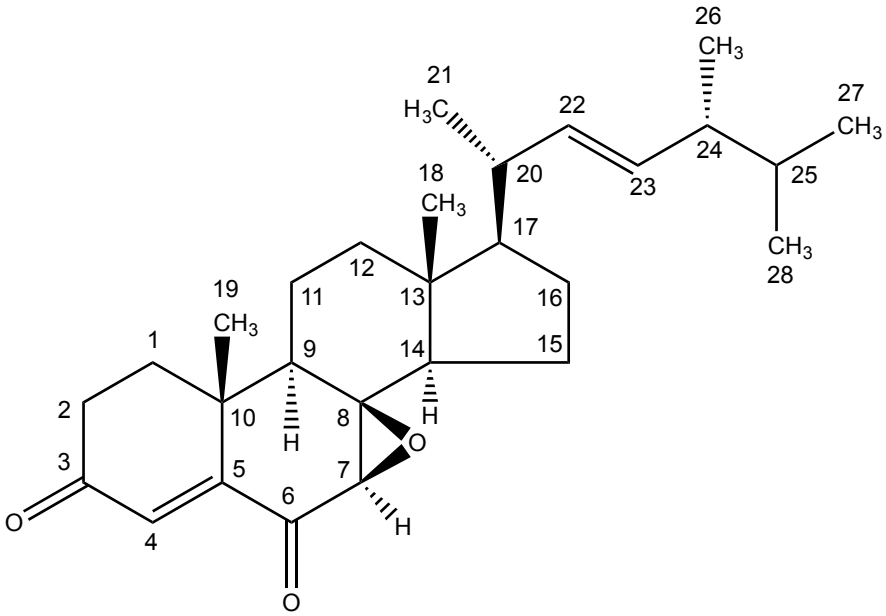

Figure 48. Structure of talarosterone (**V**).

The molecular formula $C_{28}H_{40}O_3$ of **V**, a white crystal (mp. 146-148 °C), was established based on the (+)-HRESIMS *m/z* 425.3056 $[M+H]^+$ (calculated 425.3056), indicating nine degrees of unsaturation. The IR spectrum showed absorption bands for conjugated ketone carbonyl (1689, 1670 cm^{-1}) and olefin (1593 cm^{-1}) groups. Like **IV**, the ^{13}C NMR spectra of **V** (**Table 8**) showed the presence of twenty eight carbon signals which can be classified, by DEPTs and HSQC spectra, as two conjugated ketone carbonyl (δ_C 199.5 and 195.9), one quaternary sp^2 (δ_C 155.0), three methine sp^2 (δ_C 135.0, 132.5 and 129.2), one oxyquaternary sp^3 (δ_C 66.2), two quaternary sp^3 (δ_C 44.3 and 36.8), seven methine sp^3 (δ_C 56.1, 56.0, 51.8, 43.9, 42.8, 40.0 and 33.0), six methylene sp^3 (δ_C 39.0, 37.1, 33.8, 27.7, 20.7 and 18.7), two tertiary methyl (δ_C 21.8 and 12.4) and four secondary methyl (δ_C 21.0, 20.0, 19.6 and 17.6) groups.

The ^1H NMR spectrum (**Table 8**) exhibited a doublet of an olefinic proton at δ_H 6.66 (*J* = 0.8 Hz), a singlet of one proton at δ_H 3.20, two singlets of the tertiary methyls at δ_H 1.50 and 0.89, in addition to the proton signals of the (*3E*)-5,6-dimethylhept-3-en-2-yl side chain [δ_H 0.82, d, *J* = 6.8 Hz (H_3-27), δ_H 0.84, d, *J* = 6.8 Hz (H_3-28), δ_H 1.04, d, *J* = 6.8 Hz (H_3-21), δ_H 5.15, dd, *J* = 15.3, 7.3 Hz (H-22) and δ_H 5.25, dd, *J* = 15.3, 8.0 Hz (H-23)]. As both H_3-21 and the methyl singlet at δ_H 0.89 showed HMBC cross peaks to C-17 (δ_C 56.0), the methyl singlet δ_H 0.89 was assigned to CH_3-18. Therefore, another methyl singlet (δ_H 1.50; δ_C 21.8)

was assigned to CH_3-19. Since the HMBC spectrum (**Table 8**, **Figure 49**) also exhibited cross peaks from both H_3-19 and the doublet of the olefinic proton at δ_H 6.66 (J = 0.8 Hz, H-4) to the quaternary sp^2 carbon at δ_C 155.0, the double bond was placed between C-4 (δ_C 129.2) and C-5 (δ_C 155.5). Moreover, H_3-19 also showed HMBC cross peaks to the carbon signals at δ_C 43.9, 37.1 and 36.8, therefore they were assigned to C-9, C-1 and C-10, respectively. On the other hand, the carbons at δ_C 44.3 and 51.8 were assigned to C-13 and C-14 since both showed HMBC cross peaks to H_3-18. Moreover, the HMBC spectrum also exhibited cross peaks from the singlet at δ_H 3.20 to C-5, C-14, the carbons at δ_C 66.2 and δ_C 195.9, the carbon at δ_C 66.2 was assigned to C-8 and one of the conjugated carbonyl carbon (δ_C 195.9) was placed on C-6. This was supported by the HMBC cross peak from H-4 to C-6. Therefore, another conjugated carbonyl group (δ_C 199.5) must be on C-3. The fact that there was one more oxygen atom to be accounted for, along with the presence of the oxyquaternary carbon (δ_C 66.2), the epoxide function was placed between C-7 and C-8. Therefore, the structure of **V** was elucidated as 7, 8-epoxyergosta-4, 22-dien-3, 6-dione.

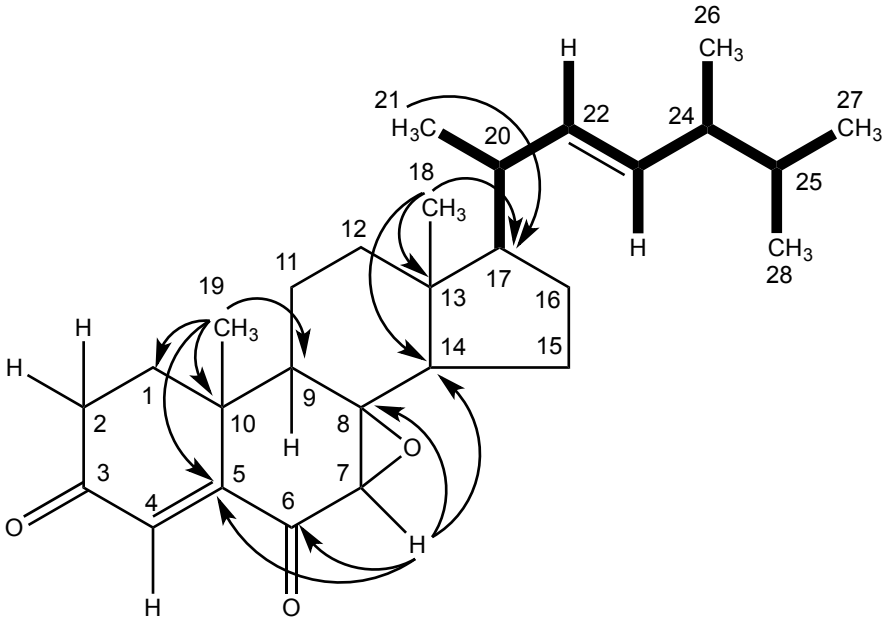

Figure 49. Key COSY (▬) and HMBC (⟶) correlations of **V.**

In order to determine the stereochemistry of **V**, the ROESY spectrum was obtained. As the ROESY spectrum (**Table 8, Figure 50**) showed cross peaks from H-7 to H-9, H-14 and H-15 (δ_H 1.25, m) but not to H_3-19, it was concluded that the epoxide ring was on the same face as CH_3-19, i. e. the relative configurations of C-7 and C-8 are 7*R* and 8*R*, respectively.

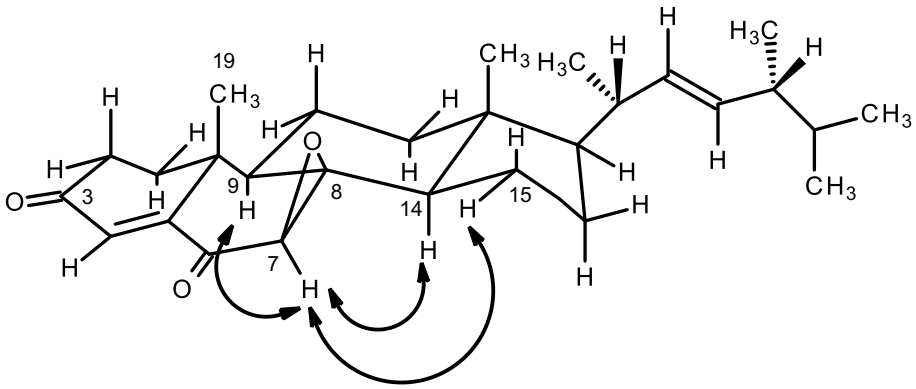

Figure 50. Key ROESY correlations (⟷) of **V**.

Since **V** was obtained in a suitable crystal, X-ray analysis was carried out, and the ORTEP view shown in **Figure 51** revealed that the absolute configurations of C-7, C-8, C-9, C-10, C-13, C-14, C-17, C-20 and C-24 are 7*R*, 8*R*, 9*R*, 10*R*, 13*R*, 14*R*, 17*R*, 20*S* and 24*R*. A literature search indicated that **V** has never been previously reported. Therefore, it is a new compound and was named talarosterone.

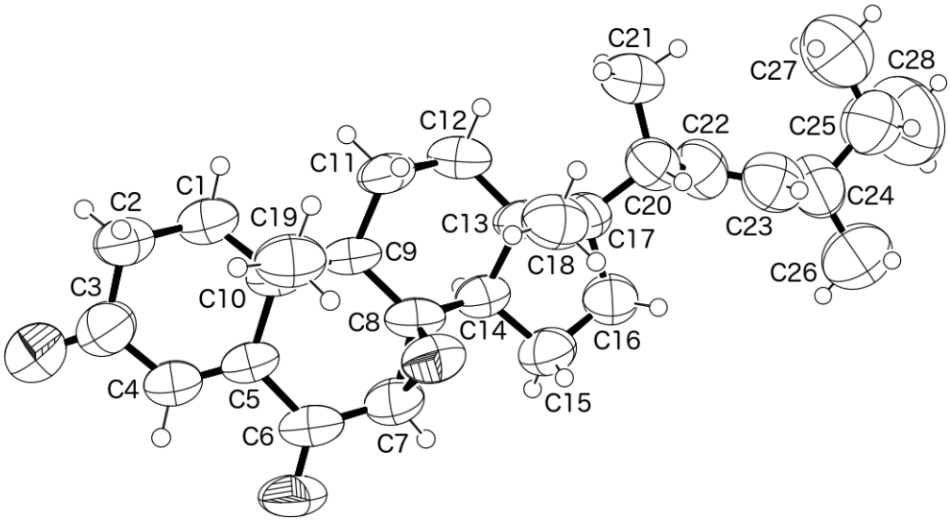

Figure 51. ORTEP diagram of **V**.

Table 8. ^{1}H and ^{13}C NMR ($CDCl_3$, 300.13 MHz and 75.4 MHz) and HMBC assignment for talarosterone (**V**).

Position	δ_C, type	δ_H, mult. (*J* in Hz)	COSY	ROESY	HMBC
1α	37.1, CH_2	1.81, m	---	---	---
β		2.18, m			
2α	33.8, CH_2	2.50, m	H-1	---	---
β		2.64, dd (17.9, 7.2)	H-1		
3	199.5, CO	---	---	---	---
4	129.2, CH	6.66, d (0.8)	---	---	C-2, 3, 5
5	155.0, C	---	---	---	---
6	195.9, CO	---	---	---	---
7	56.1, CH	3.20, s	---	H-9, 14, 15	C-5, 6, 8, 14
8	66.2, C	---	---	---	---
9	43.9, CH	1.90, m	---	---	---
10	36.8, C	---	---	---	---
11	20.7, CH_2	1.85, m	---	---	---
12	39.0, CH_2	1.21, m	---	---	---
		1.40, m			
13	44.3, C	---	---	---	---
14	51.8, CH	1.94, m	---	---	---
15	18.7, CH_2	1.25, m	---	---	---
16	27.7, CH_2	1.34, m	---	---	---
		1.75, m			
17	56.0, CH	1.30, m	---	---	---
18	12.4, CH_3	0.89, s	---	---	C-12, 13, 14, 17
19	21.8, CH_3	1.50, s	---	1β, 2β	C-1, 5, 9, 10
20	40.0, CH	2.04, m	---	---	---
21	21.0, CH_3	1.04, d (6.8)	H-20	---	C-17, 20, 22
22	135.0, CH	5.15, dd (15.3, 7.3)	H-20, 23	---	C-21, 24
23	132.5, CH	5.25, dd (15.3, 8.0)	H-22, 24	---	C-20, 24, 25, 26
24	42.8, CH	1.85, m	---	---	C-22, 23
25	33.0, CH	1.48, m	---	---	---
26	17.6, CH_3	0.92, d (6.8)	H-24	---	C-23, 24, 25
27	20.0, CH_3	0.82, d (6.8)	H-25	---	C-24, 25, 28
28	19.6, CH_3	0.84, d (6.8)	H-25	---	C-24, 25, 27

4.2.3. Structure Elucidation of Anthraquinones

4.2.3.1. Emodin (VI)

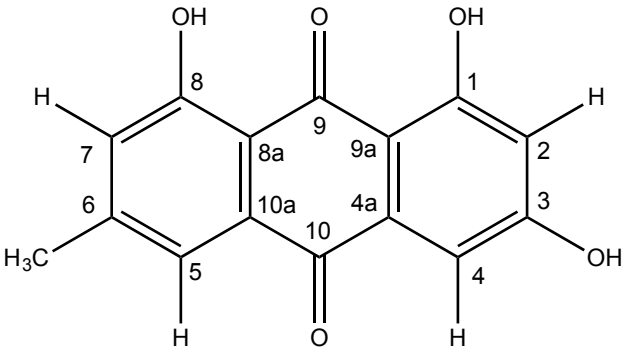

Figure 52. Structure of emodin (**VI**).

Compound **VI** was isolated as orange solid (mp. 105-110 °C). The ^{13}C NMR, DEPT and HSQC spectra (**Table 9**) exhibited the signals of two conjugated ketone carbonyls (δ_C 181.6 and 189.2), two sp^2 oxyquaternary (δ_C 164.6 and 161.4), four sp^2 quaternary (δ_C 148.0, 135.0, 132.9 and 113.5), four sp^2 methine (δ_C 124.1, 120.4, 109.2 and 108.1), and one methyl (δ_C 21.5) groups, respectively. Since the intensity of the sp^2 oxyquaternary carbon at δ_C 161.4 is nearly double of that at δ_C 164.6, the carbon signal at δ_C 161.4 must correspond to two sp^2 oxyquaternary carbons.

The ^{1}H NMR spectrum (**Table 9**) exhibited three broad singlets at δ_H 7.50, 7.17 and 6.56, and one doublet at δ_H 7.10, d, J = 2.0 Hz of the aromatic protons, and one singlet of the aromatic methyl group at δ_H 2.42, in addition to a broad singlet (integrated for two protons) of the hydrogen-bonded hydroxyl groups at δ_H 12.11. The COSY spectrum (**Table 9**) showed correlations from the aromatic proton at δ_H 7.50, brs, to the aromatic proton at δ_H 7.17, brs and the methyl proton at δ_H 2.42, s, while the latter also showed correlations to the aromatic proton at δ_H 7.50, brs and the methyl protons at δ_H 2.42, s. Therefore, the presence of a 1, 2, 3, 5-tetrasubstituted benzene ring with the methyl group on C-5 **(Figure 53 A)** was suggested. The COSY spectrum also showed a correlation between another pair of aromatic protons, i.e. δ_H 7.10, d (J = 2.0 Hz) and δ_H 6.56, brs. Therefore, another 1,2,3,5-tetrasubstituted benzene ring was present **(Figure 53 B)** in the structure of **VI**.

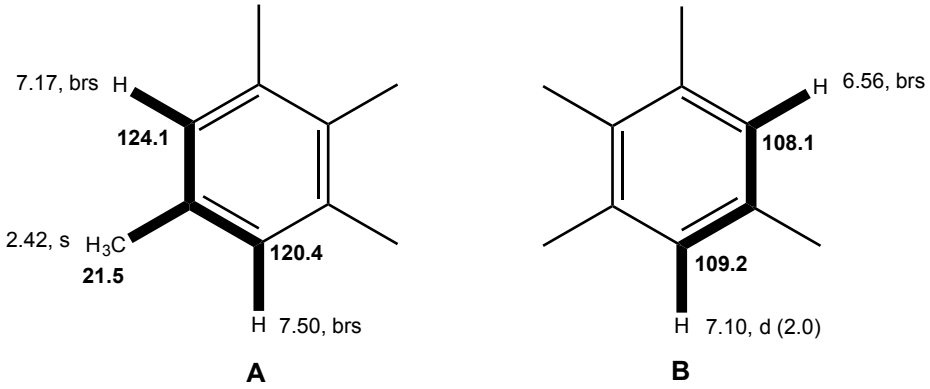

Figure 53. Key COSY correlations (—) of **VI**.

The HMBC spectrum (**Table 9**) exhibited cross peaks from the proton at δ_H 7.50, brs, to the methyl carbon at δ_C 21.5, aromatic carbons at δ_C 113.5 (C), 124.1 (CH) and the carbonyl carbon at δ_C 181.6, as well as from the proton singlet at δ_H 7.17 to the methyl carbon at δ_C 21.5, aromatic carbons at δ_C 113.5 (C), 120.4 (CH) and 161.4 (C). Therefore, it is clear that the ketone carbonyl group (δ_C 181.6) was on C-1 and the hydroxyl group was on C-6 (δ_C 161.4) (**Figure 54 C**). This was supported by the HMBC correlations of the singlet of the methyl protons (δ_H 2.42) to the aromatic carbons at δ_C 120.4 (CH), 124.1 (CH) and 148.0 (C), respectively. Moreover, the HMBC spectrum also showed cross peaks from the aromatic proton at δ_H 7.10, d (J = 2.0 Hz) to the ketone carbonyl group (δ_C 181.6) and the aromatic carbon at δ_C 108.1, as well as from the aromatic proton at δ_H 6.56, brs to the aromatic carbons at δ_C 109.2 (CH) and 161.4 (C). Therefore, the ketone carbonyl (δ_C 181.6) was on C-3 and the hydroxyl groups were on C-1 (δ_C 161.4) and C-5 (δ_C 164.6) of this 1,2,3,5-tetrasubstituted benzene ring (**Figure 54 D**), respectively.

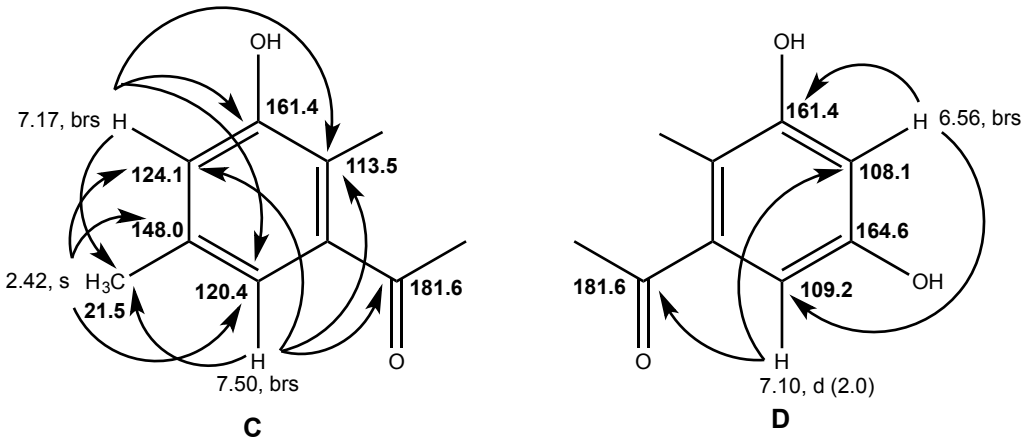

Figure 54. The HMBC correlations (⟶) of **VI**.

Since the chemical shift value of another ketone carbonyl carbon (δ_C 189.2) was nearly 8 ppm higher than the conjugated carbon at δ_C 181.6, it must be flanked by phenolic hydroxyl groups which form the hydrogen bonds with this conjugated carbonyl. Therefore, the two substituted benzene rings were linked by another carbonyl group forming an anthraquinone scaffold (**Figure 55**).

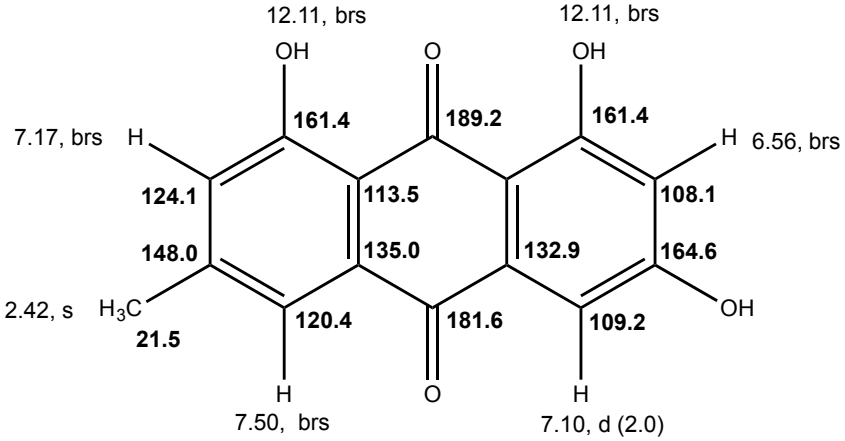

Figure 55. Structure of emodin (**VI**) indicating ^{1}H and ^{13}C chemical shifts.

Taking together all these NMR data and correlations, the structure of **VI** was deduced as **1, 3, 8-trihydroxy-6-methylanthracene-9,10-dione.**

Literature search revealed that **VI**, which is widely known as emodin, has been isolated from several natural sources including the endophytic fungus *Aspergillus versicolor* isolated from red sea algae (Hawas *et al.*, 2012), the marine derived-fungus *Penicillium oxalicum* (Wang *et al.*, 2014). Emodin has been isolated from lichenized fungi of the genus *Xanthoria* (Manojlovic *et al.*, 2000) and also from the genus *Heterodermia* (Cohen and Towers, 1995). Moreover, emodin has been isolated from several plants including *Cassia obtusifolia* (Yang *et al.*, 2003), *Polygonum cuspidatum* (Jayasuriya *et al.*, 1992) and from *Rhamnus triquerta* wall (Goel *et al.*, 1991).

Table 9. ^{1}H and ^{13}C NMR (DMSO, 500.13 MHz and 125.4 MHz) and HMBC assignment for emodin (**VI**).

Position	δ_C, type	δ_H, mult. (*J* in Hz)	COSY	HMBC
1	161.4, C	---	---	---
2	108.1, CH	6.56, brs	H-4	C-1, 4
3	164.6, C	---	---	---
4	109.2, CH	7.10, d (2.0)	H-2	C-2, 10
4a	132.9, C	---	---	---
5	120.4, CH	7.50, brs	H-7, H_3-6	C-7, 8a, 10, CH_3-6
6	148.0, C	---	---	---
7	124.1, CH	7.17, brs	H-5, H_3-6	C-5, 8, 8a, CH_3-6
8	161.4, C	---	---	---
8a	113.5, C	---	---	---
9	189.2, CO	---	---	---
9a	ND	---	---	---
10	181.6, CO	---	---	---
10a	135.0, C	---	---	---
CH_3-6	21.5, CH_3-	2.42, s	H-5, 7	C-5, 6, 7
OH-1, 8	---	12.11, brs	---	---
OH-3	---	---	---	---

4.2.3.2. Questinol (VII)

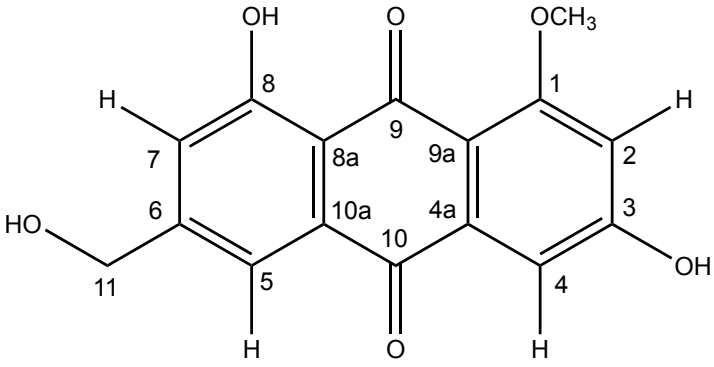

Figure 56. Structure of questinol (**VII**).

Compound **VII** was also isolated as an orange solid (mp. 255-265 °C) and its molecular formula $C_{16}H_{12}O_6$ was determined based on the (+)-HRESIMS *m/z* 301.0713 $[M+H]^+$ (calculated 301.0712), indicating eleven degrees of unsaturation. The ^{13}C NMR, DEPT and HSQC spectra (**Table 10**) exhibited the signals of two conjugated ketone carbonyls (δ_C 186.1 and 182.5), two oxyquaternary sp^2 (δ_C 163.6 and 161.8), five quaternary sp^2 (δ_C 151.2, 136.8, 132.2, 115.2 and 112.0), one oxymethylene sp^3 (δ_C 62.1) and one methoxyl (δ_C 56.2) groups. The ^1H NMR spectra exhibited a broad singlet of one hydrogen-bonded hydroxyl group at δ_C 13.40 and two pairs of doublets of the aromatic protons at δ_H 7.57, d (*J* = 1.6 Hz)/ 7.20, d (*J* = 1.6 Hz) and at δ_H 7.18, d (*J* = 2.3 Hz)/ 6.80, d (*J* = 2.3 Hz), in addition to a singlet of the methoxy protons at δ_H 3.89 and a singlet of the oxymethylene protons at δ_H 4.58. That the two pairs of the aromatic protons belong to the two *meta*-coupled benzene rings was substantiated by the COSY correlations (**Table 10, Figure 57**) from the proton at δ_H 7.57, d (*J* = 1.6 Hz) to the proton at δ_H 7.20, d (*J* = 1.6 Hz) as well as from the proton at δ_H 7.18, d (*J* = 2.3 Hz) to the proton at δ_H 6.80, d (*J* = 2.3 Hz). Moreover, the doublet at δ_H 6.80, d (*J* = 2.3 Hz) also showed cross peak to the methoxyl singlet at δ_H 3.89, suggesting that the methoxyl group is in close proximity to this aromatic proton. On the other hand, both aromatic protons at δ_H 7.57, d (*J* = 1.6 Hz) and 7.20, d (*J* = 1.6 Hz) gave cross peaks to the oxymethylene protons at δ_H 4.58, s, suggesting that this oxymethylene group was flanked by these two aromatic protons.

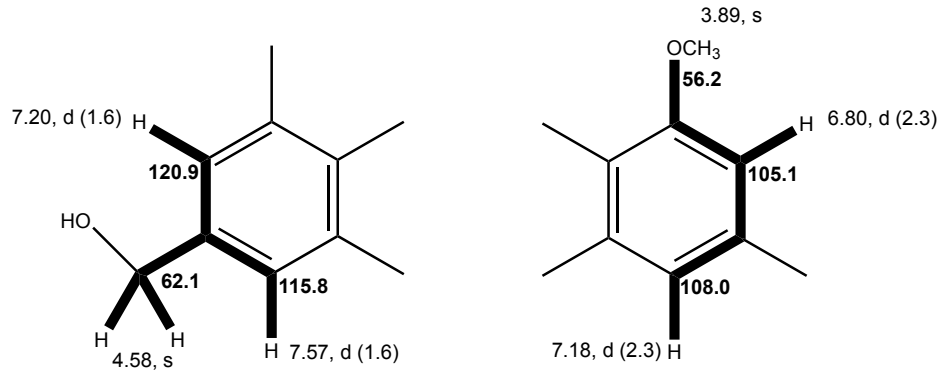

Figure 57. Key COSY correlations (—) of **VII**.

The HMBC spectrum (**Table 10, Figure 58**) exhibited cross peaks from the aromatic proton at δ_H 7.57, d (J = 1.6 Hz) to the carbons at δ_C 115.2 (C), 120.9 (CH) and the carbonyl carbon at δ_C 182.5, and from the aromatic proton at δ_H 7.20, d (J = 1.6 Hz) to the carbons at δ_C 115.2 (C), 115.8 (CH) and 161.8 (C), suggesting that this aromatic proton was next to the phenolic hydroxyl group. In turn, the singlet of the oxymethylene protons at δ_H 4.58, s gave cross peaks to the aromatic carbons at δ_C 115.8 (CH), 120.9 (CH) and the quaternary sp^2 carbon at δ_C 151.2. Therefore, one of the 1,2,3,5-tetrasubstituted benzene ring was:

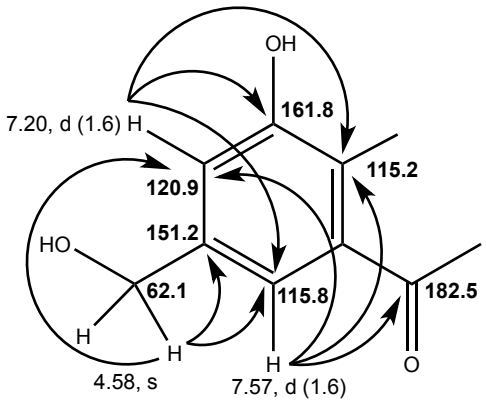

Figure 58. The HMBC correlations (⟶) of **VII**.

Moreover, the doublet at δ_H 7.18, d (J = 2.3 Hz) also gave HMBC cross peaks to the carbonyl carbon at δ_C 182.5, in addition to the aromatic carbons at δ_C 112.0 (C) and 105.1 (CH), while the doublet at δ_H 6.80, d (J = 2.3 Hz) exhibited cross peaks with the aromatic carbons at δ_C 112.0 (C) and 108.0 (CH). As the methoxyl proton (δ_H 3.89, s) gave cross peak to the oxyquaternary carbon at δ_C 163.6, the methoxyl group is on this carbon. The chemical shift value of the aromatic proton at δ_H 6.80, d (J = 2.3 Hz) suggested also that it should be flanked by two oxygenated substituents, thus another substituent in this tetrasubstituted benzene ring should be a hydroxyl group (**Figure 59**).

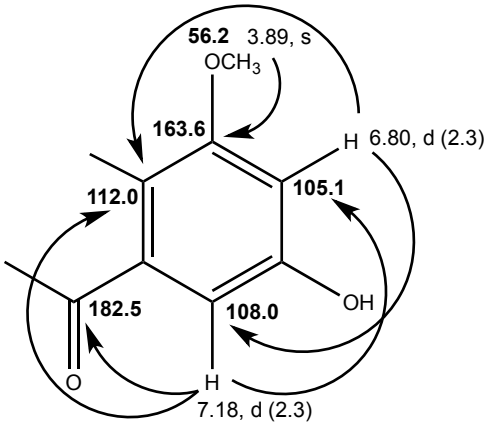

Figure 59. The HMBC correlations (⟶) of **VII**.

Since there is another carbonyl carbon at δ_C 186.1 in the structure, the two substituted benzene rings were connected by two conjugated ketone carbonyls presenting the anthraquinone scaffold similar to that of emodin **(VI)**:

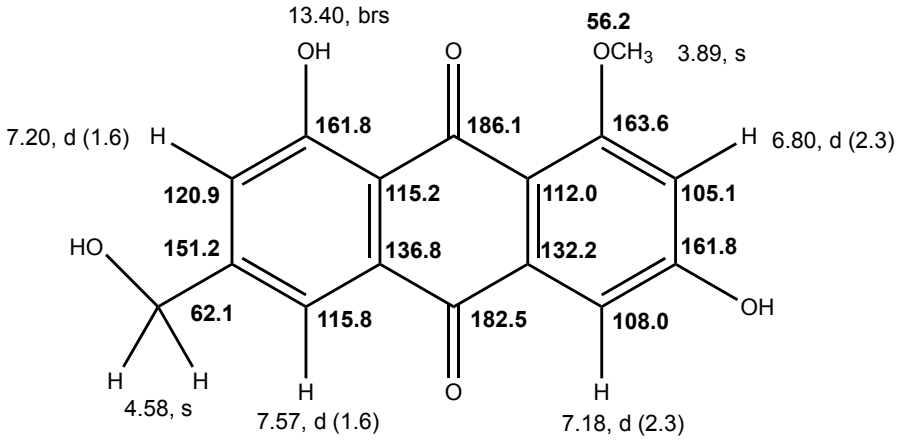

Figure 60. Structure of questinol indicating ^{1}H and ^{13}C chemical shifts.

Therefore, the structure of **VII** was identified as 3,8-dihydroxy-6-(hydroxymethyl)-1-methoxy-9,10-anthraquinone or commonly known as questinol.

Literature search revealed that questinol has been isolated from marine-derived fungus *Eurotium amstelodami* (Yang *et al.*, 2014).

Table 10. ^{1}H and ^{13}C NMR (DMSO, 300.13 MHz and 75.4 MHz) and HMBC assignment for questinol (**VII**)

Position	δ_C, type	δ_H, mult. (*J* in Hz)	COSY	HMBC
1	163.6, C	---	---	---
2	105.1, CH	6.80, d (2.3)	H-4, OCH_3	C-4, 9a
3	161.8, C	---	---	---
4	108.0, CH	7.18, d (2.3)	H-2	C-2, 9a, 10
4a	132.2, C	---	---	---
5	115.8, CH	7.57, d (1.6)	H-7, 11	C-7, 8a, 10
6	151.2, C	---	---	---
7	120.9, CH	7.20, d (1.6)	H-5, 11	C-5, 8a, 8
8	161.8, C	---	---	---
8a	115.2, C	---	---	---
9	186.1, CO	---	---	---
9a	112.0, C	---	---	---
10	182.5, CO	---	---	---
10a	136.8, C	---	---	---
11	62.1, CH_2	4.58, s	H-5, 7	C-5, 6, 7
OCH_3	56.2, CH_3	3.89, s	H-2	C-1
OH-1	---	13.40, brs	---	---

4.2.3.3. Citreorosein (VIII)

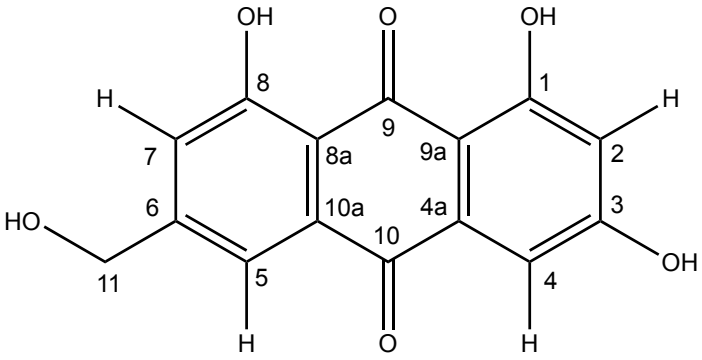

Figure 61. Structure of citreorosein (**VIII**).

Compound **VIII** was isolated as a yellow solid (mp. 287-289 °C). The ^{1}H and ^{13}C NMR spectra of **VIII** resembled those of **VII**, except for the absence of the methoxyl group. Moreover, the ^{1}H and ^{13}C NMR spectra exhibited two singlets at δ_H 12.05 and 12.03, characteristic of hydrogen-bonded phenolic hydroxyl groups. The ^{13}C NMR, DEPT and HSQC spectra (**Table 11**) exhibited the signals of two conjugated ketone carbonyls (δ_C 189.7 and 181.3), three oxyquaternary sp^2 (δ_C 165.6, 164.5 and 161.5), five quaternary sp^2 (δ_C 152.9, 135.1, 132.9, 114.0 and 109.0), four methine sp^2 (δ_C 120.8, 117.1, 108.8 and 107.9) and one oxymethylene sp^3 (δ_C 62.0), which is characteristic of hydroxymethyl anthraquinone. The ^{1}H NMR (**Table 11**) exhibited, in addition to the two singlets of hydrogen-bonded hydroxyl groups at δ_H 12.05 and 12.03, two pairs of the *meta*-coupled aromatic protons at δ_H 7.60, d (J = 1.5 Hz)/ 7.21, d (J = 1.5 Hz) and δ_H 7.09, d (J = 2.4 Hz)/ 6.56, d (J = 2.4 Hz), a singlet of the hydroxymethyl group at δ_H 4.59 and a broad singlet of a hydroxyl group at δ_H 5.58.

The COSY spectrum (**Table 11, Figure 62**) exhibited, on the one hand, cross peaks from the doublet at δ_H 7.60, d (J = 1.5 Hz) to the doublet at δ_H 7.21, d (J = 1.5 Hz), and the singlet at δ_H 4.59, as well as from the doublet at 7.21, d (J = 1.5 Hz) to the doublet at δ_H 7.60, d (J = 1.5 Hz) and the singlet at δ_H 4.59, on the other hand, from the doublet at δ_H 7.09, d (J = 2.4 Hz) to the doublet at δ_H 6.56, d (J = 2.4 Hz). These correlations not only confirmed the presence of two 1,2,3,5-tetrasubstituted benzene rings but also the position of the hydroxymethyl group between the *meta*-coupled protons in one of the benzene rings:

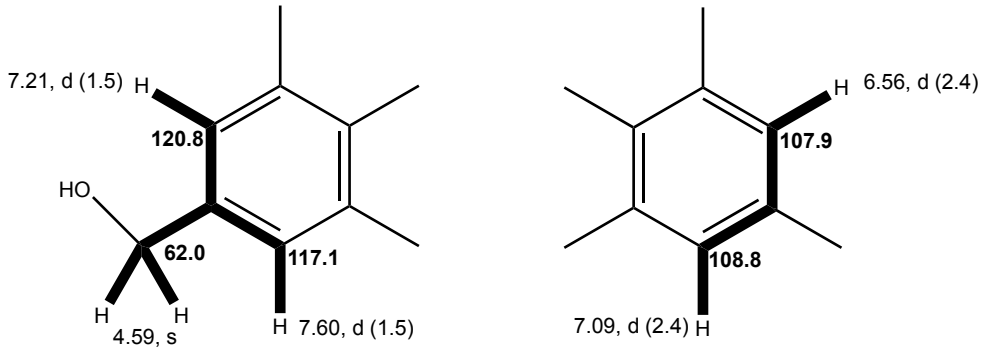

Figure 62. Key COSY correlations (—) of **VIII**.

The HMBC spectrum (**Table 11**) exhibited correlations of both aromatic protons at δ_H 7.09, d (J = 2.4 Hz) and δ_H 7.60, d (J = 1.5 Hz) to the carbonyl carbon at δ_C 181.3 whereas the singlets of the hydrogen-bonded hydroxyl protons at δ_H 12.05 and 12.03 gave cross peaks, respectively, to the oxyquaternary carbons at δ_C 164.5 and 161.5. Another carbonyl group (δ_C 189.7) was hydrogen-bonded with these two phenolic hydroxyl groups since it has a much higher resonance (δ_C 189.7). Taken together these data, it was possible to identify **VIII** as 1,3,8-trihydroxy-6-(hydroxymethyl)anthra-9,10-quinone. The HMBC correlations from the doublet at δ_H 7.09, d (J = 2.4 Hz) to the carbon at δ_C 109.0, from δ_H 6.56, d (J = 2.4 Hz) to the carbons at δ_C 109.0, 164.5 and 165.6 allow an assignment for C-3 and C-9a. Similarly, the HMBC correlations from the doublet at δ_H 7.60, d (J = 1.5 Hz) to the carbons at δ_C 62.0, 114.0, 120.8 and 181.3, and from the doublet at δ_H 7.21, d (J = 1.5 Hz) to the carbons at δ_C 114.0, 117.1 and 161.5 confirmed the assignment for C-8a, C-5 and C-8.

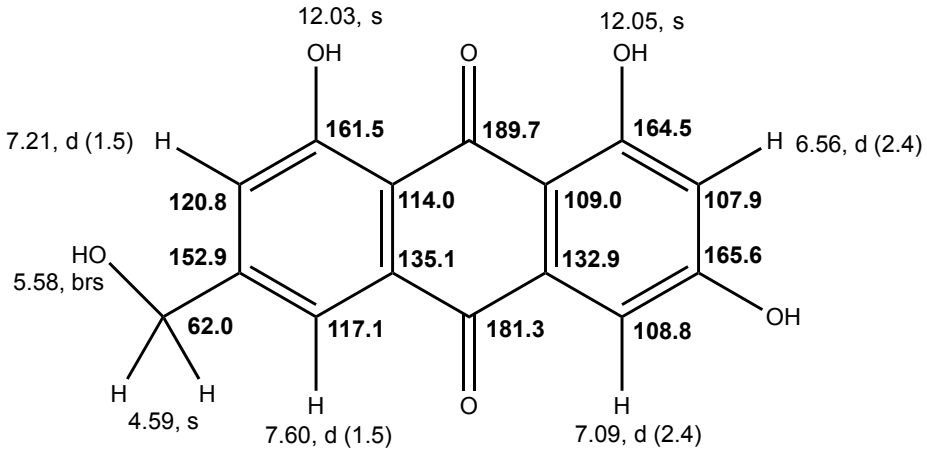

Figure 63. Structure of citreorosein indicating ^{1}H and ^{13}C chemical shifts.

Literature search revealed that **VIII,** also known as citreorosein, has been isolated from Ascomycete, *Zopfiella longicaudata* (Fujimoto *et al.*, 2004) and from a gorgonian coral-associated fungus *Penicillium* sp. (Bao *et al.*, 2013).

Table 11. ^{1}H and ^{13}C NMR (DMSO, 500.13 MHz and 125.4 MHz) and HMBC assignment for citreorosein (**VIII**).

Position	δ_C, type	δ_H, mult. (*J* in Hz)	COSY	HMBC
1	164.5, C	---	---	---
2	107.9, CH	6.56, d (2.4)	H-4	C-1, 3, 4, 9a
3	165.6, C	---	---	---
4	108.8, CH	7.09, d (2.4)	H-2	C-9a, 10
4a	132.9, C	---	---	---
5	117.1, CH	7.60, d (1.5)	H-7, 11	C-7, 8a, 10, 11
6	152.9, C	---	---	---
7	120.8, CH	7.21, d (1.5)	H-5, 11	C-5, 8, 8a
8	161.5, C	---	---	---
8a	114.0, C	---	---	---
9	189.7, CO	---	---	---
9a	109.0, C	---	---	---
10	181.3, CO	---	---	---
10a	135.1, C	---	---	---
11	62.0, CH_2	4.59, s	---	C-5, 6, 7
OH-1	---	12.05, s	---	C-1, 2
OH-8	---	12.03, s	---	C-7, 8, 8a
OH-11	---	5.58, brs	---	---

4.2.3.4. Fallacinol (IX)

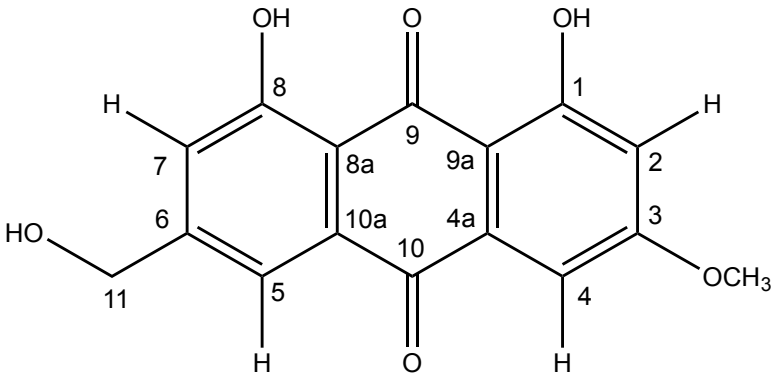

Figure 64. Structure of fallacinol (**IX**)

Compound **IX** was also isolated as a yellowish orange crystals (mp. 205-208 °C). The ^{1}H and ^{13}C NMR spectra of **IX** resembled those of citreorosein (**VIII**). The ^{1}H NMR and COSY spectra exhibited the signals of two pairs of *meta*-coupled aromatic protons at δ_H 6.87, d (J = 2.3 Hz)/ 7.24, d (J = 2.3 Hz) and δ_H 7.23, d (J = 1.5 Hz)/ 7.61, d (J = 1.5 Hz), the signals of the hydroxymethylene group at δ_H 4.59, d (J = 5.6 Hz) and δ_H 5.53, t (J = 5.9 Hz), in addition to the singlets of the hydrogen-bonded hydroxyl at δ_H 13.30 and the methoxyl group at δ_H 3.92 (**Table 12**). The ^{13}C NMR spectrum (**Table 12**) exhibited sixteen carbon signals which can be categorized, through DEPTs and HSQC spectra, into two conjugated ketone carbonyls (δ_C 182.3 and 186.4), eight quaternary sp^2 (δ_C 164.5, 163.5, 161.7, 151.4, 136.9, 132.1, 115.1 and 112.7), four methine sp^2 (δ_C 120.9, 115.8, 107.0 and 105.0), one oxymethylene sp^2 (δ_C 62.0), and one methyl (δ_C 56.4) groups. The COSY spectrum (**Table 12, Figure 65**) exhibited correlations from the oxymethylene protons (H_2-11) at δ_H 4.59, d (J = 5.6 Hz) to the *meta*-coupled aromatic protons at δ_H 7.23, d, J = 1.5 Hz (H-7)/ 7.61, d, J = 1.5 Hz (H-5) as well as from the methoxyl proton at δ_H 3.92 to the *meta*-coupled aromatic protons at δ_H 6.87, d, J = 2.3 Hz (H-2)/ 7.24, d, J = 2.3 Hz (H-4). Therefore, the structure of **IX** consisted of two 1,2,3,5-tetrasubstituted benzene rings:

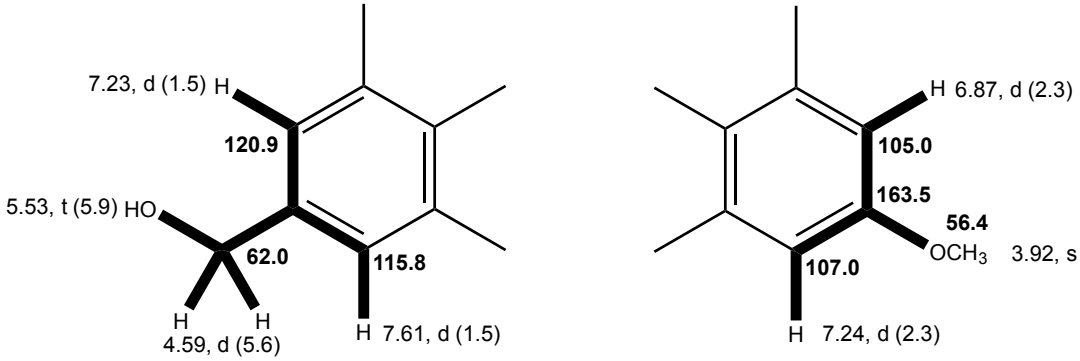

Figure 65. Key COSY correlations (—) of compound **IX**.

Since the HMBC spectrum (**Table 12, Figure 66**) exhibited correlations of the aromatic protons at δ_H 7.24, d, (*J* = 2.3 Hz, H-4) and 7.61, d (*J* = 1.5 Hz, H-5) to the carbonyl at δ_C 182.3, this carbonyl group was placed on C-10. Moreover, the singlet of the hydrogen-bonded proton (δ_H 13.30) gave cross peaks to the carbons at δ_C 161.7 (C-8), 120.9 (C-7) and 115.1 (C-8a), while the singlet of the methoxyl protons showed cross peaks to the carbon at δ_C 163.5, the hydroxyl and the methoxyl groups were placed on C-8 and C-3, respectively. Moreover, as the doublet of the oxymethylene protons at δ_H 4.59, d, *J* = 5.6 Hz (H_2-11) gave the HMBC cross peak to the carbon at δ_C 151.4, this carbon was assigned to C-6. On the other hand, both of the aromatic protons at δ_H 6.87, d, (*J* = 2.3 Hz, H-2)/ 7.24, d, (*J* = 2.3 Hz, H-4) exhibited cross peaks to the carbon at δ_C 112.7, this carbon was assigned to C-9a. Taken together these correlations, the partial structure of compound **IX** is:

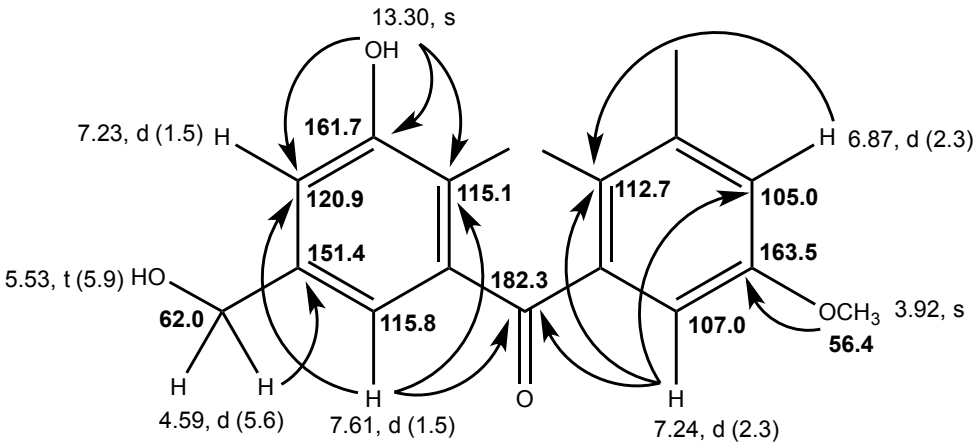

Figure 66. The HMBC correlations (⟶) of **IX**.

Since there is another conjugated carbonyl with hydrogen-bonding (δ_C 186.4), this carbonyl was placed on C-9, completing the structure of 1,8-dihydroxy-2-methoxy-6-(hydroxymethyl)-9,10-anthraquinone (**IX**).

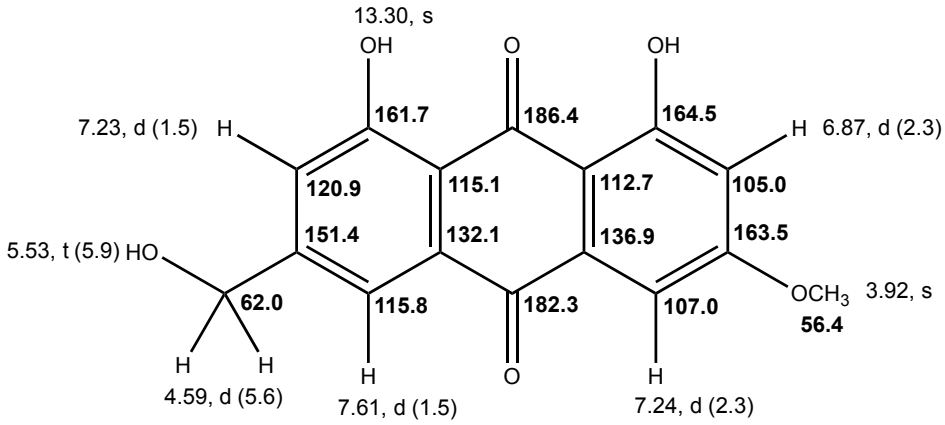

Figure 67. Structure of fallacinol indicating ^{1}H and ^{13}C chemical shifts.

Literature search revealed that **IX**, named fallacinol, has been previously isolated from lichenized fungi *Xanthoria fallax* (Murakami, 1956), *Xanthoria parientina* (Piattelli and de Nicola, 1968) and *Caloplaca schaereri* (Manojlovic *et al.*, 2002). Later on, fallacinol has been discovered from marine-derived fungi *Aspergillus variecolor* (Wang *et al.*, 2007).

Table 12. ^{1}H and ^{13}C NMR (DMSO, 500.13 MHz and 125.4 MHz) and HMBC assignment for fallacinol (**IX**).

Position	δ_C, type	δ_H, mult. (*J* in Hz)	COSY	HMBC
1	164.5, C	---	---	---
2	105.0, CH	6.87, d (2.3)	H-4, OMe	C-1, 4, 9a
3	163.5, C	---	---	---
4	107.0, CH	7.24, d (2.3)	H-2, OMe	C-2, 9a, 10
4a	136.9, C	---	---	---
5	115.8, CH	7.61, d (1.5)	H-7, 11	C-7, 8a, 10
6	151.4, C	---	---	---
7	120.9, CH	7.23, d (1.5)	H-5, 11	C-5, 8a
8	161.7, C	---	---	---
8a	115.1, C	---	---	---
9	186.4, CO	---	---	---
9a	112.7, C	---	---	---
10	182.3, CO	---	---	---

Position	δ_C, type	δ_H, mult. (*J* in Hz)	COSY	HMBC
10a	132.1, C	---	---	---
11	62.0, CH_2	4.59, d (5.6)	H-5, 7	C-5, 6, 7
OCH_3-3	56.4, CH_3	3.92, s	H-2, 4	C-3
OH-8	---	13.30, s	---	C-7, 8, 8a
OH-11	---	5.53, t (5.9)	H-11	---

4.2.3.5. 1,3,6,8-tetrahydroxy-9,10-anthraquinone = Rheoemodin (X)

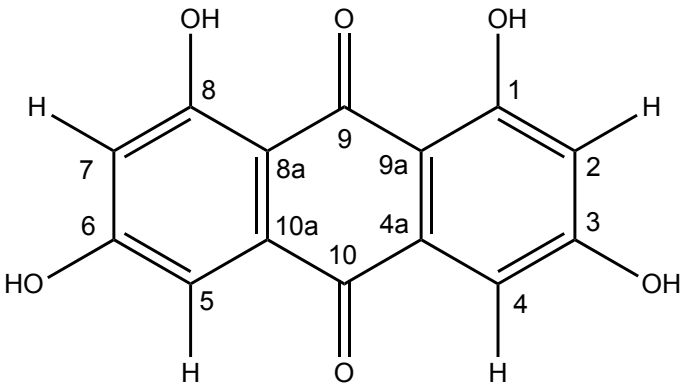

Figure 68. Structure of rheoemodin (**X**).

Compound **X** was isolated as a brown solid (mp. 164-167 °C). The ^{1}H and ^{13}C NMR spectra of **X** resemble those of emodin (**VI**), except for the absence of the methyl group. Additionally, the ^{13}C NMR, DEPT and HSQC spectra (**Table 13**) exhibited the signals of two conjugated ketone carbonyls (δ_C 189.2 and 180.9), four oxyquarternary sp^2 (δ_C 166.3, 165.6, 164.8 and 161.1), four quaternary sp^2 (δ_C 135.1, 133.5, 118.3 and 109.2), four methine sp^2 (δ_C 124.2, 118.9, 109.3 and 108.1), respectively. The ^{1}H NMR spectrum (**Table 13**) exhibited two pairs of doublets of aromatic protons at δ_H 8.08, d (J = 1.6 Hz)/ 7.71, d (J = 1.6 Hz) and at δ_H 7.13, d (J = 2.3 Hz)/ 6.60, d (J = 2.3 Hz), in addition to two broad singlets of hydrogen-bonded hydroxyl groups at δ_H 12.03. That the two pairs of the aromatic protons belong to the two *meta*-coupled benzene rings was substantiated by COSY correlations (**Table 13, Figure 69**) from the proton at δ_H 8.08, d (J = 1.6 Hz, H-5) to the proton at δ_H 7.71, d (J = 1.6 Hz, H-7), as well as from the proton at δ_H 7.13, d (J = 2.3 Hz, H-4) to the proton at δ_H 6.60, d (J = 2.3 Hz, H-2). Therefore, the structure of **X** consisted of two 1,2,3,5-tetrasubstituted benzene rings.

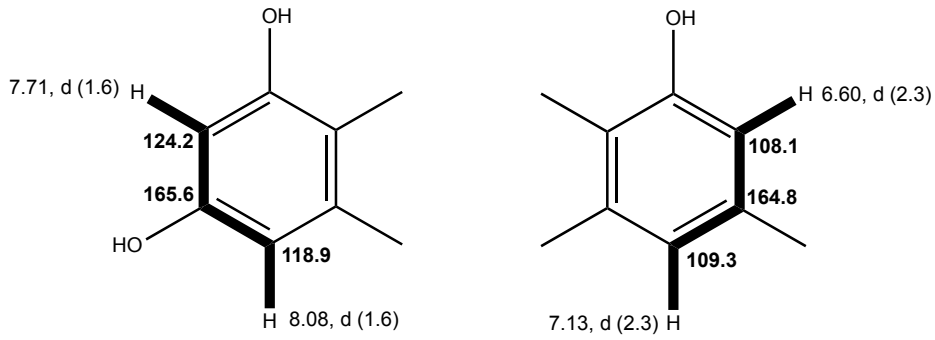

Figure 69. Key COSY correlations (—) of **X**.

The HMBC spectrum (**Table 13, Figure 70**) showed cross peaks from the aromatic proton at δ_H 8.08, d (*J* = 1.6 Hz, H-5) to the ketone carbonyl group (δ_C 180.9, C-10), aromatic carbons at δ_C 118.3 (C-8a) and 124.2 (CH-7), as well as from the aromatic proton at δ_H 7.71, d (*J* = 1.6 Hz, H-7) to the aromatic carbons at δ_C 165.6 (C-6), 161.1 (C-8) and 118.3 (C-8a), suggesting that this aromatic proton was next to the phenolic hydroxyl group. On the other hand, the HMBC spectrum also showed cross peaks from the aromatic proton at δ_H 7.13, d (*J* = 2.3 Hz, H-4) to the ketone carbonyl (δ_C 180.9, C-10) and the aromatic carbon at δ_C 109.2 (C-9a), as well as from the aromatic proton at δ_H 6.60, d (*J* = 2.3 Hz, H-2) to the aromatic carbons at δ_C 166.3 (C-1) and δ_C 109.3 (CH-4). The chemical shift value of the aromatic protons at δ_H 6.60 (C-2) and δ_H 7.71 (C-7) suggested also that they should be flanked by two oxygenated substituents. Therefore, these substituents should be the hydroxyl groups.

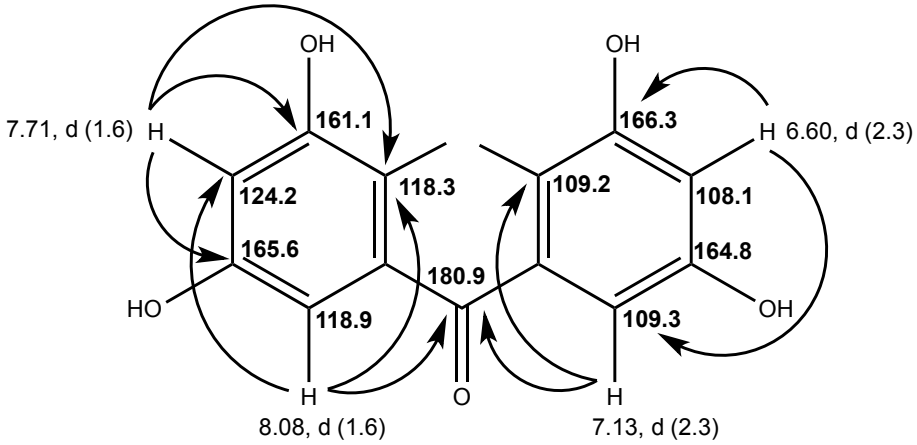

Figure 70. The HMBC correlations (⟶) of **X.**

Moreover, HMBC spectrum also exhibited correlations of both aromatic protons at δ_H 8.08, d (*J* = 1.6 Hz, H-5) and δ_H 7.13, d (*J* = 2.3 Hz, H-4) to the carbonyl carbon at δ_C 180.9 (C-10). Another carbonyl group (δ_C 189.2, C-9) was hydrogen-bonded with two phenolic hydroxyl groups since it has a very high resonance (δ_C 189.2, C-9). Thus, the two substituted benzene rings were connected by two conjugated ketone carbonyls rendering the anthraquinone scaffold similar to emodin (**VI**).

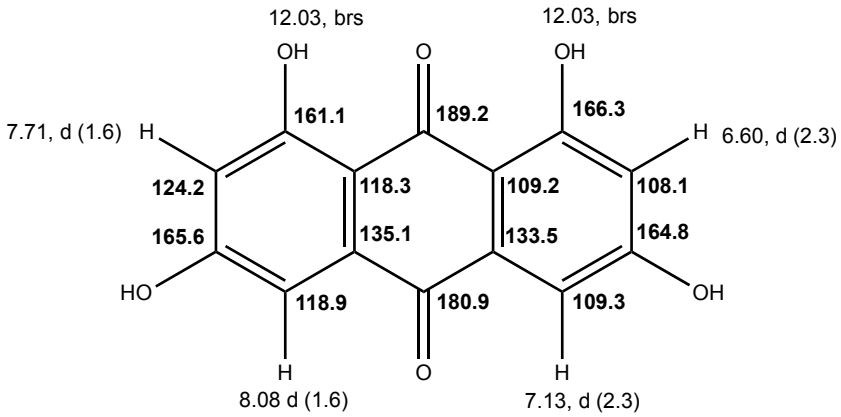

Figure 71. Structure of rheoemodin (**X**) indicating ^{1}H and ^{13}C chemical shifts.

Therefore, the structure of **X** is identified as 1,3,6,8-tetrahydroxy-9,10-anthraquinone or commonly known as rheoemodin.

Literature search revealed that rheoemodin (**X**) has been isolated from *Geomithia* species (Stodůlková *et al.*, 2009) and also from the endophytic fungus *Nigrospora* sp. (Huang *et al.*, 2016).

Table 13. ^{1}H and ^{13}C NMR (DMSO, 300.13 MHz and 75.4 MHz) and HMBC assignment for rheoemodin (**X**)

Position	δ_C, type	δ_H, mult. (*J* in Hz)	COSY	HMBC
1	166.3, C	---	---	---
2	108.1, CH	6.60, d (2.3)	H-4	C-1, 4, 8a
3	164.8, C	---	---	---
4	109.3, CH	7.13, d (2.3)	H-2	C-9a, 10
4a	133.5, C	---	---	---
5	118.9, CH	8.08, d (1.6)	H-7	C-7, 8a, 10
6	165.6, C	---	---	---
7	124.2, CH	7.71, d (1.6)	H-5	C-6, 8, 8a
8	161.1, C	---	---	---
8a	118.3, C	---	---	---
9	189.2, CO	---	---	---
9a	109.2, C	---	---	---
10	180.9, CO	---	---	---
10a	135.1, C	---	---	---
OH-1	---	12.03, brs	---	---
OH-8	---	12.03, brs	---	---

4.2.4. Structure Elucidation of *Bis* - Xanthone and *Bis* - Anthraquinone

4.2.4.1. Secalonic acid A (XI)

Compound **XI** was also isolated as yellow crystal (mp. 268-270 °C). The ^{13}C NMR spectrum (**Table 14**) exhibited sixteen carbon signals which were categorized, through DEPT and HSQC spectra (**Table 14**), as one conjugated ketone carbonyl (δ_C 186.5), one ketone or enolic (δ_C 178.2), one ester carbonyl (δ_C 170.0), two oxyquaternary sp^2 (δ_C 158.9 and 158.5), three quaternary sp^2 (δ_C 117.3, 106.3 and 101.7), two methine sp^2 (δ_C 140.2 and 107.5), one oxyquaternary sp^3 (δ_C 85.2), one oxymethine sp^3 (δ_C 75.2), one methine sp^3 (δ_C 29.9), one methylene sp^3 (δ_C 35.8), one methyl (δ_C 17.7) and one methoxyl (δ_C 52.9) groups. The ^{1}H NMR spectrum (**Table 14**) exhibited two *ortho*-coupled aromatic protons at δ_H 7.46, d, (J = 8.5 Hz) and 6.63, d, (J = 8.5 Hz), a broad singlet of one hydrogen-bonded phenolic hydroxyl at δ_H 11.62, one broad signal of one enolic hydroxyl at δ_H 13.70, one double doublet of the hydroxyl at δ_H 6.04, dd, (J = 5.7, 2.5 Hz), one double doublet at δ_H 3.82, dd, (J = 10.0, 5.7 Hz), three multiplets at δ_H 2.50 (1H), 2.67 (1H), 2.30 (1H), a doublet of one methyl at δ_H 1.04, d, (J = 6.0 Hz) and a methoxyl singlet at δ_H 3.62. That the *ortho*-coupled aromatic protons belonged to the 2,3,5-trisubstituted phenol was supported by the HMBC correlations from the hydrogen-bonded phenolic hydroxyl group at δ_H 11.62 to the oxyquaternary sp^2 carbon at δ_C 158.5 (C-1) and the quaternary sp^2 carbons at δ_C 117.3 (C-2) and 106.3 (C-9a), from the doublet at δ_H 7.46, d, (J = 8.5 Hz) to C-1, C-2 and another oxyquaternary sp^2 carbon at δ_C 158.9, the latter was assigned to C-4a, as well as from the doublet at δ_H 6.63, d, (J = 8.5 Hz) to C-2, C-4a and C-9a (**Figure 72**).

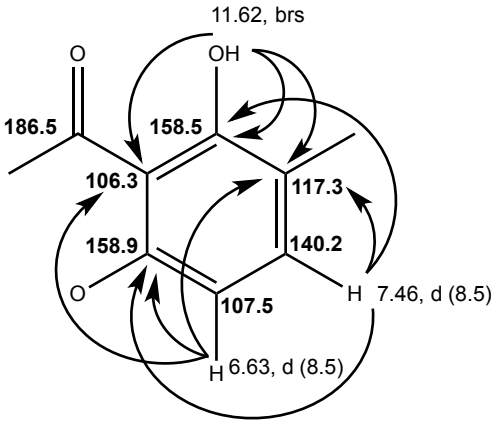

Figure 72. The HMBC correlations (⟶) of **XI**.

The COSY spectrum (**Table 14, Figure 73**) exhibited cross peaks from the double doublet of the methine proton at δ_H 3.82 (*J* = 10.0, 5.7 Hz, H-5) to the double doublet of the hydroxyl proton at δ_H 6.04 (*J* = 5.7, 2.5 Hz) and a multiplet of another methine proton at δ_H 2.30 (H-6), while the latter also showed cross peaks to the methyl doublet at δ_H 1.04 (*J* = 6.0 Hz) as well as the multiplets at δ_H 2.50 and 2.67 (H_2-7), suggesting the presence of the following coupling system:

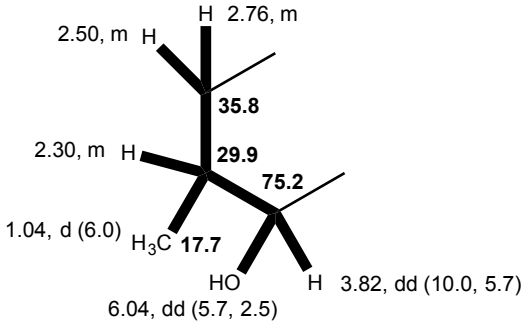

Figure 73. Key COSY correlations (—) of **XI**.

This coupling system was supported by HMBC correlations (**Table 14, Figure 74**) from the double doublet of the hydroxyl proton at δ_H 6.04, dd, (*J* = 5.7, 2.5 Hz) to the oxymethine sp^3 at δ_C 75.2 (C-5) and the methine sp^3 carbon at δ_C 29.9 (C-6) as well as from the double doublet of the methine proton at δ_H 3.82, dd, (*J* = 10.0, 5.7 Hz, H-5) to the methyl carbon at δ_C 17.7 (C-11) and the methine carbon at δ_C 29.9 (C-6). Furthermore, the methine proton at δ_H 3.82, dd, (*J* = 10.0, 5.7 Hz, H-5) showed also HMBC cross peaks to the oxyquaternary sp^3 carbon at δ_C 85.2 (C-10a) and the ester carbonyl at δ_C 170.0 (C-12), suggesting that C-10a is connected to the ester group. Since the methoxyl singlet at δ_H 3.62 (δ_C 52.9) showed also a cross peak to this ester carbonyl group, it was clear that one of the substituents on the oxyquaternary sp^3 carbon at δ_C 85.2 was an acetyl group. Moreover, the HMBC spectrum also exhibited cross peaks from the multiplets at δ_H 2.50 and 2.67 to the enolic carbon at δ_C 178.2 and the quaternary sp^2 carbon at δ_C 101.7, suggesting the presence of the following moiety:

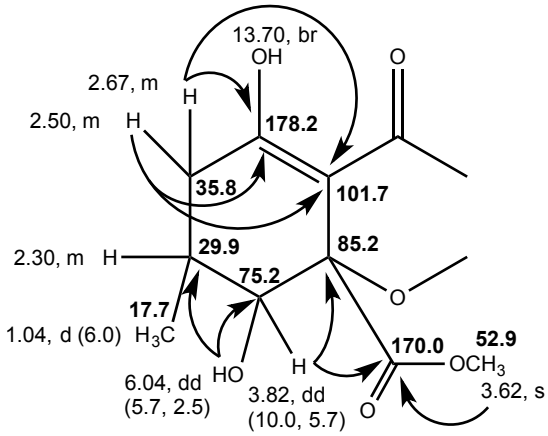

Figure 74. The HMBC correlations (⟶) of **XI**.

Taking together the two-partial structures deduced from the NMR data, the structure of **XI** was purposed as methyl 1,4-dihydroxy-3-methyl-9-oxo-2,3,4,9-tetrahydro-4a*H*-xanthene-4a-carboxylate:

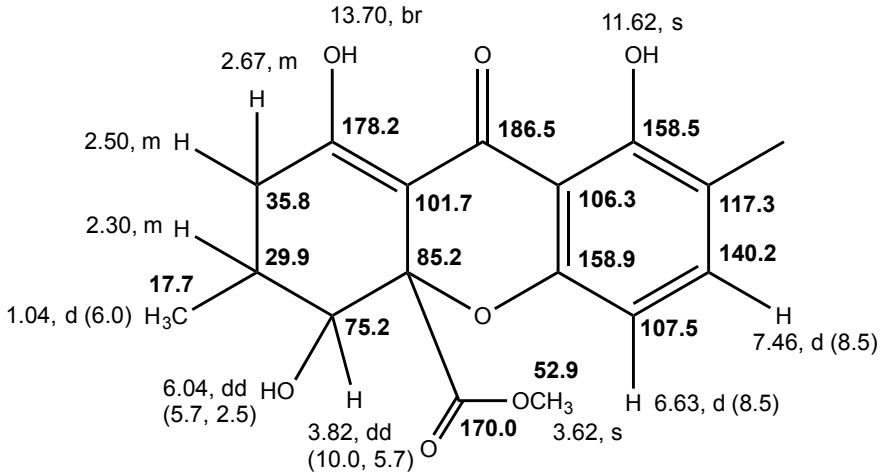

Figure 75. The partial structure of **XI** indicating the ^{1}H and ^{13}C chemical shift values.

However, this structure lacks a substituent on the carbon at δ_C 117.3 of the phenolic moiety. This structure also accounts for $C_{16}H_{15}O_7$. Since the (+)-HRESIMS of **XI** gave the *m/z* 639.1714 for its $[M+H]^+$ (calculated for $C_{32}H_{31}O_{14}$, 639.1714) its molecular formula was established as $C_{32}H_{30}O_{14}$, which is double of the proposed structure established by the NMR data. Therefore, **XI** must correspond to a dimer of the proposed structure, linked through its carbon at δ_C 117.3, i.e.:

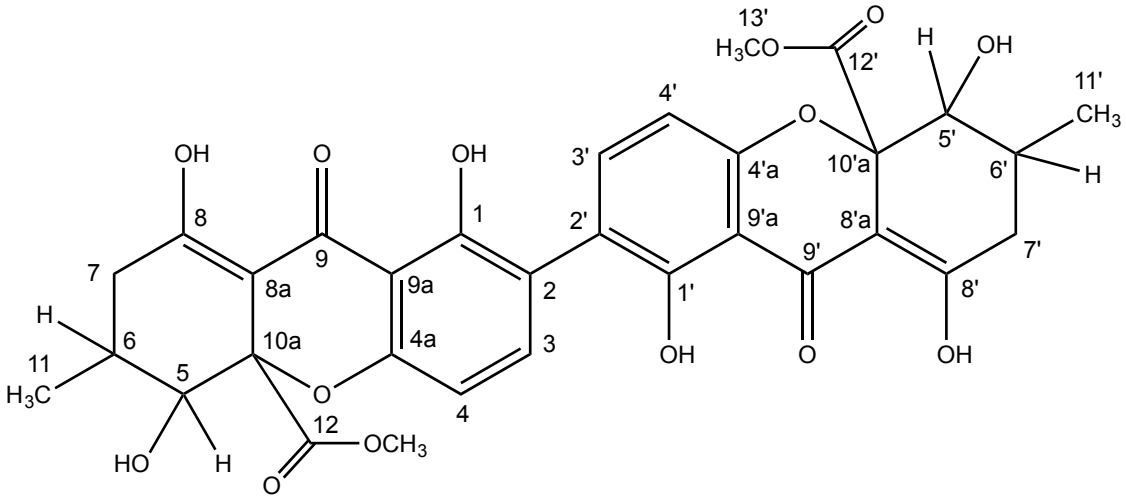

Figure 76. The structure of **XI**.

This hypothesis was also supported by the HMBC correlation from H-3 (δ_H 7.46, d, J = 8.5 Hz) to C-2' (δ_C 117.3). This structure also accounts for the molecular formula $C_{32}H_{30}O_{14}$ which corresponds to eighteen degrees of unsaturation.

The structure of **XI** has six stereogenic carbons in total (three for each monomer), i.e. C-5/C-5', C-6/C-6' and C-10a/C-10'a. Since **XI** was obtained as a suitable crystal, X-ray analysis was performed. The Ortep view (**Figure 77**) not only confirms the structure of **XI** but also determines the absolute configurations of C-5/C-5', C-6/C-6' and C-10a/C-10'a, respectively as C-5*S*/C-5'*S*, C-6*R*/C-6'*R*, and C-10a*S*/C-10'a*S*.

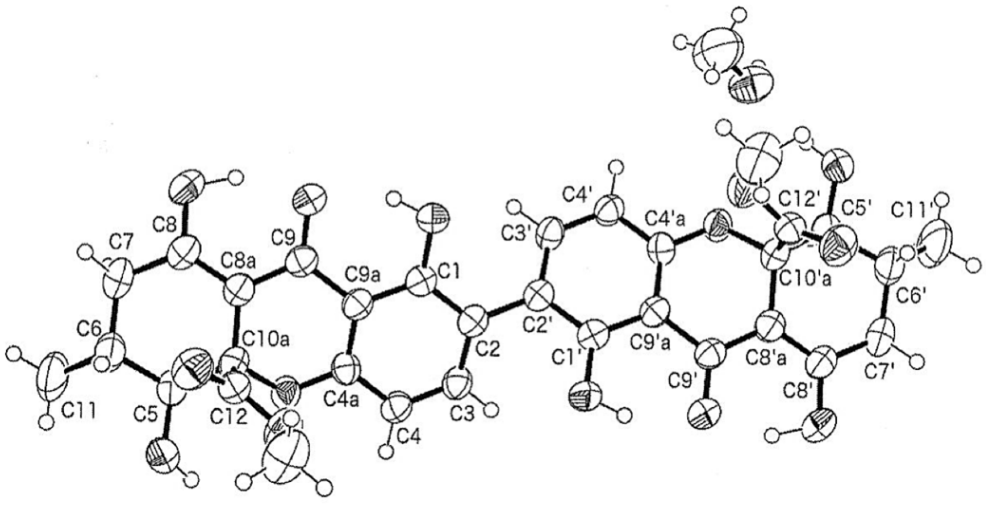

Figure 77. Ortep view of **XI**.

Thus, the complete structure of **XI** is proposed to be:

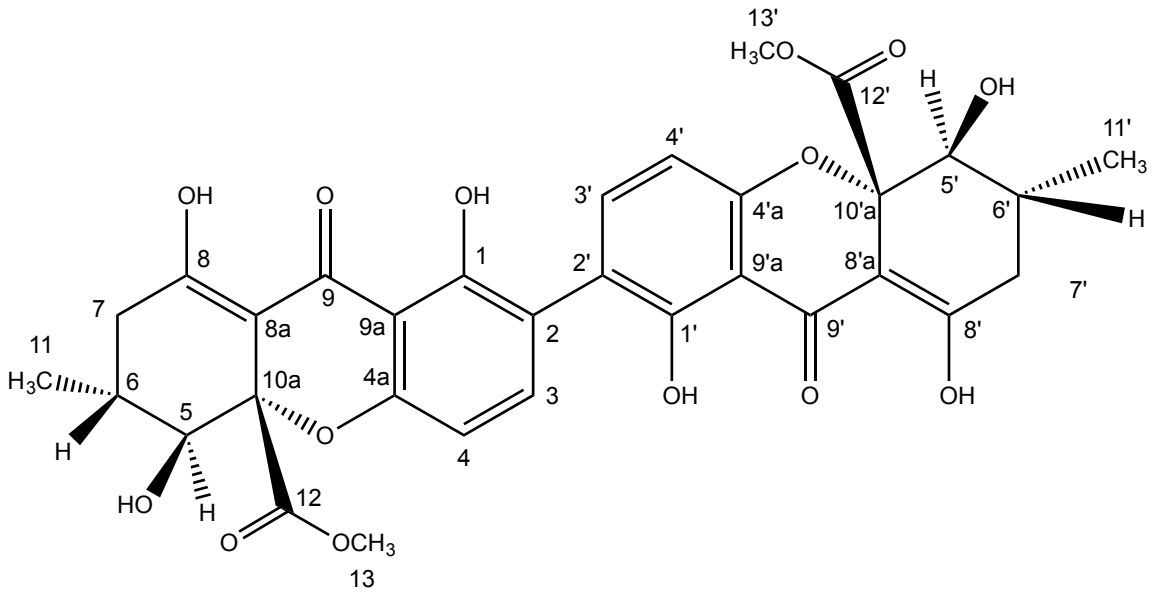

Figure 78. The complete structure of **XI**.

Literature search revealed that the structure of **XI** corresponds to secalonic acid A, a secondary metaboilite isolated from various fungi including *Aspergillus ochraceus* (Yamazaki *et al.*, 1971), *Pyrenochaeta terrestris* (Kurobane *et al.*, 1979) and *Pseudoparmelia sphaerospora* (Honda *et al.*, 1995).

Table 14. ^{1}H and ^{13}C NMR (DMSO, 300.13 MHz and 75.4 MHz) and HMBC assignment for secalonic acid A (**XI**).

Position	δ_C, type	δ_H, mult. (*J* in Hz)	COSY	HMBC
1 (1')	158.5, C	---	---	---
2 (2')	117.3, C	---	---	---
3 (3')	140.2, CH	7.46, d (8.5)	H-4 (4')	C-1 (1'), 4a (4'a), 2 (2')
4 (4')	107.5, CH	6.63, d (8.5)	H-3 (3')	C-2 (2'), 4a (4'a), 9a (9'a)
4a (4'a)	158.9, C	---	---	---
5 (5')	75.2, CH	3.82, dd (10.0, 5.7)	OH-5 (5'), 6 (6')	C-6 (6'), 10a (10'a), 11 (11'), 12 (12')
6 (6')	29.9, CH	2.30, m	H-5 (5'), 7 (7'), 11 (11')	---
7 (7')	35.8, CH_2	2.50, m 2.67, m	H-6(6') H-6(6')	C-8 (8'), 8a (8'a) C-8 (8'), 8a (8'a)
8 (8')	178.2, CO	---	---	---
8a (8'a)	101.7, C	---	---	---
9 (9')	186.5, CO	---	---	---
9a (9'a)	106.3, C	---	---	---
10a (10'a)	85.2, C	---	---	---
11 (11')	17.7, CH_3	1.04, d (6.0)	H-6 (6')	---
12 (12')	170.0, CO	---	---	---
OCH_3	52.9, CH_3	3.62, s	---	C-12 (12')
OH-5 (5')	---	6.04, dd (5.7, 2.5)	H-5 (5')	C-5 (5'), 6 (6')
OH-1 (1')	---	11.62, brs	---	C-1 (1'), 2 (2'), 9a (9'a)
OH-8 (8')	---	13.70, br	---	---

4.2.4.2. *Bis*-(7-methyl-1,4,5-trihydroxy-anthracene-9,10-dione) (XII)

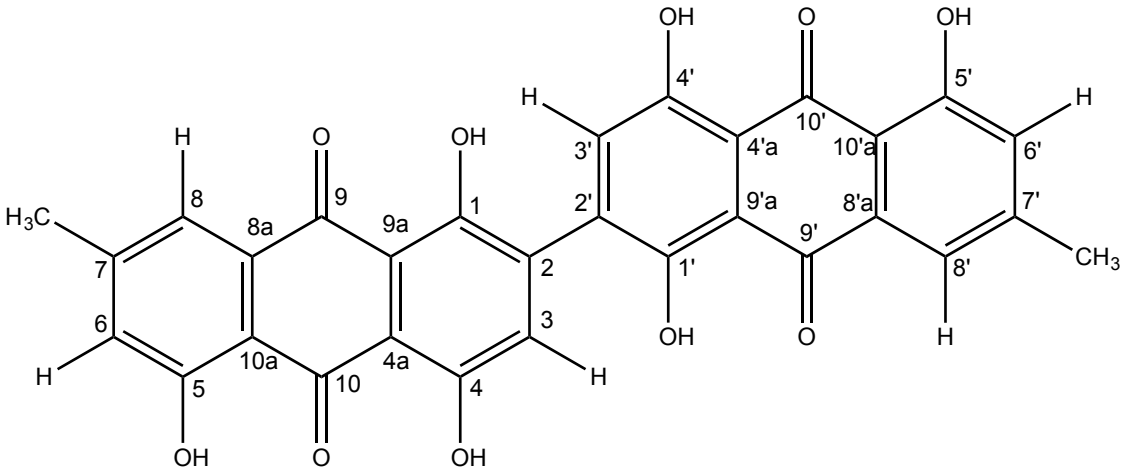

Figure 79. Structure of **XII**.

Compound **XII** was isolated as a reddish orange solid (mp. 258-260 °C). The IR spectrum showed absorption bands for hydroxyl (3463 cm^{-1}), conjugated ketone carbonyl (1622 cm^{-1}) and aromatic (1550 cm^{-1}) groups.

The ^{13}C NMR spectrum (**Table 15**) exhibited fifteen carbon signals which, in conjunction with DEPTs and HSQC spectra, can be categorized as two conjugated ketone carbonyls (δ_C 189.6 and 182.1), nine quaternary sp^2 (δ_C 164.4, 164.3, 161.1, 148.2, 133.2, 131.3, 123.5, 113.1 and 108.9), three methine sp^2 (δ_C 123.6, 120.5 and 107.2) and one tertiary methyl (δ_C 21.5) groups. The ^1H NMR spectrum (**Table 15**) showed one singlet at δ_H 6.73 and two double doublets at δ_H 7.15, dd (J = 1.0, 0.5 Hz) and 7.28, dd (J = 1.0, 0.5 Hz) of the aromatic protons and one singlet of the tertiary methyl (δ_H 2.33), in addition to two singlets of the hydrogen bonded hydroxyl groups at δ_H 12.04 and δ_H 12.79.

The ^1H and ^{13}C NMR features suggested that compound **XII** was a polyhydroxy-methyl anthraquinone. That one of the benzene rings of **XII** was a 3-hydroxy-5-methyl-1,2,3,5-tetrasubstituted was supported by the COSY correlations from the aromatic protons at δ_H 7.15 (J = 1.0, 0.5 Hz, H-6) and 7.28 (J = 1.0, 0.5 Hz, H-8) to the methyl protons at δ_H 2.33 as well as by the HMBC correlations from H-6 to C-8 (δ_C 120.5), C-5 (δ_C 161.1), C-10a (δ_C 113.1) and CH_3-7 (δ_C 21.5), from H-8 to C-6 (δ_C 123.6), C-10a and CH_3-7, as well as from OH-5 (δ_H 12.04, s) to C-5 (δ_C 161.1), C-6 and C-10a (**Table 15, Figure 80**). Since the methyl protons showed HMBC correlation with the carbon at δ_C 148.2, it was assigned to C-7.

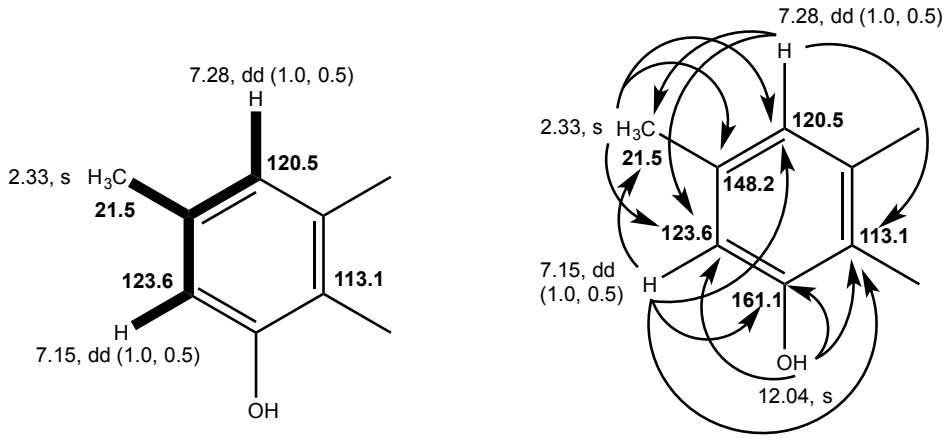

Figure 80. Key COSY (—) and HMBC (⟶) correlations of **XII.**

On the other hand, another benzene ring of **XII** was 3,6-dihydroxy-1,2,3,4,6-substituted since the HMBC spectrum (**Table 15, Figure 81**) exhibited correlations from the aromatic proton singlet at δ_H 6.73 (H-3) to C-1 (δ_C 164.3), C-4 (δ_C 164.4), C-4a (δ_C 108.9) as well as from the hydroxyl singlet at δ_H 12.79 (OH-4) to C-3 (δ_C 107.2), C-4 (δ_C 164.4) and C-4a (δ_C 108.9).

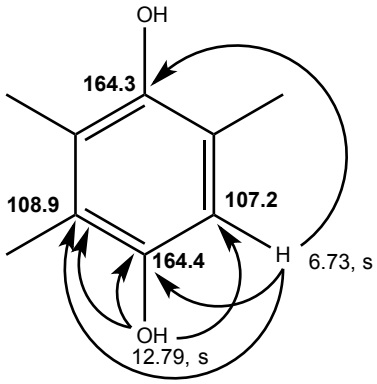

Figure 81. HMBC (⟶) correlations of compound **XII.**

Moreover, the HMBC spectrum (**Table 15**) also exhibited a cross peak from H-8 to the carbonyl carbon at δ_C 182.1, the latter was assigned to C-9. Since, there was no cross peak from H-3 to either of the carbonyl carbons, the carbonyl carbon at δ_C 189.6 was assigned to C-10. The higher chemical shift value of C-10 than that of C-9 was justified by its hydrogen bonding with both OH-4 and OH-5. By comparing the ^{13}C NMR spectrum of XII to those of other anthraquinones isolated from this fungus, i.e. emodin (**VI**), citreorosein (**VIII**), fallacinol (**IX**) and rheoemodin (**X**), the carbons at δ_C 131.3 and δ_C 133.2 were assigned to C-8a and C-9a, respectively. Therefore, the structure of **XII** was tentatively established as 7-methyl-1,4,5-trihydroxy-9,10-anthraquinone (**Figure 82**).

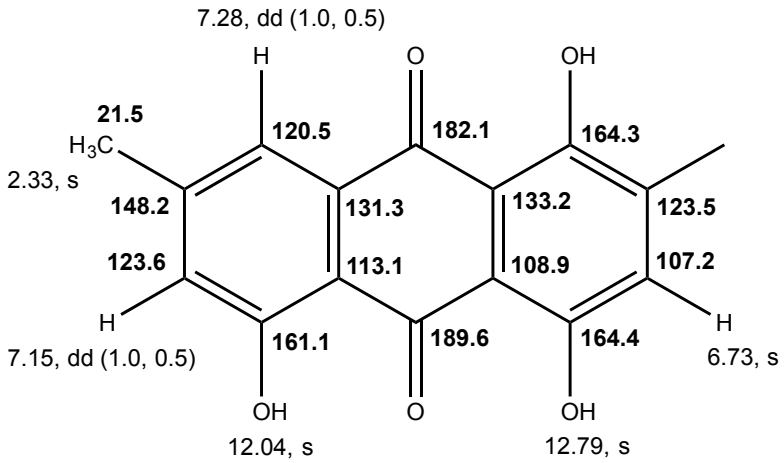

Figure 82. Partial structure of 7-methyl-1,4,5-trihydroxy-9,10-anthraquinone.

However, this structure ($C_{15}H_9O_5$) was not complete since there was no substituent on C-2 (δ_C 123.5) to be accounted for. Since the (+)-HRESIMS of **XII** gave the $[M+H]^+$ peak at *m/z* 539.0942 $[M+H]^+$, corresponding to $C_{30}H_{19}O_{10}$ (calculated 539.0978), the molecular formula of **XII** was $C_{30}H_{18}O_{10}$ (twenty two degrees of unsaturation). Therefore, the structure of **XII** was a dimer of 7-methyl-1,4,5-trihydroxy-9,10-anthraquinone.

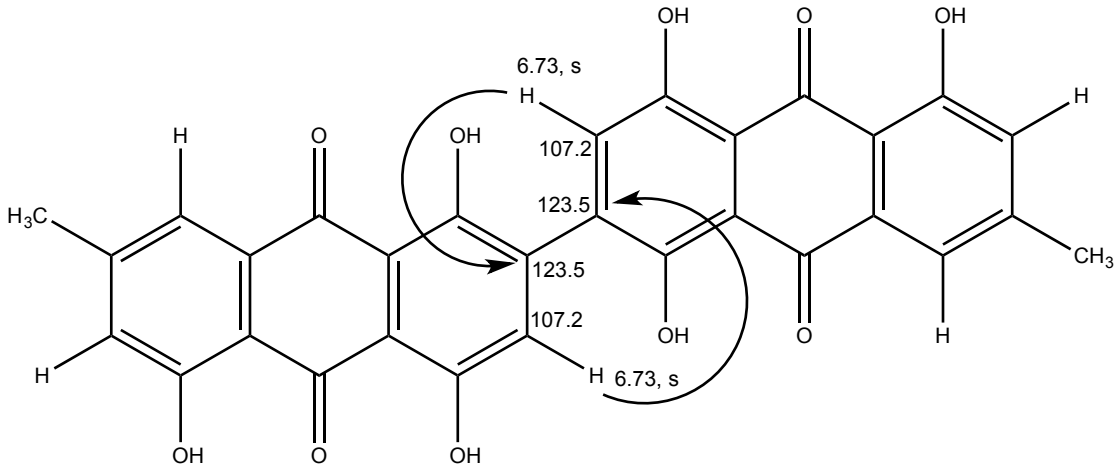

Figure 83. HMBC correlations of the dimer of 7-methyl-1,4,5-trihydroxy-9,10-anthraquinone.

This structure was also supported by the HMBC correlation (**Figure 83)** from H-2 to the quaternary sp^2 carbon at δ_C 123.5 (C-2'). Therefore, the structure of **XII** was established as 2, 2'-*bis*-(7-methyl-1,4,5-trihydroxy-anthracene-9,10-dione).

Literature search revealed that Tan *et al.* (2008) have reported isolation of the structurally similar *bis*-anthraquinone, named 2240A, from an unidentified endophytic fungus (strain no 2240), isolated from the estuarine mangrove from the South China Sea Coast. The structure of 2240A is also a dimer of 7-methyl-1,4,5-trihydroxy-9,10-anthraquinone, however, the two anthraquinone monomers are linked between C-3 and C-3' (i.e. C-1/1' for the numbering used by Tan *et al.* (2008)) instead of C-2 and C-2' as in **XII**. Surprisingly, the ^{1}H and ^{13}C NMR chemical shift values reported for 2240A by Tan *et al.* (2008) were very similar to those of **XII**. Although the structures of **XII** and 2240A cannot be distinguished by HMBC correlations, careful analysis of the ^{1}H and ^{13}C NMR data of 2240A revealed that Tan *et al.* (2008) assigned the chemical shift values to some of the carbons differently from what we assigned for **XII**. Tan *et al.* (2008) assigned the carbon signal at δ_C 108.7 to C-9a/9'a (i.e. C-14/14' for the numbering used by Tan *et al.* (2008)) instead of C-4a/4'a (i.e. C-13/13' for the numbering used by Tan *et al.* (2008)) and the carbon signal at δ_C 131.8 to C-4a/4'a (i.e. C-13/C-13' for the numbering use by Tan *et al.* (2008)) instead of C-9a/9'a (i.e. C-13/C-13' for the numbering used by Tan *et al.* (2008)). This assignment seems to be incorrect since the chemical values of C-4a and C-10a of a series of anthraquinones with the hydroxyl groups on C-4 and C-5 isolated from this extract, i.e. emodin (**VI**), citreorosein (**VIII**), fallacinol (**IX**) and rheoemodin (**X**), are δ_C 108 and 115 ppm, which is far from δ_C 133 ppm proposed by Tan *et al.* (2008). Consequently, we are convinced that the structure proposed for 2240A is not correct (**Figure 84**).

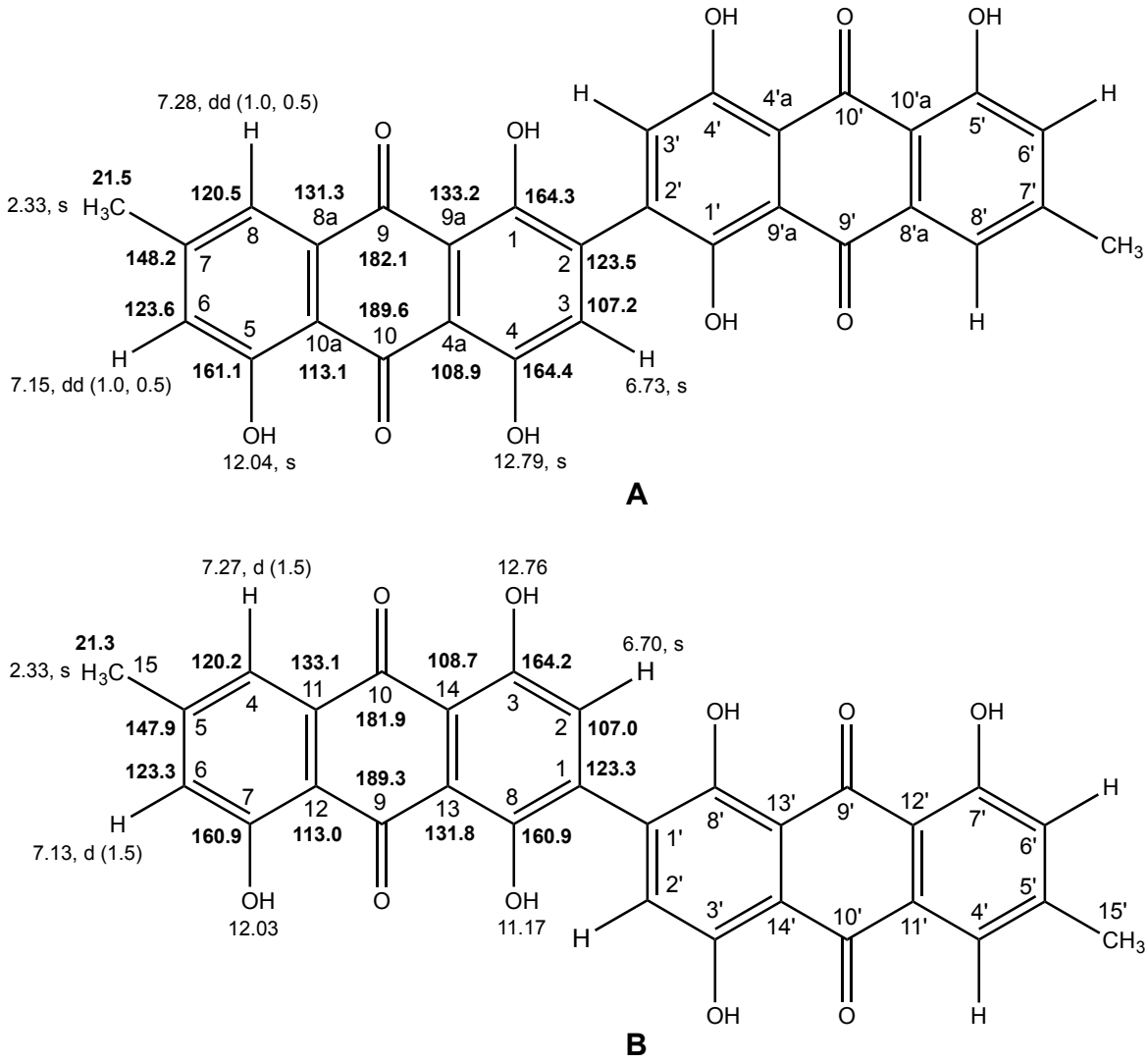

Figure 84. Comparison of the ^{1}H and ^{13}C NMR data of **XII** (**A**) and 2240A (**B**) (Tan *et al.* 2008).

Interestingly, Tan *et al.* (2008) reported 2240A as dextrorotatory, displaying $[\alpha]^{20}_{D}$ +62.50 (*c* 0.08, dioxin). On the contrary, **XII** is levorotatory having $[\alpha]^{20}_{D}$ -40 (*c* 0.05, dioxin) and -100 (*c* 0.05, MeOH), respectively. Since **XII** can be considered as a bridged biphenyl, it can have a phenomenon of atropisomerism due to a restricted rotation of the phenyl rings around the C-2/C-2' bond. Therefore, **XII** and 2240A, previously reported by Tan *et al.* (2008) are different and could probably be atropisomers (**Figure 85**).

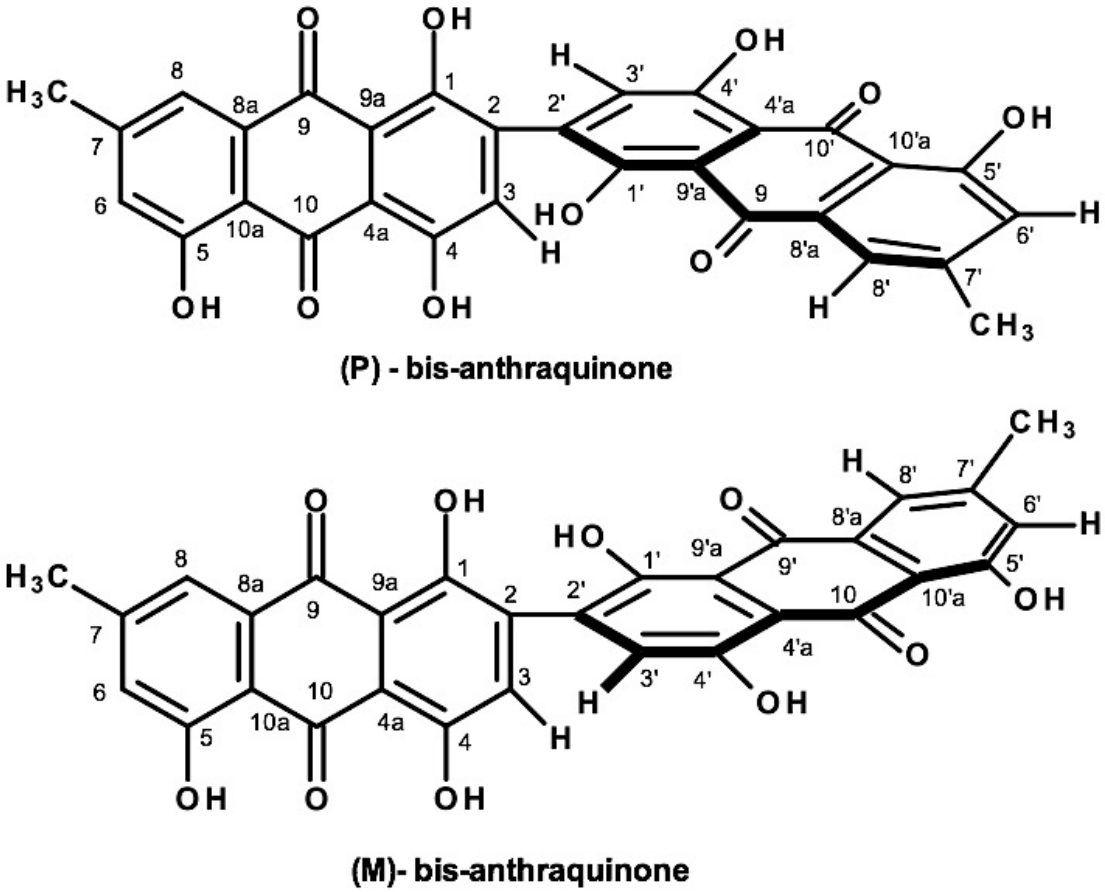

Figure 85. Atropisomers of **XII**, (**P**): right-handed helix, (**M**): left-handed helix.

The structure of **XII** can be viewed as a dimer of helminthosporin, the anthraquinone previously isolated from the subterranean stems of *Aloe saponaria* Haw.(Yagi *et al.*, 1977) and also from the roots of *Berchemia floribunda* (Wei *et al.*, 2008). However, to the best of our knowledge, there is no report so far on the isolation of *bis*-anthraquinone with this structure.

Table 15. ^{1}H and ^{13}C NMR (DMSO, 500.13 MHz and 125.4 MHz) and HMBC assignment for *2, 2'-bis*-(7-methyl-1,4,5-trihydroxy-anthracene-9,10-dione) (**XII**).

Position	δ_C, type	δ_H, mult. (*J* in Hz)	COSY	HMBC
1 (1')	164.3, C	---	---	---
2 (2')	123.5, C	---	---	---
3 (3')	107.2, CH	6.73, s	---	C-1 (1'), 4 (4'), 2 (2'), 4a (4'a)
4 (4')	164.4, C	---	---	---
4a (4'a)	108.9, C	---	---	---
5 (5')	161.1, C	---	---	---
6 (6')	123.6, CH	7.15, dd (1.0, 0.5)	H-8 (8'), Me-7 (7')	C-5 (5'), 7 (7'), 8 (8'), 10a (10'a)
7 (7')	148.2, C	---	---	---
8 (8')	120.5, CH	7.28, dd (1.0, 0.5)	H-6 (6'), Me-7 (7')	C-6 (6'), 7 (7'), 9 (9'), 10a (10'a)
8a (8'a)	131.3, C*	---	---	---
9 (9')	182.1, CO	---	---	---
9a (9'a)	133.2, C*	---	---	---
10 (10')	189.6, CO	---	---	---
10a (10'a)	113.1, C	---	---	---
CH_3-7 (7')	21.5, CH_3	2.33, s	H-6 (6'), 8 (8')	C-6 (6'), 7 (7'), 8 (8')
OH-4 (4')	---	12.79, s	---	C-3 (3'), 4 (4'), 4a (4'a)
OH-5 (5')	---	12.04, s	---	C-5 (5'), 6 (6'), 10a (10'a)

*can be interchanged.

4.3. Biological Activity Tests

4.3.1. Anti-obesity activity on the zebrafish Nile red assay

Emodin (**VI**), questinol (**VII**), citreorosein (**VIII**), fallacinol (**IX**), rheoemodin (**X**) and secalonic acid A (**XI**) were tested for their anti-obesity activity on the zebrafish Nile red assay using resveratrol as a positive control as described in Jones et al. (Jones *et al.*, 2008). The result showed that only the anthraquinones questinol (**VII**) and citreorosein (**VIII**) reduced > 60% and > 90% of the stained lipids with the IC_{50} values of 0.95 and 0.17 µM, respectively. The positive control resveratrol (REV) had an IC_{50} value of 0.6 µM (**Figure 86**).

Interestingly, emodin (**VI**) and secalonic acid A (**XI**) caused toxicity (death) for all exposed zebrafish larvae after 24h while fallacinol (**IX**) and rheoemodin (**X**) did not have any significant effects (**Figure 87**).

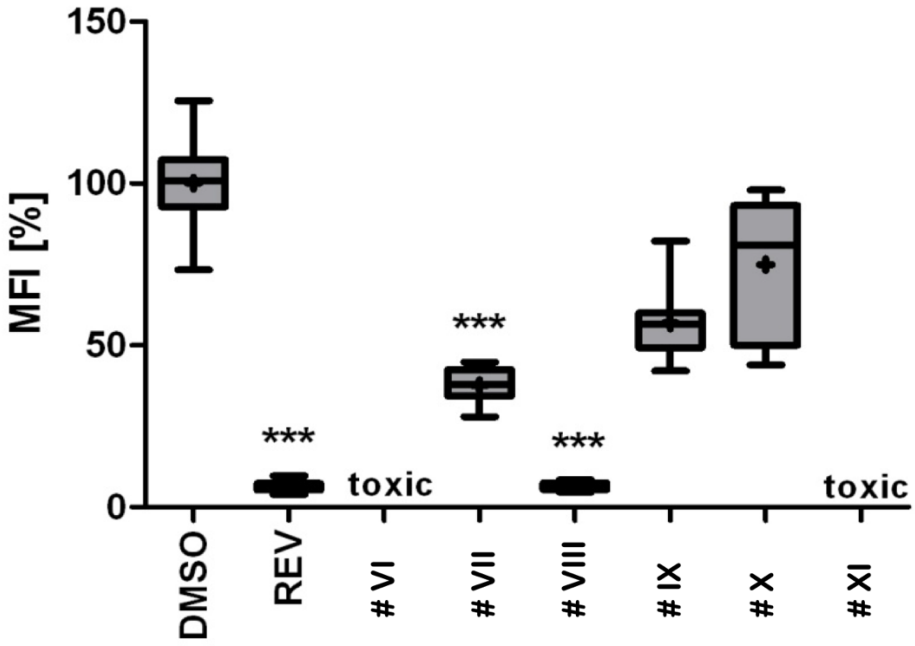

Figure 86. Anti-obesity activity of compounds **VI-XI** in the zebrafish larvae Nile red assay. The solvent control had 0.1% DMSO and the positive control received 50 µM resveratrol (REV). Values are presented as mean fluorescent intensity (MFI) relative to the DMSO group, and are derived from 10-12 individual larvae per treatment group. Statistical differences to the solvent control are indicated with asterisks, *** = $p < 0.001$.

It is interesting to observe that questinol (**VII**), citreorosein (**VIII**) and fallacinol (**IX**) are structurally similar, all having a hydroxymethyl group on C-6 and a hydroxyl group on

C-8. Replacing the hydroxyl group on C-1 by a methoxyl group, as in questinol (**VII**), diminishes the activity whereas replacing the hydroxyl group on C-3 with a methoxyl group, as in fallacinol (**IX**), completely removes the anti-obesity activity. Therefore, it seems that the hydroxymethyl group on C-6 and the hydroxyl groups on C-3 and C-8 are necessary for the anti-obesity activity of the polyhydroxy anthraquinones.

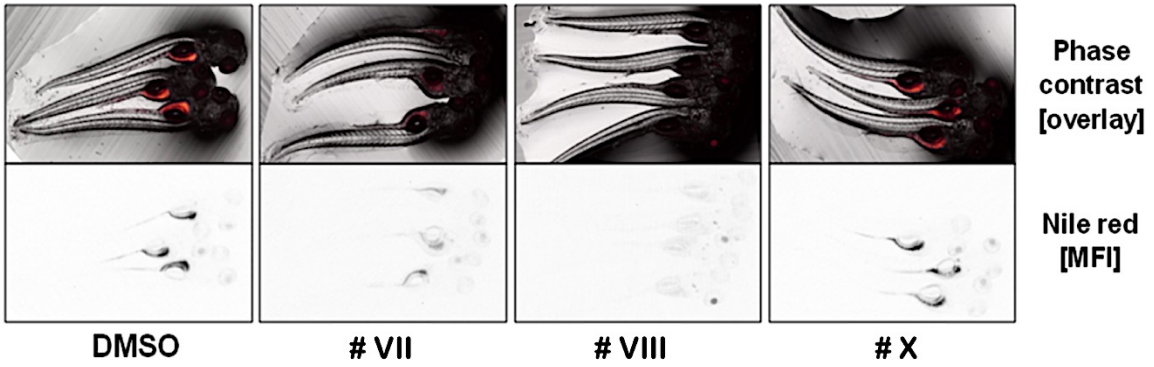

Figure 87. Representative images of the zebrafish Nile red assay. The upper images show the overlay of the fluorescence and phase contrast; the lower images show the mean fluorescence intensity (MFI) given as black and white picture. DMSO, solvent control 0.1%.

CHAPTER 5

5. Conclusion

This study describes the isolation, purification, structure elucidation and anti-obesity activity evaluation of the secondary metabolites produced by the fungus *Talaromyces stipitatus* KUFA 0207, isolated from the marine sponge *Stylissa flabelliformis* which was collected from the Gulf of Thailand.

Isolated from the crude ethyl acetate extract of the culture of this fungus are a new ergosterol derivative, talarosterone (**V**), a new *bis*-anthraquinone derivative, *bis*-(7-methyl-1,4,5-trihydroxy-anthracene-9,10-dione) (**XII**), in addition to ten known compounds including palmitic acid (**I**), ergosterol-5,8-endoperoxide (**II**), ergosta-4,6,8 (14),22-tetraen-3-one (**III**), cyathisterone (**IV**) and the previous reported anthraquinones include emodin (**VI**), questinol (**VII**), citreorosein (**VIII**), fallacinol (**IX**), rheoemodin (**X**) as well as secalonic acid A (**XI**).

Emodin (**VI**) has been previously reported from the fungus *Talaromyces stipitatus* chemotype II (Frisvad *et al.*, 1990), while the other obtained metabolites have never been reported from this fungal species. Interestingly, talarosterone (**V**) and the *bis*-anthraquinone derivative (**XII**) are new compounds whose structure and stereochemistry were established by 1D and 2D NMR techniques, including ^{1}H, ^{13}C NMR, DEPT, COSY, HSQC, and HMBC. Moreover, talarosterone (**V**) was also determined the stereochemistry by X-ray crystallographic analysis.

Compound **VI**–**XI** were tested for their anti-obesity activity by the zebrafish Nile red assay using resveratrol as a positive control. Citreorosein (**VIII**) exhibited a strong anti-obesity activity (IC_{50} = 0.17 μM) while questinol (**IX**) showed moderate activity (IC_{50} = 0.95 μM) in this test system. Analysis of the structures of the anthraquinones tasted revealed that the hydroxymethyl group on C-6 and the hydroxyl groups on C-3 and C-8 are required for the anti-obesity activity. The results obtained from this study suggested that marine-derived fungi of the genus *Talaromyces* can be a promising source of compounds with potential anti-obesity activity.

CHAPTER 6

6. Appendix

6.1 NMR Spectra of Isolated Compounds

6.1.1 NMR Spectrum of Palmitic acid (I)

^{1}H NMR spectrum (500.13 MHz)

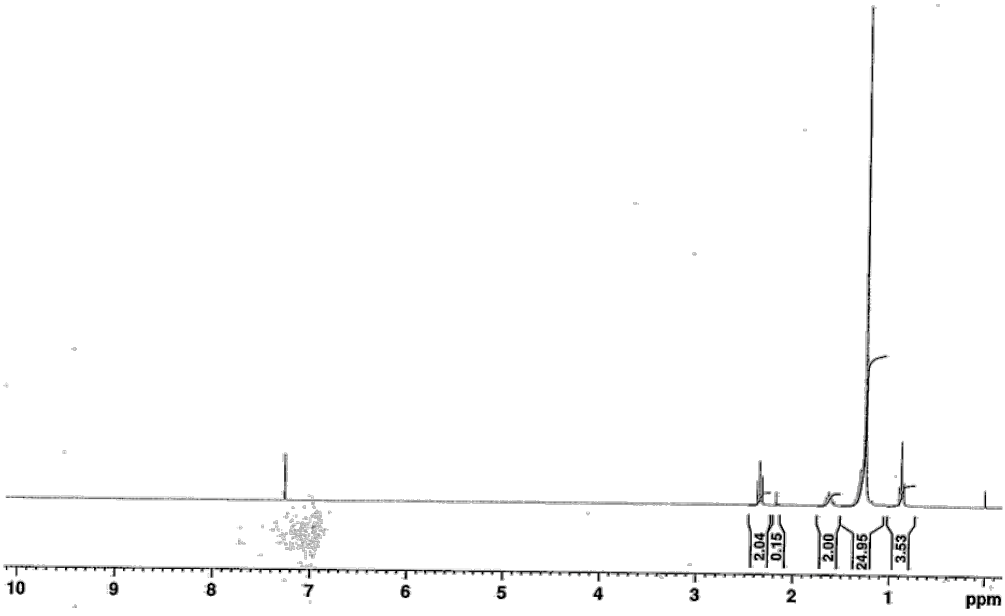

^{13}C NMR spectrum (125.4 MHz)

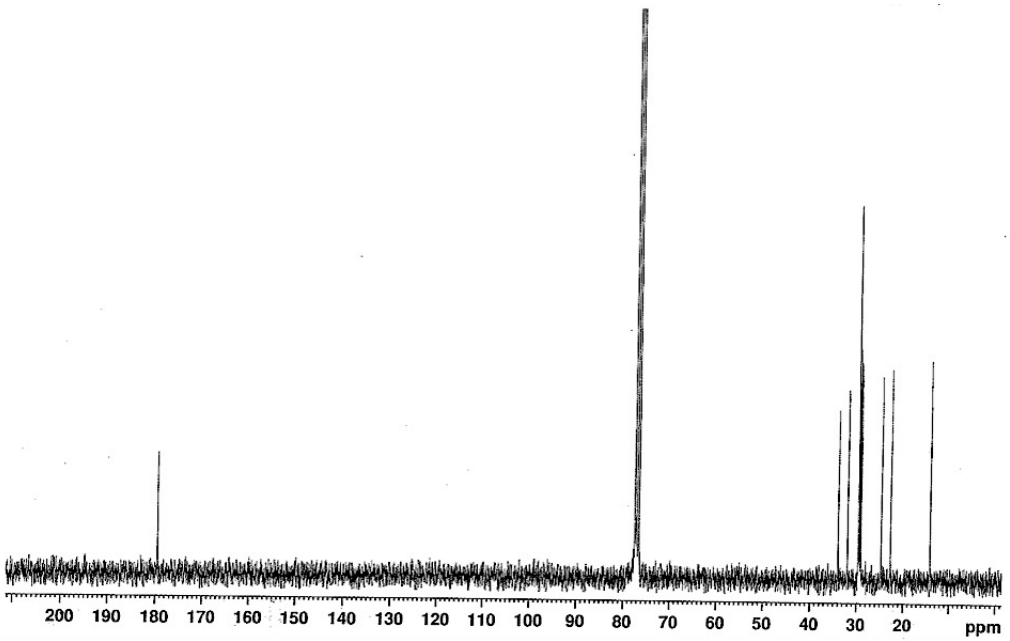

6.1.2 NMR Spectrum of Ergosterol-5,8-endoperoxide (II)

^{1}H NMR spectrum (300.13 MHz)

^{13}C NMR spectrum (75.4 MHz)

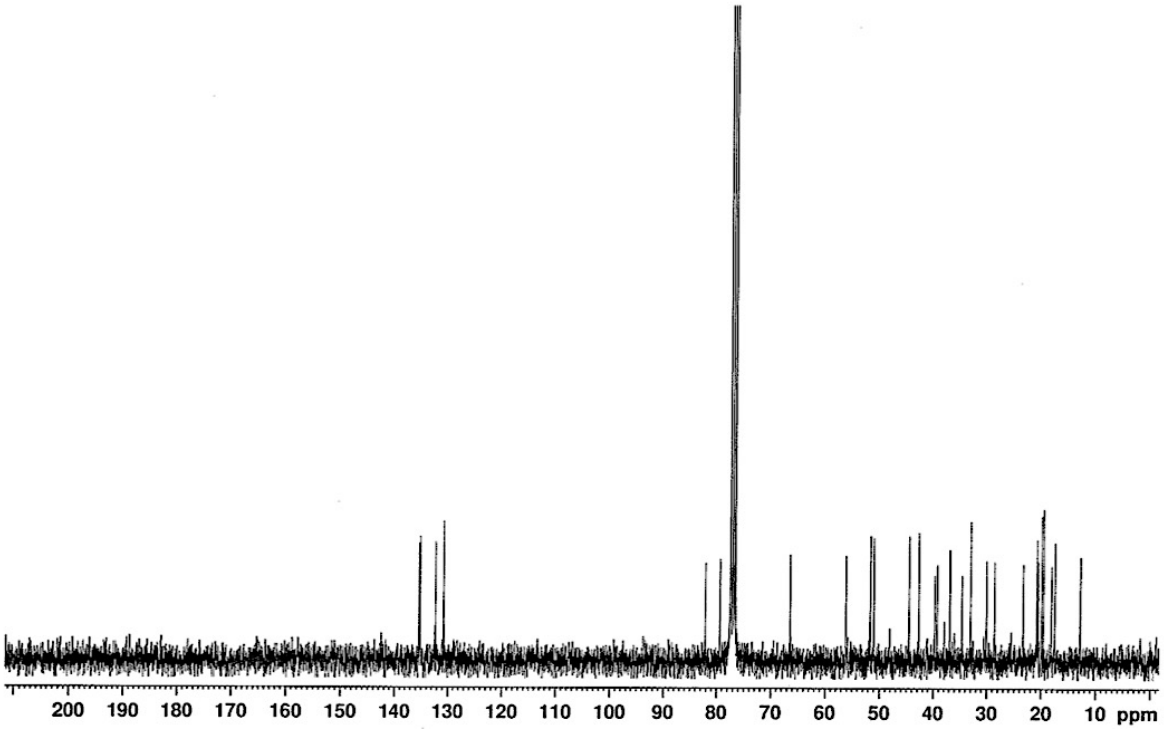

6.1.3 NMR Spectrum of Ergosta-4,6,8(14),22-tetraen-3-one (III)

^{1}H NMR spectrum (300.13 MHz)

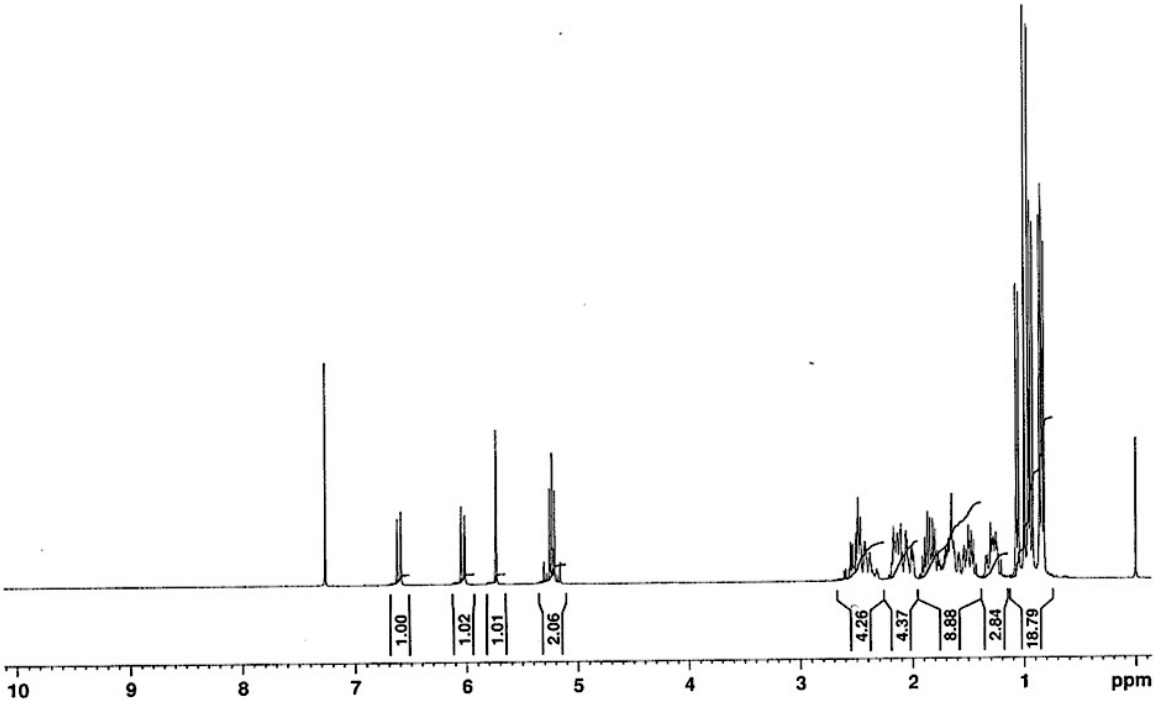

^{13}C NMR spectrum (75.4 MHz)

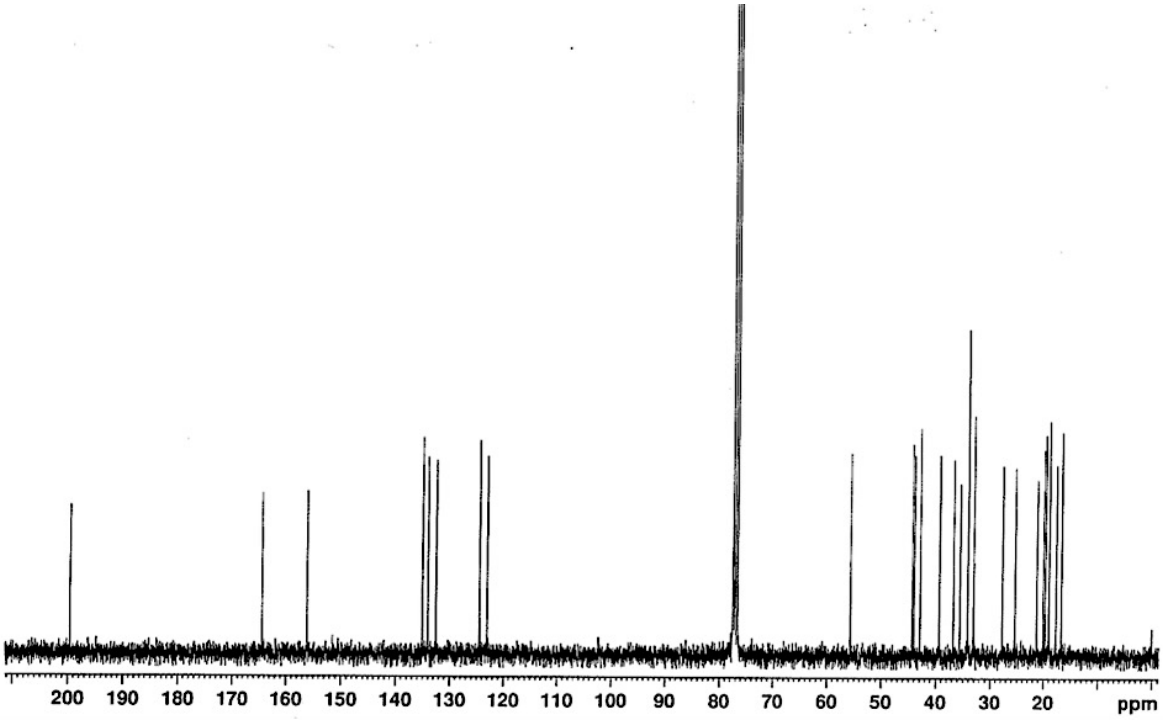

6.1.4 NMR Spectrum of Cyathisterone (IV)

^{1}H NMR spectrum (300.13 MHz)

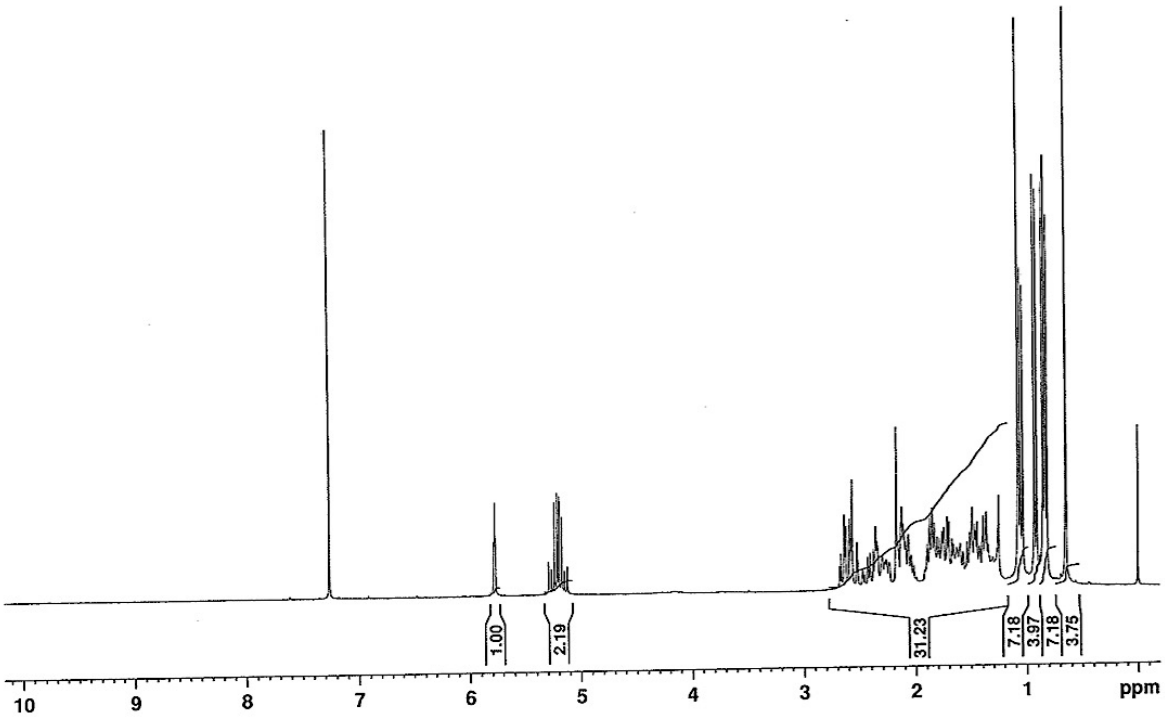

^{13}C NMR spectrum (75.4 MHz)

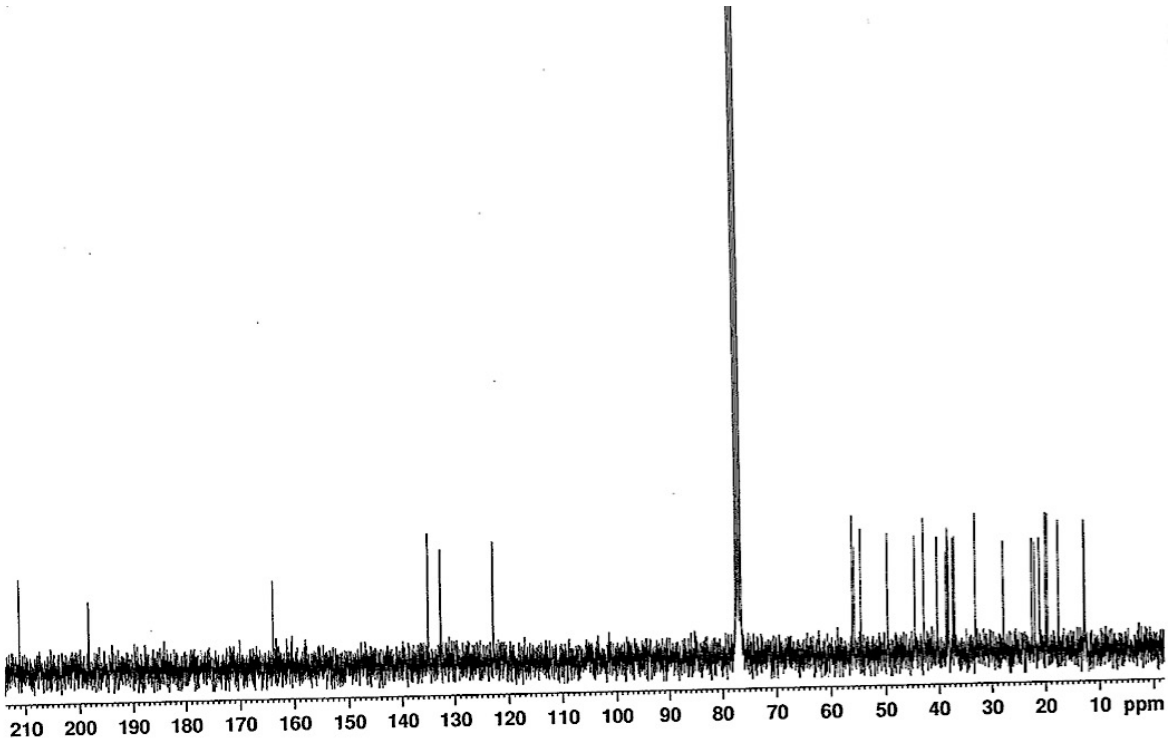

6.1.5 NMR Spectrum of Talarosterone (V)

^{1}H NMR spectrum (300.13 MHz)

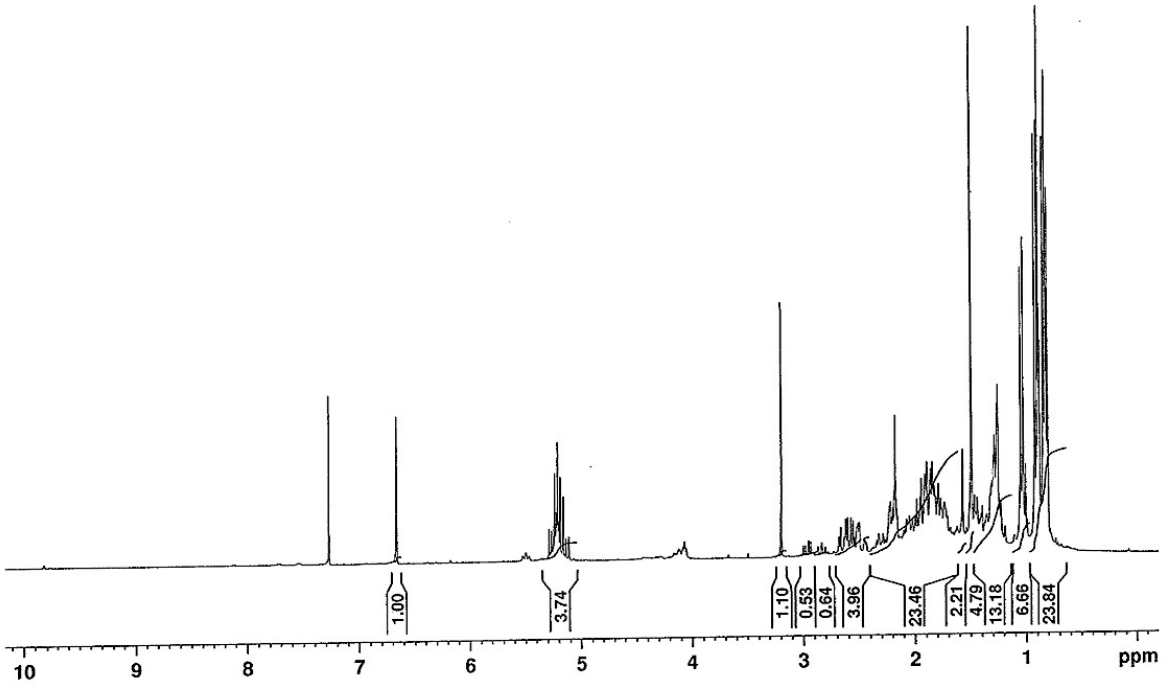

^{13}C NMR spectrum (75.4 MHz)

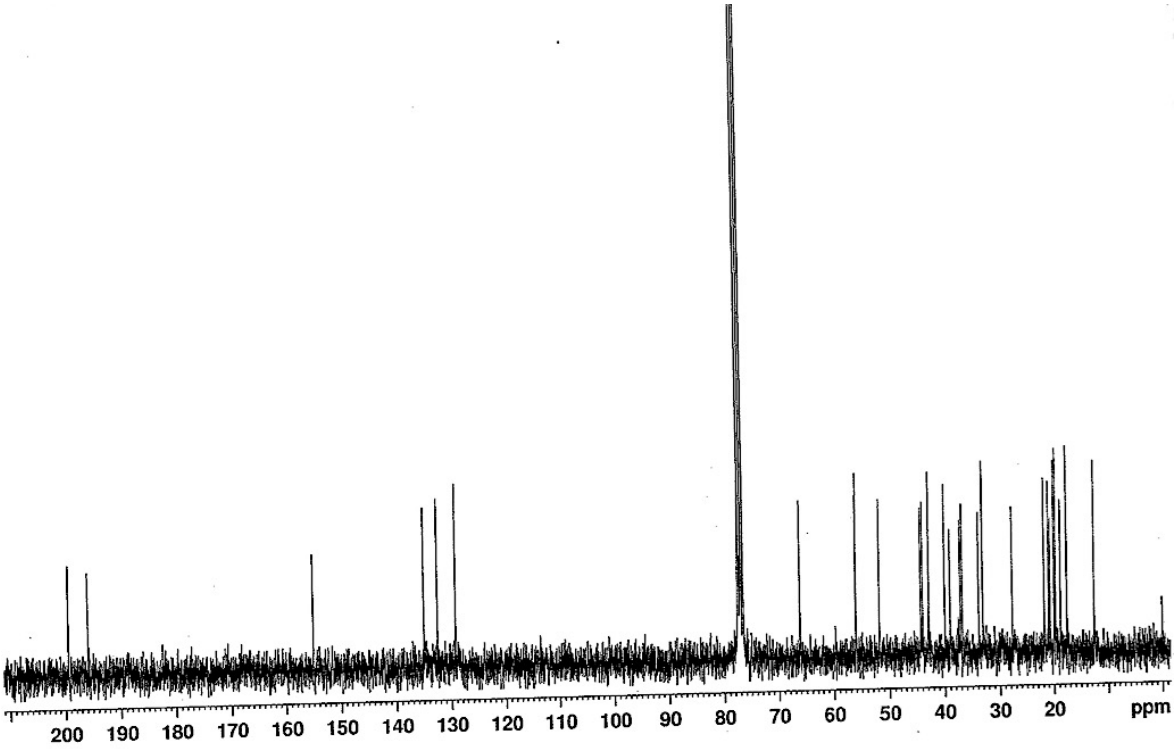

6.1.6 NMR Spectrum of Emodin (VI)

^{1}H NMR spectrum (500.13 MHz)

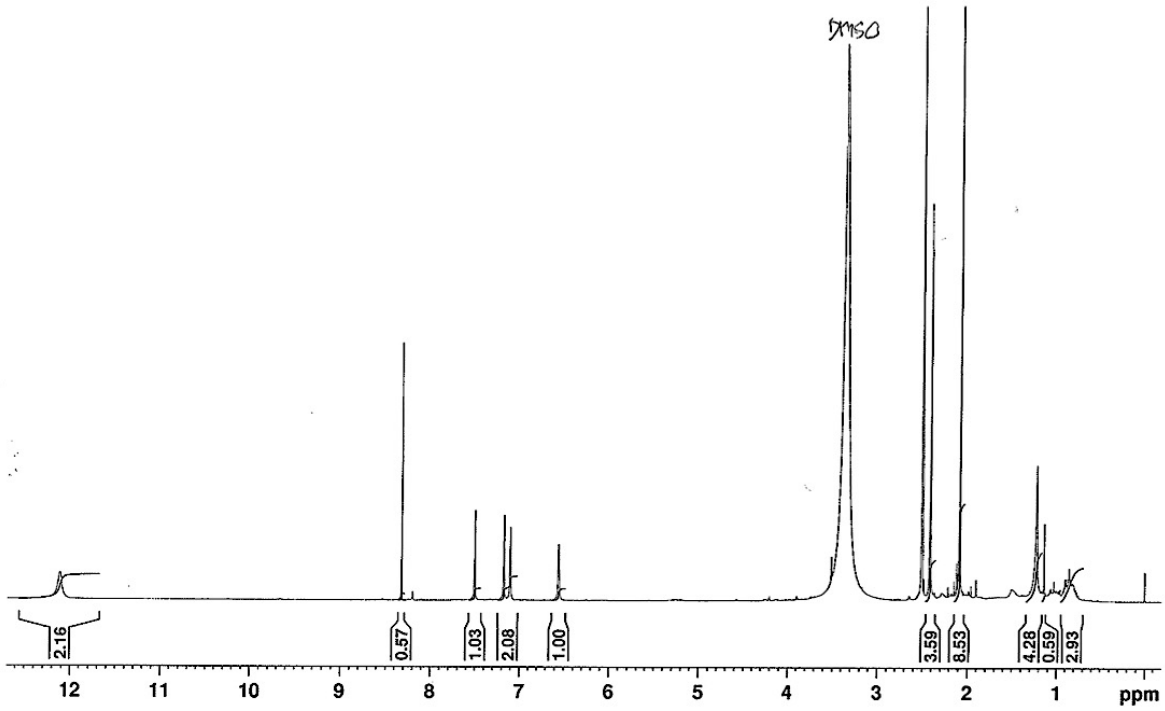

^{13}C NMR spectrum (125.4 MHz)

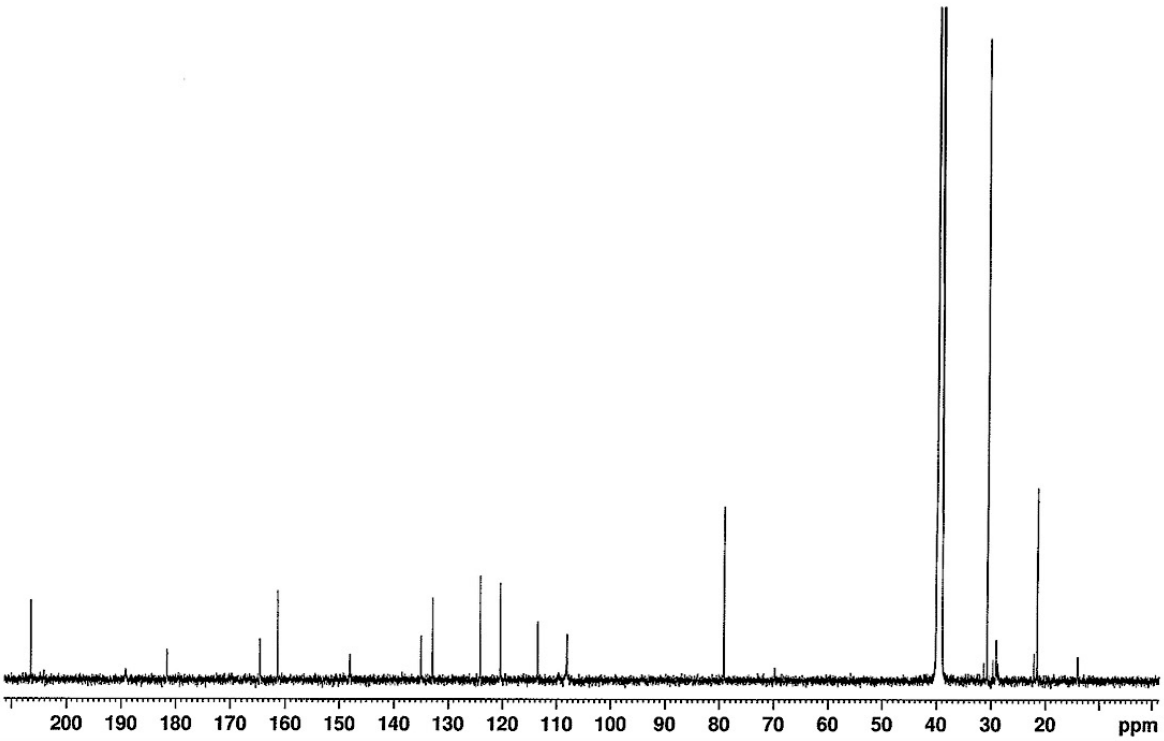

6.1.7 NMR Spectrum of Questinol (VII)

^{1}H NMR spectrum (300.13 MHz)

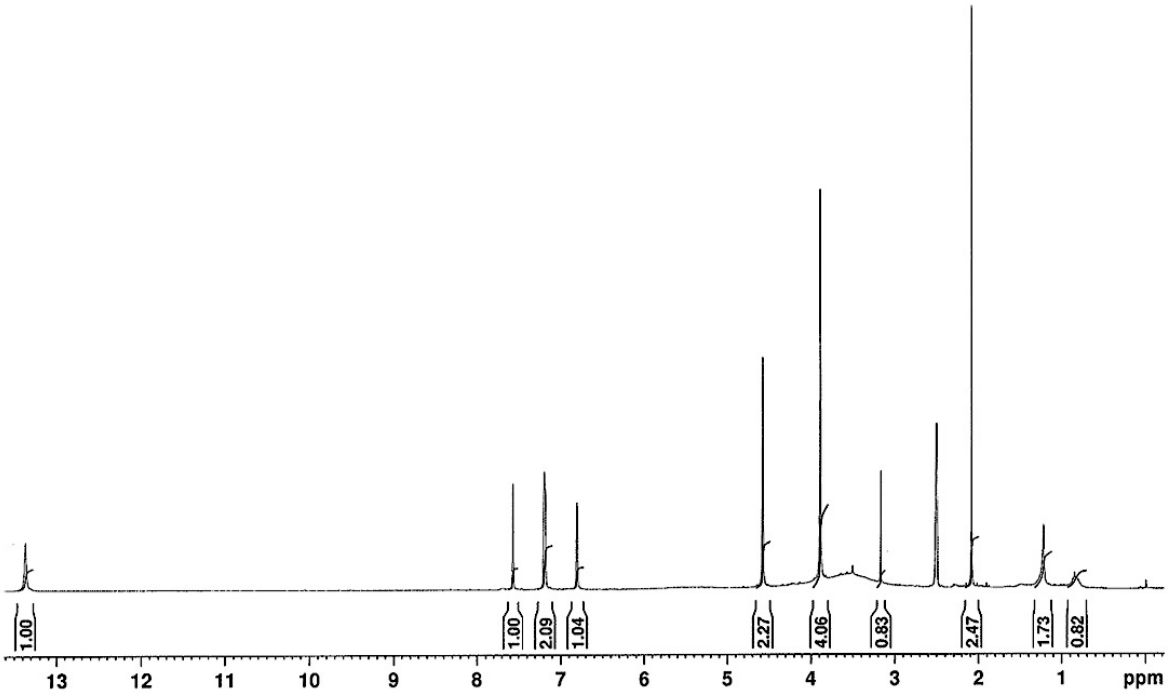

^{13}C NMR spectrum (75.4 MHz)

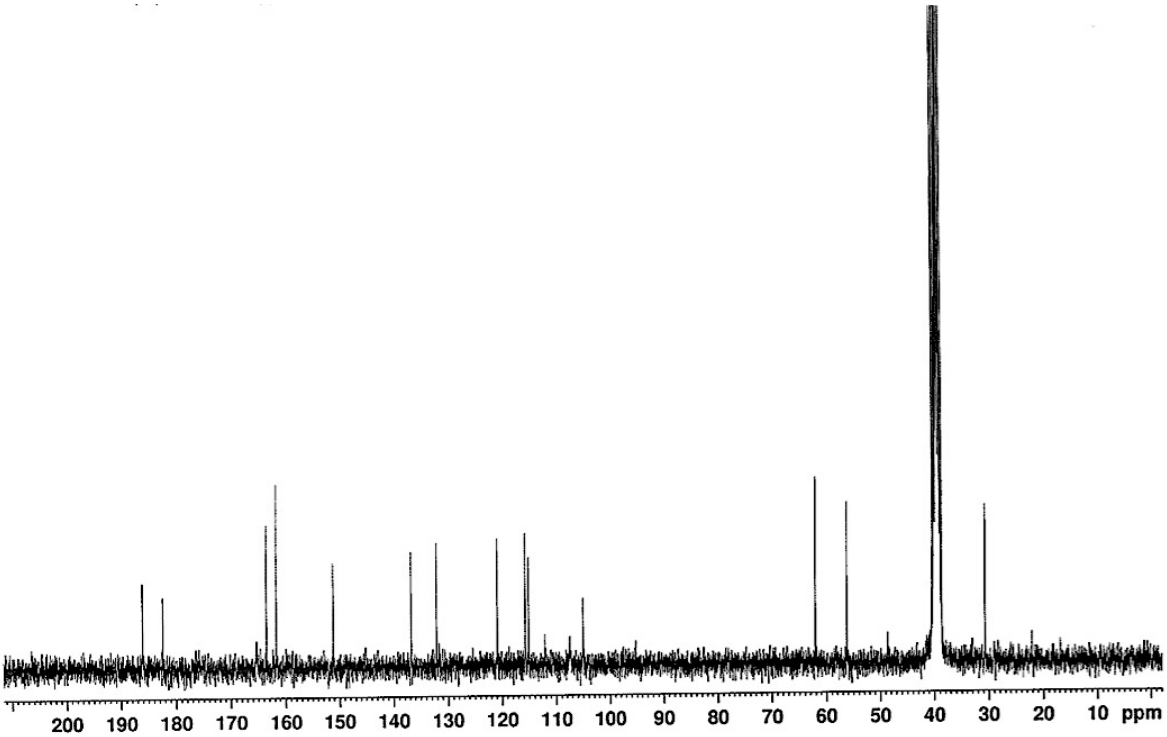

6.1.8 NMR Spectrum of Citreorosein (VIII)

^{1}H NMR spectrum (500.13 MHz)

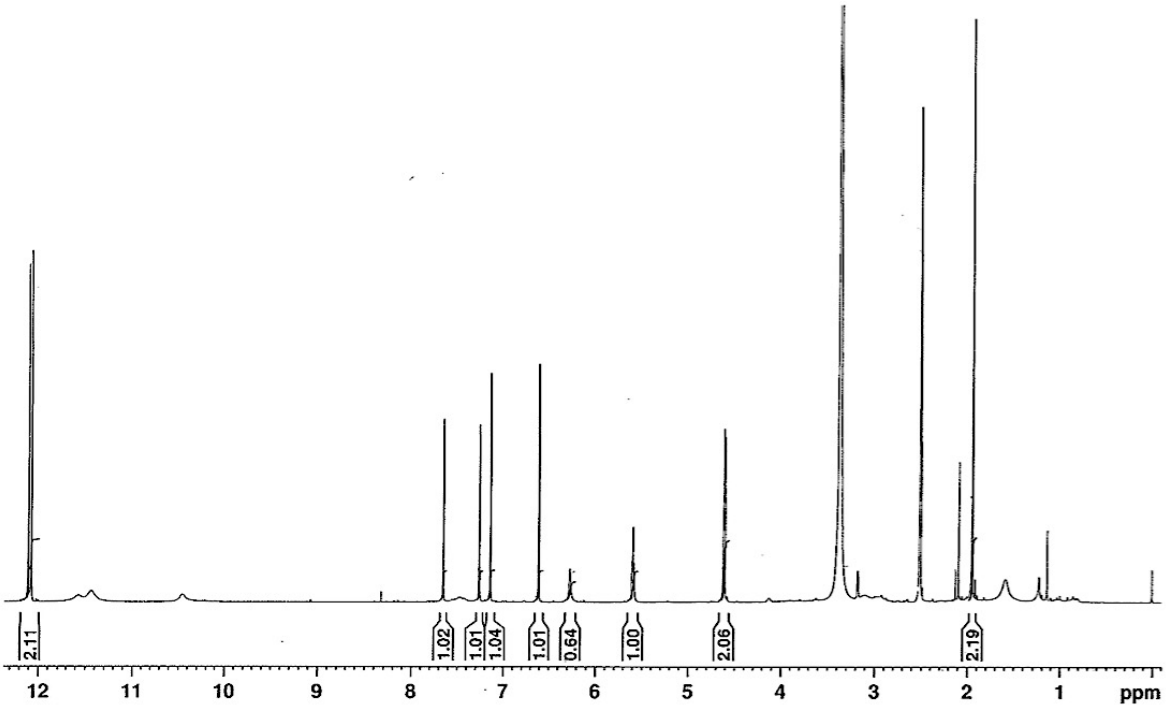

^{13}C NMR spectrum (125.4 MHz)

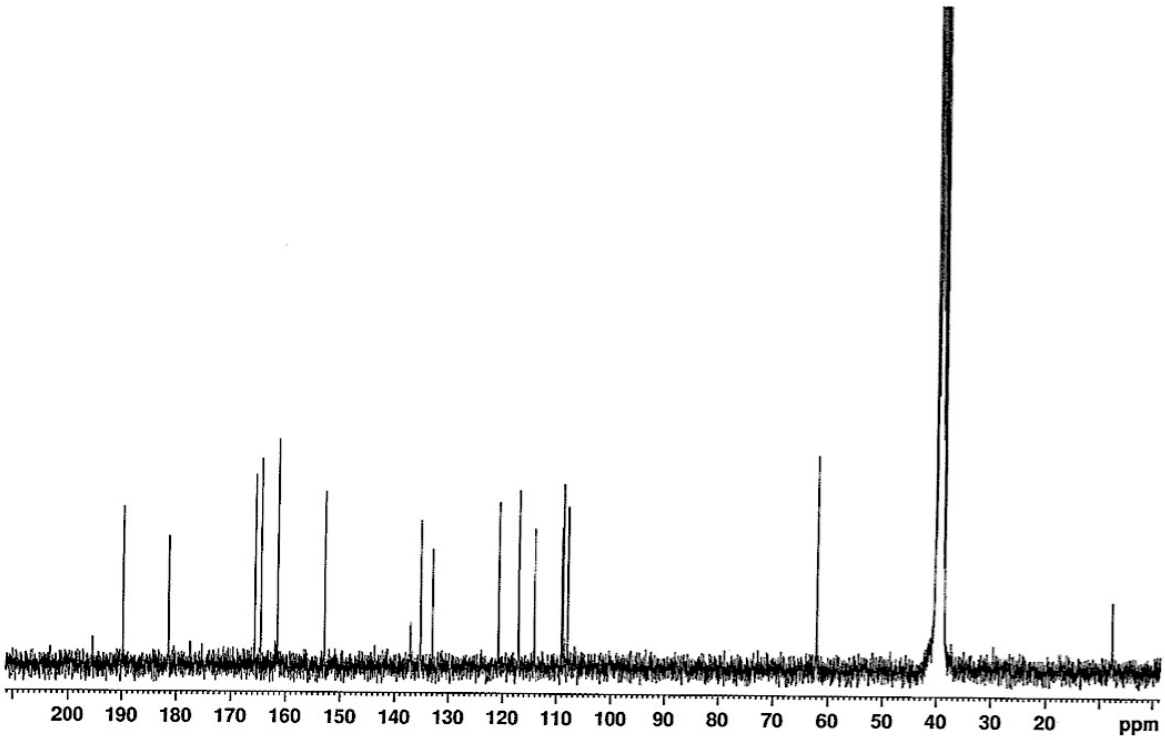

6.1.9 NMR Spectrum of Fallacinol (IX)

^{1}H NMR spectrum (500.13 MHz)

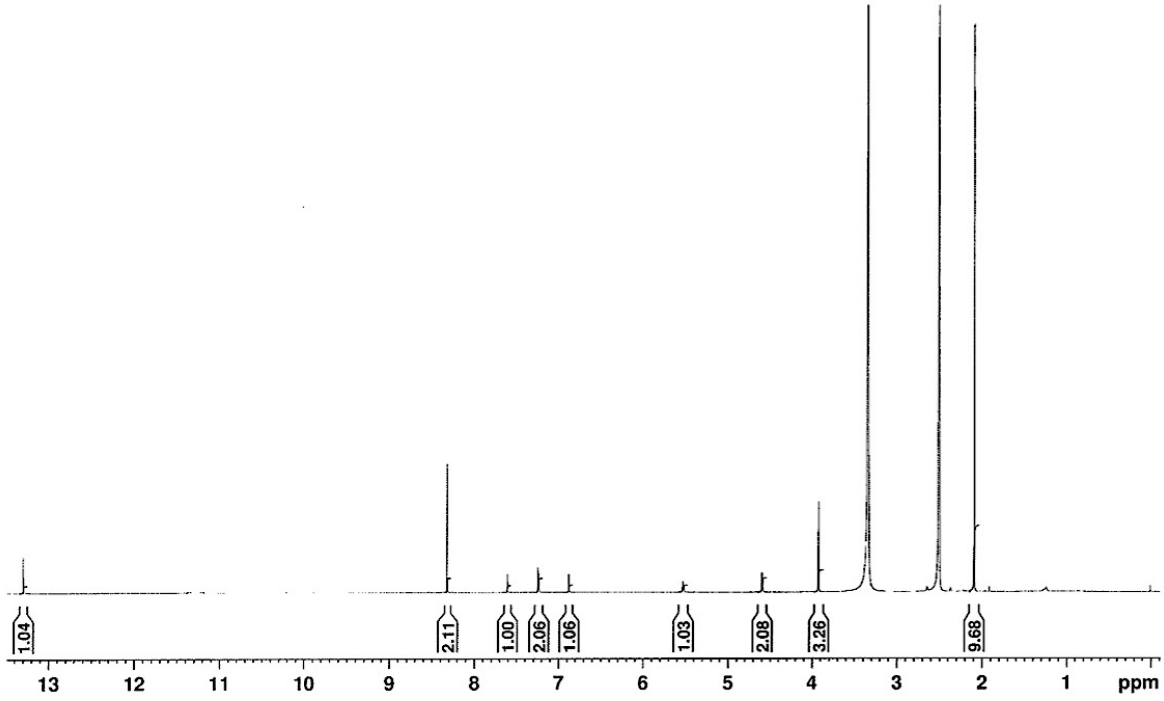

^{13}C NMR spectrum (125.4 MHz)

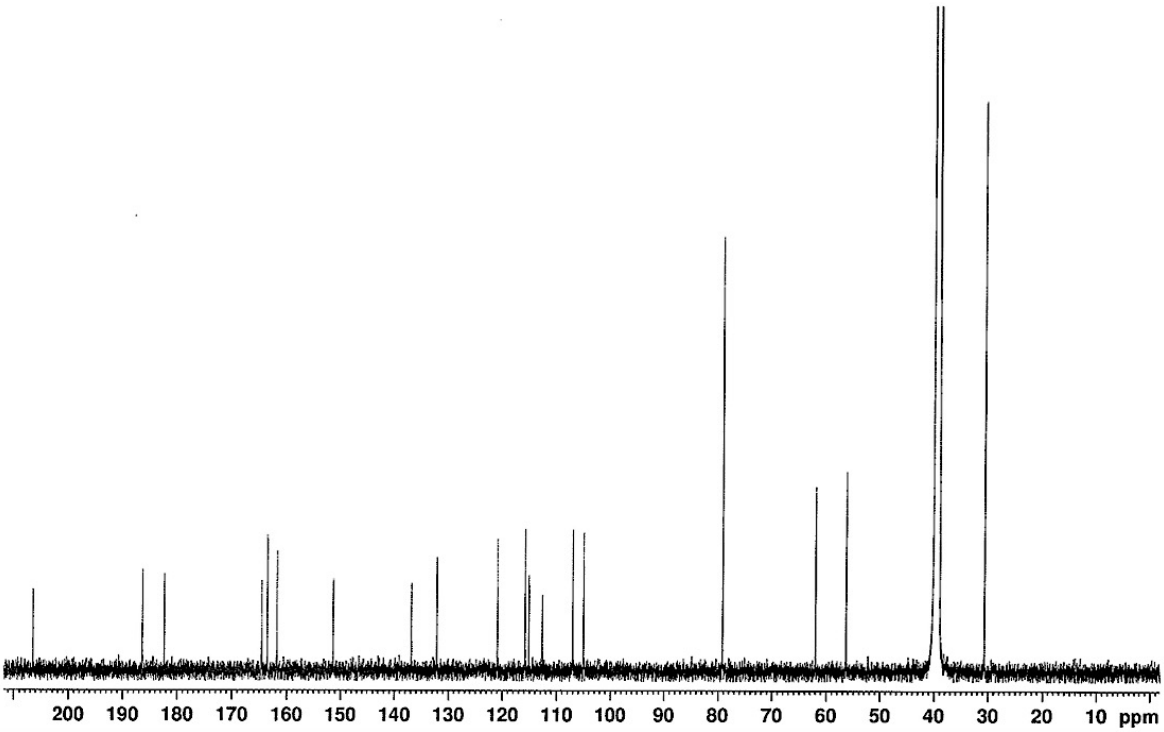

6.1.10 NMR Spectrum of Rheoemodin (X)

^{1}H NMR spectrum (300.13 MHz)

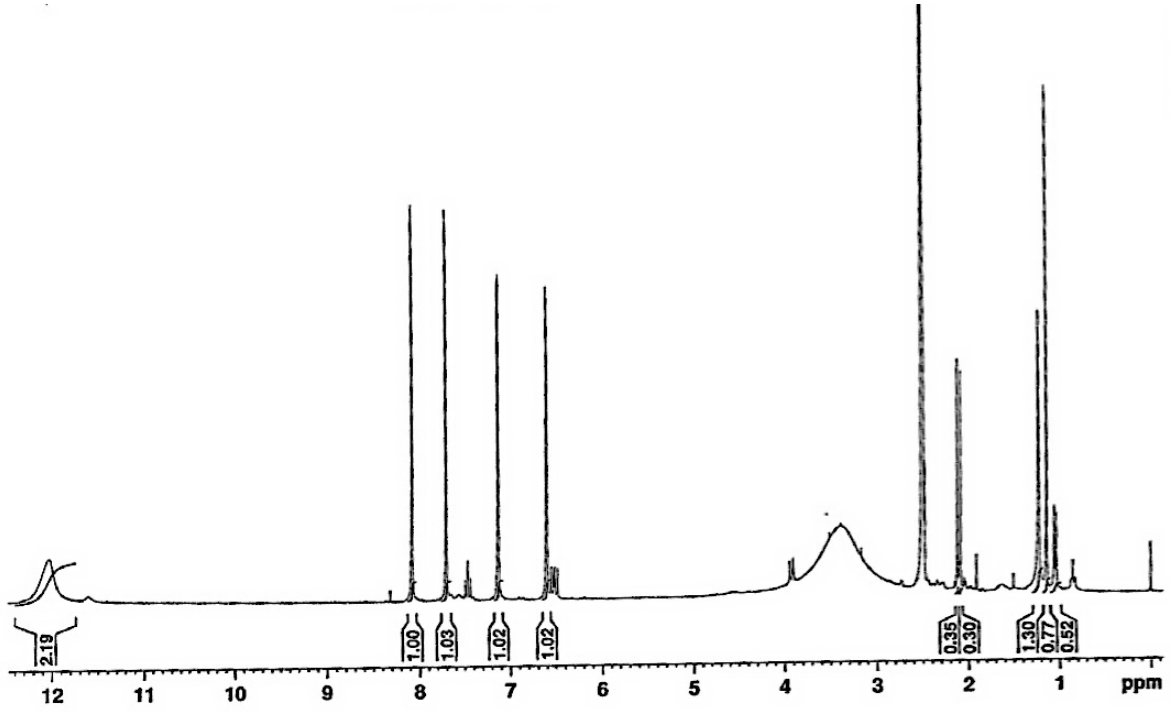

^{13}C NMR spectrum (75.4 MHz)

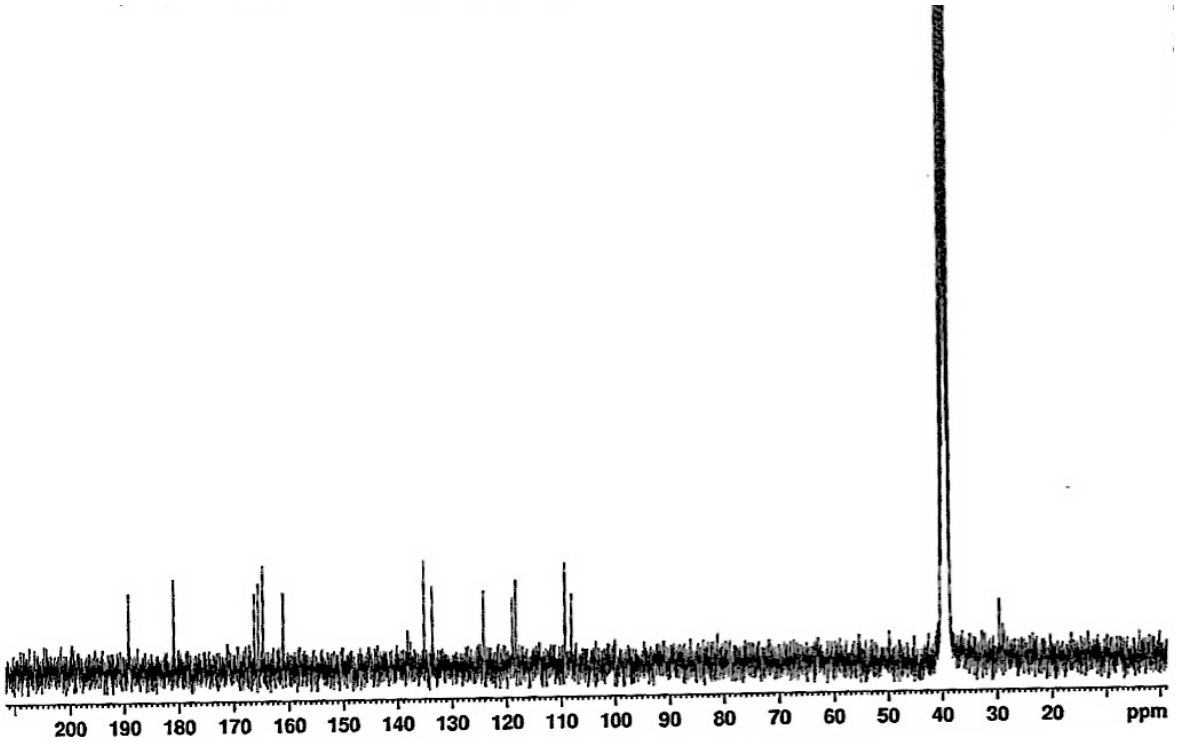

6.1.11 NMR Spectrum of Secalonic Acid A (XI)

^{1}H NMR spectrum (300.13 MHz)

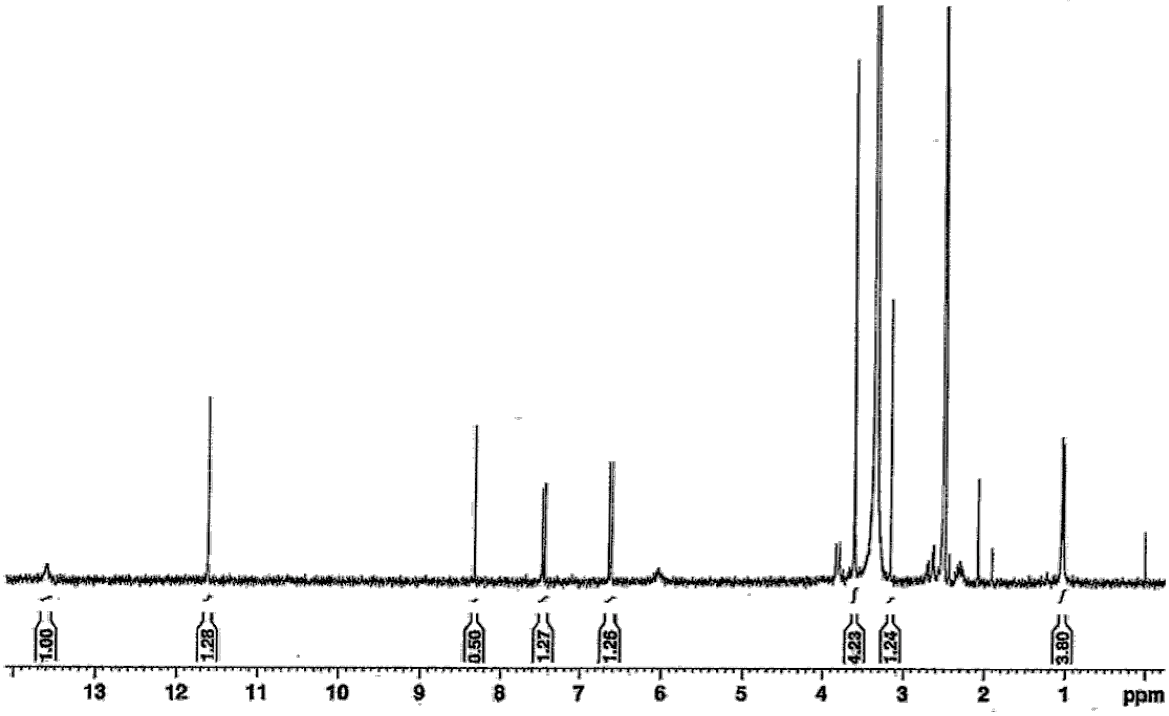

^{13}C NMR spectrum (75.4 MHz)

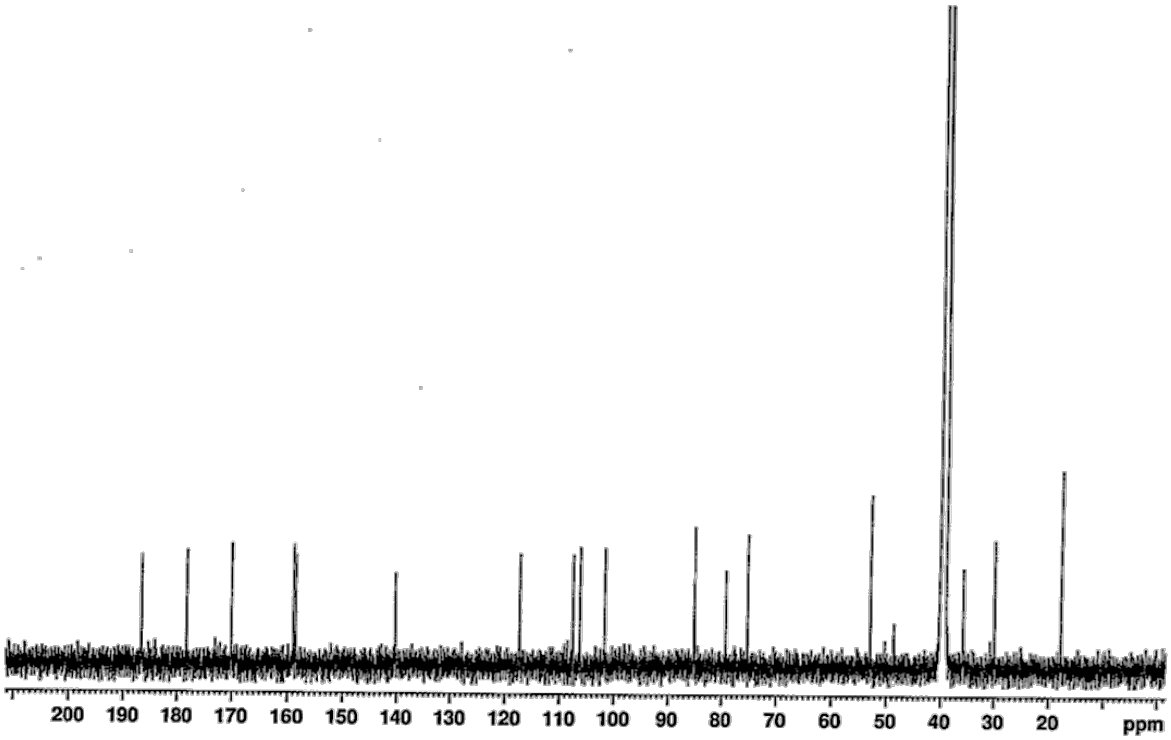

6.1.12 NMR Spectrum of *Bis*- Anthraquinone (XII)

^{1}H NMR spectrum (500.13 MHz)

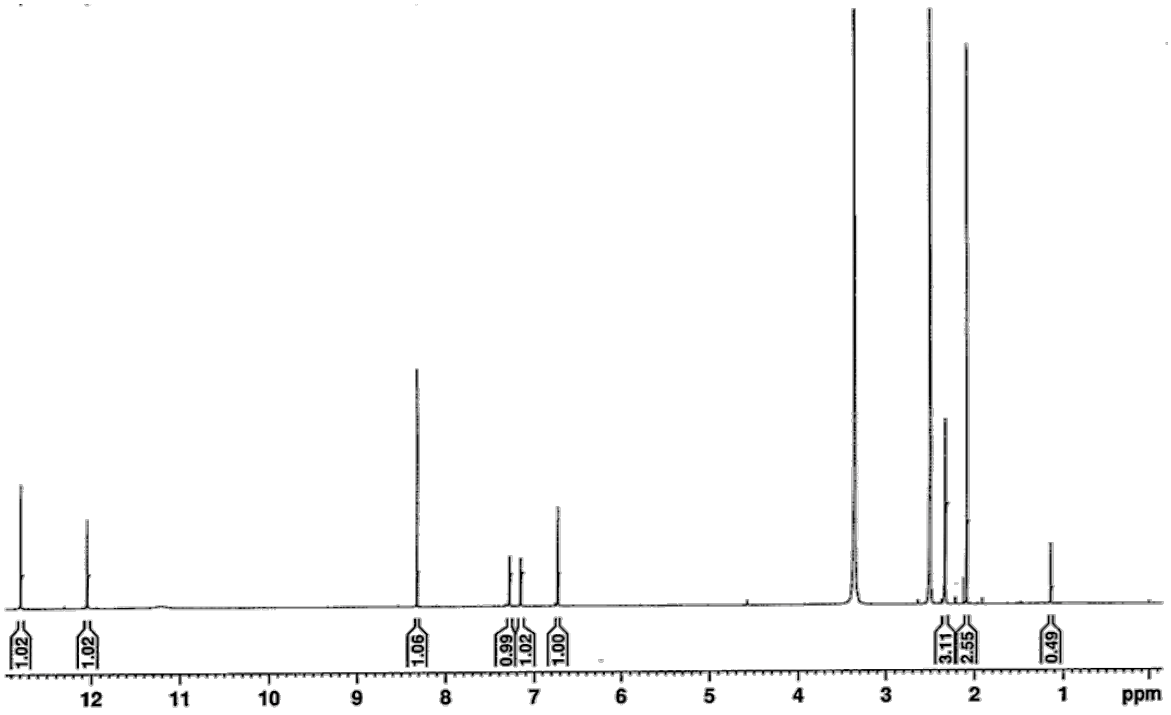

^{13}C NMR spectrum (125.4 MHz)

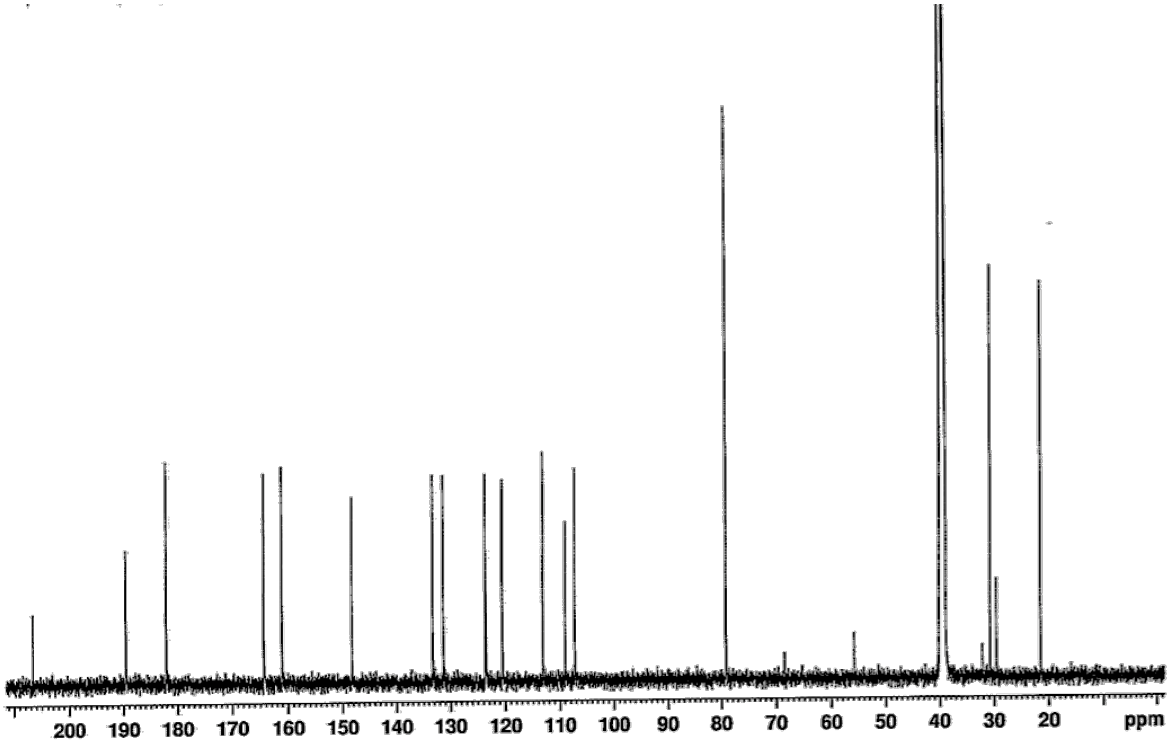

CHAPTER 7

7. References

Adams, P. B. (1990). The Potential of Mycoparasites for Biological Control of Plant Diseases*. *Annual review of phytopathology* 28, 59-72.

Arai, M., Tomoda, H., Okuda, T., Wang, H., Tabata, N., Masuma, R., Yamaguchi, Y., and Omura, S. (2002). Funicone-related Compounds, Potentiators of Antifungal Miconazole Activity, Produced by *Talaromyces flavus* FKI-0076. *The Journal of antibiotics* 55, 172-180.

Atalay, A., Koc, A. N., Akyol, G., Cakır, N., Kaynar, L., and Ulu-Kilic, A. (2016). Pulmonary infection caused by *Talaromyces purpurogenus* in a patient with multiple myeloma. *Le infezioni in medicina: rivista periodica di eziologia, epidemiologia, diagnostica, clinica e terapia delle patologie infettive* 24, 153.

Ayer, W. A., and Racok, J. S. (1990). The metabolites of *Talaromyces flavus*: Part 1. Metabolites of the organic extracts. *Canadian journal of chemistry* 68, 2085-2094.

Aziz, N. H., Mattar, Z. A., and Mahrous, S. R. (2006). Contamination of Grains by Mycotoxin-Producing Molds and Mycotoxins and Control by Gamma Irradiation. *Journal of food safety* 26, 184-201.

Bao, J., Sun, Y.-L., Zhang, X.-Y., Han, Z., Gao, H.-C., He, F., Qian, P.-Y., and Qi, S.-H. (2013). Antifouling and antibacterial polyketides from marine gorgonian coral-associated fungus *Penicillium* sp. SCSGAF 0023. *The Journal of antibiotics* 66, 219-223.

Bara, R., Aly, A. H., Pretsch, A., Wray, V., Wang, B., Proksch, P., and Debbab, A. (2013a). Antibiotically active metabolites from *Talaromyces wortmannii*, an endophyte of *Aloe vera*. *Journal of Antibiotics* 66, 491.

Bara, R., Aly, A. H., Wray, V., Lin, W., Proksch, P., and Debbab, A. (2013b). Talaromins A and B, new cyclic peptides from the endophytic fungus *Talaromyces wortmannii*. *Tetrahedron Letters* 54, 1686-1689.

Bara, R., Zerfass, I., Aly, A. H., Goldbach-Gecke, H., Raghavan, V., Sass, P., Mándi, A., Wray, V., Polavarapu, P. L., and Pretsch, A. (2013c). Atropisomeric dihydroanthracenones as inhibitors of multiresistant *Staphylococcus aureus*. *Journal of medicinal chemistry* 56, 3257-3272.

Benjamin, C. R. (1955). Ascocarps of *Aspergillus* and *Penicillium*. *Mycologia* 47, 669-687.

Blunt, J. W., Copp, B. R., Keyzers, R. A., Munro, M. H., and Prinsep, M. R. (2015). Marine natural products. *Natural Product Reports* 32, 116-211.

Blunt, J. W., Copp, B. R., Keyzers, R. A., Munro, M. H., and Prinsep, M. R. (2016). Marine natural products. *Natural Product Reports* 33, 382-431.

Boosalis, M. (1956). Effect of soil temperature and green-manure amendment of unsterilized soil on parasitism of *Rhizoctonia solani* by *Penicillium vermiculatum* and *Trichoderma* sp. *Phytopathology* 46, 473-478.

Bugni, T. S., and Ireland, C. M. (2004a). Marine-derived fungi: a chemically and biologically diverse group of microorganisms. *Nat Prod Rep* 21, 143-63.

Bugni, T. S., and Ireland, C. M. (2004b). Marine-derived fungi: a chemically and biologically diverse group of microorganisms. *Natural Product Reports* 21, 143-163.

Butler, M. S. (2004). The role of natural product chemistry in drug discovery. *Journal of natural products* 67, 2141-2153.

Cantrell, C. L., Rajab, M. S., Franzblau, S. G., Fronczek, F. R., and Fischer, N. H. (1999). Antimycobacterial ergosterol-5, 8-endoperoxide from *Ajuga remota*. *Planta medica* 65, 732-734.

Carte, B. K. (1996). Biomedical potential of marine natural products. *Bioscience* 46, 271-286.

Castro, M., Preto, M., Vasconcelos, V., and Urbatzka, R. (2016). Obesity: The Metabolic Disease, Advances on Drug Discovery and Natural Product Research. *Current topics in medicinal chemistry* 16, 2577-2604.

Choudhary, M. I. (2011). "Anti-Obesity Drug Discovery and Development," Bentham Science Publishers.

Cohen, P. A., and Towers, G. N. (1995). The anthraquinones of *Heterodermia obscurata*. *Phytochemistry* 40, 911-915.

Cruz, L. J., Insua, M. M., Baz, J. P., Trujillo, M., Rodriguez-Mias, R. A., Oliveira, E., Giralt, E., Albericio, F., and Canedo, L. M. (2006). IB-01212, a new cytotoxic cyclodepsipeptide isolated from the marine fungus *Clonostachys* sp. ESNA-A009. *The Journal of organic chemistry* 71, 3335-3338.

Dijksterhuis, J. (2007). Heat-resistant ascospores. *Mycology Series* 25, 101.

Ding, H.-E., Yang, Z.-D., Sheng, L., Zhou, S.-Y., Li, S., Yao, X.-J., Zhi, K.-K., Wang, Y.-G., and Zhang, F. (2015a). Secovironolide, a novel furanosteroid scaffold with a five-membered B ring from the endophytic fungus *Talaromyces wortmannii* LGT-4. *Tetrahedron Letters* 56, 6754-6757.

Ding, L.-J., Gu, B.-B., Jiao, W.-H., Yuan, W., Li, Y.-X., Tang, W.-Z., Yu, H.-B., Liao, X.-J., Han, B.-N., and Li, Z.-Y. (2015b). New Furan and Cyclopentenone Derivatives from the Sponge-Associated Fungus *Hypocrea Koningii* PF04. *Marine drugs* 13, 5579-5592.

Dong, Y., Lin, J., Lu, X., Zheng, Z., Ren, X., Zhang, H., He, J., and Yang, J. (2009). Cathepsin B inhibitory tetraene lactones from the fungus *Talaromyces wortmannii*. *Helvetica Chimica Acta* 92, 567-574.

Dong, Y., Yang, J., Zhang, H., Lin, J., Ren, X., Liu, M., Lu, X., and He, J. (2006). Wortmannilactones AD, 22-Membered Triene Macrolides from *Talaromyces wortmannii*. *Journal of natural products* 69, 128-130.

Duarte, K., Rocha-Santos, T. A., Freitas, A. C., and Duarte, A. C. (2012). Analytical techniques for discovery of bioactive compounds from marine fungi. *TrAC Trends in Analytical Chemistry* 34, 97-110.

Dufosse, L., Fouillaud, M., Caro, Y., Mapari, S. A., and Sutthiwong, N. (2014). Filamentous fungi are large-scale producers of pigments and colorants for the food industry. *Current opinion in biotechnology* 26, 56-61.

Enigl, D., King, A., and Török, T. (1993). *Talaromyces trachyspermus*, a heat-resistant mold isolated from fruit juice. *Journal of Food Protection*® 56, 1039-1042.

Firn, R. D., and Jones, C. G. (2000). The evolution of secondary metabolism–a unifying model. *Molecular microbiology* 37, 989-994.

Fleming, A. (1944). The discovery of penicillin. *British Medical Bulletin* 2, 4-5.

Frisvad, J., and Filtenborg, O. (1988). Specific Mycotoxin Producing *Penicillium* and *Aspergillus* Mycoflora of Different Foods. *Japanese Society of Mycotoxicology* 1988, 163-166.

Frisvad, J., Filtenborg, O., Samson, R., and Stolk, A. (1990). Chemotaxonomy of the genus *Talaromyces*. *Antonie van Leeuwenhoek* 57, 179-189.

Frisvad, J. C., Yilmaz, N., Thrane, U., Rasmussen, K. B., Houbraken, J., and Samson, R. A. (2013). *Talaromyces atroroseus*, a new species efficiently producing industrially relevant red pigments. *PloS one* 8, e84102.

Fujii, T., Hoshino, T., Inoue, H., and Yano, S. (2014). Taxonomic revision of the cellulose-degrading fungus A*cremonium cellulolyticus* nomen nudum to *Talaromyces* based on phylogenetic analysis. *FEMS microbiology letters* 351, 32-41.

Fujimoto, H., Matsudo, T., Yamaguchi, A., and Yamazaki, M. (1990). Two new fungal azaphilones from *Talaromyces luteus*, with monoamine oxidase inhibitory effect. *Heterocycles* 30, 607-616.

Fujimoto, H., Nakamura, E., Okuyama, E., and Ishibashi, M. (2004). Six immunosuppressive features from an ascomycete, *Zopfiella longicaudata*, found in a screening study monitored by immunomodulatory activity. *Chemical and pharmaceutical bulletin* 52, 1005-1008.

Galeano, E., Rojas, J. J., and Martinez, A. (2011). Pharmacological developments obtained from marine natural products and current pipeline perspective. *Natural product communications* 6, 287-300.

Gao, J., Shen, J., Zhang, A., Zhu, W., Zhang, X., and Liu, J. (2003). Chemical constituents of the fungus *Leccinum extremiorientale*. *Chinese Journal of Organic Chemistry* 23, 853-857.

Giacomotto, J., and Ségalat, L. (2010). High-throughput screening and small animal models, where are we? *British journal of pharmacology* 160, 204-216.

Gill, M., and Steglich, W. (1987). Pigments of fungi (macromycetes). *Natural Product Reports* 51.

Goel, R., Das, G. G., Ram, S., and Pandey, V. (1991). Antiulcerogenic and anti-inflammatory effects of emodin, isolated from *Rhamnus triquerta* wall. *Indian journal of experimental biology* 29, 230-232.

Gottlieb, D., and Van Etten, J. L. (1964). Biochemical changes during the growth of fungi I. Nitrogen Compounds and Carbohydrate Changes in *Penicillium atrovenetum*. *Journal of bacteriology* 88, 114-121.

Gu, X.-l., and Tian, Y.-p. (2013). Isolation and characterization of urethanase from *Penicillium variabile* and its application to reduce ethyl carbamate contamination in Chinese rice wine. *Applied biochemistry and biotechnology* 170, 718-728.

Hamilton, G. R., and Baskett, T. F. (2000). In the arms of Morpheus: the development of morphine for postoperative pain relief. *Canadian journal of anesthesia* 47, 367-374.

Harvey, A. L. (2008). Natural products in drug discovery. *Drug discovery today* 13, 894-901.

Hashimoto, M., Wakana, D., Ueda, M., Kobayashi, D., Goda, Y., and Fujii, I. (2015). Product identification of non-reducing polyketide synthases with C-terminus methyltransferase domain from *Talaromyces stipitatus* using *Aspergillus oryzae* heterologous expression. *Bioorganic & medicinal chemistry letters* 25, 1381-1384.

Hawas, U. W., El-Beih, A. A., and El-Halawany, A. M. (2012). Bioactive anthraquinones from endophytic fungus *Aspergillus versicolor* isolated from red sea algae. *Archives of pharmacal research* 35, 1749-1756.

He, J.-W., Liang, H.-X., Gao, H., Kuang, R.-Q., Chen, G.-D., Hu, D., Wang, C.-X., Liu, X.-Z., Li, Y., and Yao, X.-S. (2014a). Talaflavuterpenoid A, a new nardosinane-type sesquiterpene from *Talaromyces flavus*. *Journal of Asian natural products research* 16, 1029-1034.

He, J.-W., Mu, Z.-Q., Gao, H., Chen, G.-D., Zhao, Q., Hu, D., Sun, J.-Z., Li, X.-X., Li, Y., and Liu, X.-Z. (2014b). New polyesters from *Talaromyces flavus*. *Tetrahedron* 70, 4425-4430.

He, J.-W., Qin, D.-P., Gao, H., Kuang, R.-Q., Yu, Y., Liu, X.-Z., and Yao, X.-S. (2014c). Two New Coumarins from *Talaromyces flavus*. *Molecules* 19, 20880-20887.

Hirata, Y., and Uemura, D. (1986). Halichondrins-antitumor polyether macrolides from a marine sponge. *Pure and Applied Chemistry* 58, 701-710.

Honda, N. K., Devincenzi, I. A., and Xavier Filho, L. (1995). Secalonic Acid A from *Pseudoparmelia sphaerospora* (Nyl.) Hale and *Pseudoparmelia. hypomilta* (Fée) Hale (Parmeliaceae). *Tropical Bryology* 10, 201-204.

Horré, R., Gilges, S., Breig, P., Kupfer, B., De Hoog, G., Hoekstra, E., Poonwan, N., and Schaal, K. (2001). Case report. Fungaemia due to *Penicillium piceum*, a member of the *Penicillium marneffei* complex. *Mycoses* 44, 502-504.

Hu, Y., Chen, J., Hu, G., Yu, J., Zhu, X., Lin, Y., Chen, S., and Yuan, J. (2015). Statistical research on the bioactivity of new marine natural products discovered during the 28 years from 1985 to 2012. *Marine Drugs* 13, 202-21.

Huang, H., Bremer, E., Hynes, R., and Erickson, R. (2000). Foliar application of fungal biocontrol agents for the control of white mold of dry bean caused by *Sclerotinia sclerotiorum*. *Biological Control* 18, 270-276.

Huang, R., Wang, T., Xie, X.-S., Ma, K.-X., Fang, X.-W., and Wu, S.-H. (2016). Secondary Metabolites from an Endophytic Fungus *Nigrospora* sp. *Chemistry of Natural Compounds* 52, 697-699.

Jayasuriya, H., Koonchanok, N. M., Geahlen, R. L., McLaughlin, J. L., and Chang, C.-J. (1992). Emodin, a protein tyrosine kinase inhibitor from *Polygonum cuspidatum*. *Journal of Natural Products* 55, 696-698.

Jennings, D. (1983). Some aspects of the physiology and biochemistry of marine fungi. *Biological Reviews* 58, 423-459.

Jin, L., Quan, C., Hou, X., and Fan, S. (2016). Potential Pharmacological Resources: Natural Bioactive Compounds from Marine-Derived Fungi. *Marine Drugs* 14.

Jones, D., Anderson, H., Russell, J., Fraser, A., and Onions, A. H. (1984). Vermiculine, a metabolic product from *Talaromyces wortmannii*. *Transactions of the British Mycological Society* 83, 718-721.

Jones, E., Sakayaroj, J., Suetrong, S., Somrithipol, S., and Pang, K. (2009). Classification of marine Ascomycota, anamorphic taxa and Basidiomycota. *Fungal Diversity* 35, 187.

Jones, K. S., Alimov, A. P., Rilo, H. L., Jandacek, R. J., Woollett, L. A., and Penberthy, W. T. (2008). A high throughput live transparent animal bioassay to identify non-toxic small molecules or genes that regulate vertebrate fat metabolism for obesity drug development. *Nutrition & metabolism* 5, 23.

Kakvan, N., Heydari, A., Zamanizadeh, H. R., Rezaee, S., and Naraghi, L. (2013). Development of new bioformulations using *Trichoderma* and *Talaromyces* fungal antagonists for biological control of sugar beet damping-off disease. *Crop Protection* 53, 80-84.

Kawahara, N., Sekita, S., and Satake, M. (1994). Steroids from *Calvatia cyathiformis*. *Phytochemistry* 37, 213-215.

Kijjoa, A., and Sawangwong, P. (2004). Drugs and cosmetics from the sea. *Marine Drugs* 2, 73-82.

Kim, D.-H., Jung, S. J., Chung, I.-S., Lee, Y.-H., Kim, D.-K., Kim, S.-H., Kwon, B.-M., Jeong, T.-S., Park, M.-H., and Seoung, N.-S. (2005). Ergosterol peroxide from flowers of *Erigeron annuus* L. as an anti-atherosclerosis agent. *Archives of pharmacal research* 28, 541-545.

Kim, S.-W., Park, S.-S., Min, T.-J., and Yu, K.-H. (1999). Antioxidant activity of ergosterol peroxide (5, 8-epidioxy-5α, 8α-ergosta-6, 22E-dien-3β-ol) in *Armillariella mellea*. *Bulletin Korean Chemical Society* 20, 819-823.

Kobayashi, M., Krishna, M. M., Ishida, K., and Anjaneyulu, V. (1992). Marine Sterols. XXII. Occurrence of 3-Oxo-4, 6, 8 (14)-triunsaturated Steroids in the Sponge *Dvsidea herbacea*. *Chemical and pharmaceutical bulletin* 40, 72-74.

Koehn, F. E., and Carter, G. T. (2005). The evolving role of natural products in drug discovery. *Nature reviews Drug discovery* 4, 206-220.

Kohlmeyer, J., and Kohlmeyer, E. (1979). Marine Mycology: The Higher Fungi (Academic, New York). *KohlmeyerMarine Mycology: The Higher Fungi1979*.

Koski, R. R. (2008). Omega-3-acid ethyl esters (Lovaza) for severe hypertriglyceridemia. *Pharmacy and Therapeutics* 33, 271.

Kubanek, J., Jensen, P. R., Keifer, P. A., Sullards, M. C., Collins, D. O., and Fenical, W. (2003). Seaweed resistance to microbial attack: a targeted chemical defense against marine fungi. *Proceedings of the National Academy of Sciences* 100, 6916-6921.

Kuml, D., Dethoup, T., Buttachon, S., Singburaudom, N., Silva, A., and Kijjoa, A. (2014). Spiculisporic acid E, a new spiculisporic acid derivative and ergosterol derivatives from the marine-sponge associated fungus *Talaromyces trachyspermus* (KUFA 0021). *Natural product communications* 9, 1147-1150.

Kurobane, I., Vining, L. C., and MCINNES, A. G. (1979). Biosynthetic relationships among the secalonic acids. *The Journal of antibiotics* 32, 1256-1266.

Larsen, T. O., Smedsgaard, J., Nielsen, K. F., Hansen, M. E., and Frisvad, J. C. (2005). Phenotypic taxonomy and metabolite profiling in microbial drug discovery. *Natural product reports* 22, 672-695.

Li, H., Huang, H., Shao, C., Huang, H., Jiang, J., Zhu, X., Liu, Y., Liu, L., Lu, Y., and Li, M. (2011). Cytotoxic norsesquiterpene peroxides from the endophytic fungus *Talaromyces flavus* isolated from the mangrove plant *Sonneratia apetala*. *Journal of natural products* 74, 1230-1235.

Li, J. W.-H., and Vederas, J. C. (2009). Drug discovery and natural products: end of an era or an endless frontier? *Science* 325, 161-165.

Lin, Y.-L., Wang, T.-H., Lee, M.-H., and Su, N.-W. (2008). Biologically active components and nutraceuticals in the *Monascus*-fermented rice: a review. *Applied microbiology and biotechnology* 77, 965-973.

Link, E. M., Hardiman, G., Sluder, A. E., Johnson, C. D., and Liu, L. X. (2000). Therapeutic target discovery using *Caenorhabditis elegans*. *Pharmacogenomics* 1, 203-217.

Lowenberg, B., Pabst, T., Vellenga, E., Farag, S., Ruppert, A., and Mrozek, K. (2011). Cytarabine dose for acute myeloid leukemia. *New England Journal of Medicine* 2011, 2166-2169.

Lynn, D. G., Phillips, N. J., Hutton, W. C., Shabanowitz, J., Fennell, D., and Cole, R. (1982). Talaromycins: application of homonuclear spin correlation maps to structure assignment. *Journal of the American Chemical Society* 104, 7319-7322.

Madi, L., Katan, T., Katan, J., and Henis, Y. (1997). Biological control of *Sclerotium rolfsii* and *Verticillium dahliae* by *Talaromyces flavus* is mediated by different mechanisms. *Phytopathology* 87, 1054-1060.

Manojlovic, N., Solujic, S., Sukdolak, S., and Krstic, L. (2000). Isolation and antimicrobial activity of anthraquinones from some species of the lichen genus *Xanthoria*. *Jornal of the Serbian Chemical Society* 65, 555-560.

Manojlovic, N. T., Solujic, S., and Sukdolak, S. (2002). Antimicrobial activity of an extract and anthraquinones from *Caloplaca schaereri*. *The Lichenologist* 34, 83-85.

Mapari, S. A., Hansen, M. E., Meyer, A. S., and Thrane, U. (2008). Computerized screening for novel producers of *Monascus*-like food pigments in *Penicillium* species. *Journal of agricultural and food chemistry* 56, 9981-9989.

Marois, J., Fravel, D., and Papavizas, G. (1984). Ability of *Talaromyces flavus* to occupy the rhizosphere and its interaction with *Verticillium dahliae*. *Soil Biology and Biochemistry* 16, 387-390.

Marois, J., Johnston, S., Dunn, M., and Papavizas, G. (1982). Biological control of *Verticillium wilt* of eggplant in the field. *Plant Disease* 66, 1166-1168.

Martinez, M. (2016). Ergosterol from the mushroom *laetiporus* sp.; isolation and structural characterization. *Revista Boliviana de Química* 32.

Martins, A., Vieira, H., Gaspar, H., and Santos, S. (2014). Marketed marine natural products in the pharmaceutical and cosmeceutical industries: Tips for success. *Marine drugs* 12, 1066-1101.

Mayer, A. M., Glaser, K. B., Cuevas, C., Jacobs, R. S., Kem, W., Little, R. D., McIntosh, J. M., Newman, D. J., Potts, B. C., and Shuster, D. E. (2010). The odyssey of marine

pharmaceuticals: a current pipeline perspective. *Trends in pharmacological sciences* 31, 255-265.

McLaren, D., Huang, H., and Rimmer, S. (1986). Hyperparasitism of *Sclerotinia sclerotiorum* by *Talaromyces flavus*. *Canadian Journal of Plant Pathology* 8, 43-48.

Moulé, Y., Douce, C., Moreau, S., and Darracq, N. (1981). Effects of the mycotoxin botryodiplodin on mammalian cells in culture. *Chemico-biological interactions* 37, 155-164.

Murakami, T. (1956). The coloring matters of *Xanthoria fallax* (HEPP.) ARN. Fallacinal and fallacinol. *Pharmaceutical bulletin* 4, 298-302.

Naraghi, L., Heydari, A., and Ershad, D. (2006). Sporulation and survival of *Talaromyces flavus* on different plant material residues for biological control of cotton wilt caused by *Verticillium dahliae*. *Iranian Journal of Plant Pathology* 42.

Naraghi, L., Heydari, A., Rezaee, S., and Razavi, M. (2012). Biocontrol agent *Talaromyces flavus* stimulates the growth of cotton and potato. *Journal of plant growth regulation* 31, 471-477.

Naraghi, L., Heydari, A., Rezaee, S., Razavi, M., and Afshari-Azad, H. (2011). Biological control of Verticillium wilt of greenhouse cucumber by *Talaromyces flavus*. *Phytopathologia Mediterranea* 49, 321-329.

Naraghi, L., Heydari, A., Rezaee, S., Razavi, M., and Jahanifar, H. (2010). Study on antagonistic effects of *Talaromyces flavus* on *Verticillium albo-atrum*, the causal agent of potato wilt disease. *Crop Protection* 29, 658-662.

Narikawa, T., Shinoyama, H., and Fujii, T. (2000). A β-rutinosidase from *Penicillium rugulosum* IFO 7242 that is a peculiar flavonoid glycosidase. *Bioscience, biotechnology, and biochemistry* 64, 1317-1319.

Newman, D. J., and Cragg, G. M. (2014). Marine-sourced anti-cancer and cancer pain control agents in clinical and late preclinical development. *Marine drugs* 12, 255-278.

Ng, M., Fleming, T., Robinson, M., Thomson, B., Graetz, N., Margono, C., Mullany, E. C., Biryukov, S., Abbafati, C., and Abera, S. F. (2014). Global, regional, and national prevalence of overweight and obesity in children and adults during 1980–2013: a systematic analysis for the Global Burden of Disease Study 2013. *The Lancet* 384, 766-781.

Nicoletti, R., Manzo, E., and Ciavatta, M. L. (2009). Occurence and bioactivities of funicone-related compounds. *International journal of molecular sciences* 10, 1430-1444.

Nicoletti, R., and Trincone, A. (2016). Bioactive compounds produced by strains of *Penicillium* and *Talaromyces* of marine origin. *Marine drugs* 14, 37.

Osmanova, N., Schultze, W., and Ayoub, N. (2010). Azaphilones: a class of fungal metabolites with diverse biological activities. *Phytochemistry Reviews* 9, 315-342.

Petruzzi, L., Bevilacqua, A., Ciccarone, C., Gambacorta, G., Irlante, G., Lamacchia, C., and Sinigaglia, M. (2012). Artificial aging of Uva di Troia and Primitivo wines using oak chips inoculated with *Penicillium purpurogenum*. *Journal of the Science of Food and Agriculture* 92, 343-350.

Petzinger, E., and Weidenbach, A. (2002). Mycotoxins in the food chain: the role of ochratoxins. *Livestock Production Science* 76, 245-250.

Phillips, N., Cole, R., and Lynn, D. (1987). Talaromycins C, D, E, and F. *Tetrahedron letters* 28, 1619-1621.

Piattelli, M., and de Nicola, M. G. (1968). Anthraquinone pigments from *Xanthoria parientina* (L.). *Phytochemistry* 7, 1183-1187.

Pitt, J. I., and Hocking, A. D. (2009). "Fungi and food spoilage," Springer.

Pitt, J. I., Samson, R. A., and Frisvad, J. C. (2000). List of accepted species and their synonyms in the family Trichocomaceae.

Pol, D., Laxman, R. S., and Rao, M. (2012). Purification and biochemical characterization of endoglucanase from *Penicillium pinophilum* MS 20. *Indian Journal of Biochemistry & Biophysics*.

Proksch, P., Ebel, R., Edrada, R., Riebe, F., Liu, H., Diesel, A., Bayer, M., Li, X., Han Lin, W., Grebenyuk, V., Müller, W. E. G., Draeger, S., Zuccaro, A., and Schulz, B. (2008). Sponge-associated fungi and their bioactive compounds: the Suberites case. *Botanica Marina* 51.

Prompanya, C., Fernandes, C., Cravo, S., Pinto, M. M., Dethoup, T., Silva, A., and Kijjoa, A. (2015). A new cyclic hexapeptide and a new isocoumarin derivative from the marine sponge-associated fungus *Aspergillus similanensis* KUFA 0013. *Marine drugs* 13, 1432-1450.

Quang, D. N., Hashimoto, T., Nomura, Y., Wollweber, H., Hellwig, V., Fournier, J., Stadler, M., and Asakawa, Y. (2005). Cohaerins A and B, azaphilones from the fungus *Hypoxylon cohaerens*, and comparison of HPLC-based metabolite profiles in *Hypoxylon* sect. *Annulata*. *Phytochemistry* 66, 797-809.

Raghukumar, C. (2008). Marine fungal biotechnology: an ecological perspective. *Fungal Diversity* 31, 19-35.

Rateb, M. E., and Ebel, R. (2011). Secondary metabolites of fungi from marine habitats. *Natural product reports* 28, 290-344.

Reyes, I., Bernier, L., Simard, R. R., Tanguay, P., and Antoun, H. (1999). Characteristics of phosphate solubilization by an isolate of a tropical *Penicillium rugulosum* and two UV-induced mutants. *FEMS Microbiology Ecology* 28, 291-295.

Rinehart, K. L., Holt, T. G., Fregeau, N. L., Stroh, J. G., Keifer, P. A., Sun, F., Li, L. H., and Martin, D. G. (1990). Ecteinascidins 729, 743, 745, 759A, 759B, and 770: potent antitumor agents from the Caribbean tunicate *Ecteinascidia turbinata*. *The Journal of Organic Chemistry* 55, 4512-4515.

Roh, C., and Jung, U. (2012). Screening of crude plant extracts with anti-obesity activity. *International Journal of Molecular Sciences* 13, 1710-1719.

Rollinger, J. M., Stuppner, H., and Langer, T. (2008). Virtual screening for the discovery of bioactive natural products. *In* "Natural Compounds as Drugs Volume I", pp. 211-249. Springer.

Ruiz-Ojeda, F. J., Rupérez, A. I., Gomez-Llorente, C., Gil, A., and Aguilera, C. M. (2016). Cell models and their application for studying adipogenic differentiation in relation to obesity: a review. *International Journal of Molecular Sciences* 17, 1040.

Sakai, A., Tanaka, H., Konishi, Y., Hanazawa, R., Ota, T., Nakahara, Y., Sekiguchi, S., Oshida, E., Takino, M., and Ichinoe, M. (2005). Mycological examination of domestic unpolished rice and mycotoxin production by isolated *Penicillium islandicum*. *Shokuhin eiseigaku zasshi. Journal of the Food Hygienic Society of Japan* 46, 205-212.

Saleem, M., Ali, M. S., Hussain, S., Jabbar, A., Ashraf, M., and Lee, Y. S. (2007). Marine natural products of fungal origin. *Natural product reports* 24, 1142-1152.

Santos, P., Piontelli, E., Shea, Y., Galluzzo, M., Holland, S., Zelazko, M., and Rosenzweig, S. (2006). *Penicillium piceum* infection: diagnosis and successful treatment in chronic granulomatous disease. *Medical mycology* 44, 749-753.

Schafhauser, T., Wibberg, D., Rückert, C., Winkler, A., Flor, L., van Pée, K.-H., Fewer, D. P., Sivonen, K., Jahn, L., and Ludwig-Müller, J. (2015). Draft genome sequence of *Talaromyces islandicus* ("*Penicillium islandicum*") WF-38-12, a neglected mold with significant biotechnological potential. *Journal of biotechnology* 211, 101-102.

Schmidtko, A., Lötsch, J., Freynhagen, R., and Geisslinger, G. (2010). Ziconotide for treatment of severe chronic pain. *The Lancet* 375, 1569-1577.

Schueffler, A., and Anke, T. (2014). Fungal natural products in research and development. *Natural product reports* 31, 1425-1448.

Scott, V. N., and Bernard, D. T. (1987). Heat resistance of *Talaromyces flavus* and *Neosartorya fischeri* isolated from commercial fruit juices. *Journal of Food Protection®* 50, 18-20.

Senter, P. D., and Sievers, E. L. (2012). The discovery and development of brentuximab vedotin for use in relapsed Hodgkin lymphoma and systemic anaplastic large cell lymphoma. *Nature biotechnology* 30, 631-637.

Sheldrick, G. M. (2008). A short history of SHELX. *Acta Crystallographica Section A: Foundations of Crystallography* 64, 112-122.

Shiozawa, H., Takahashi, M., Takatsu, T., Kinoshita, T., Tanzawa, K., Hosoya, T., Furuya, K., Takahashi, S., Furihata, K., and Seto, H. (1995). Trachyspic acid, a new metabolite produced by *Talaromyces trachyspermus*, that inhibits tumor cell heparanase: taxonomy of the producing strain, fermentation, isolation, structural elucidation, and biological activity. *The Journal of antibiotics* 48, 357-362.

Shulman, J. M., Shulman, L. M., Weiner, W. J., and Feany, M. B. (2003). From fruit fly to bedside: translating lessons from *Drosophila* models of neurodegenerative disease. *Current opinion in neurology* 16, 443-449.

Sigler, L., Abbott, S., and Frisvad, J. (1996). Rubratoxin mycotoxicosis by *Penicillium crateriforme* following ingestion of homemade rhubarb wine. *In* "Abstracts, 96th ASM, New Orleans. F-22", pp. 77.

Singh, J. (1999). Ethnomycology and folk remedies: Fact and fiction. *In* "From Ethnomycology to Fungal Biotechnology", pp. 11-17. Springer.

Singh, J., and Aneja, K. (2012). "From ethnomycology to fungal biotechnology: exploiting fungi from natural resources for novel products," Springer Science & Business Media.

Singh, S. B., Jayasuriya, H., Dewey, R., Polishook, J. D., Dombrowski, A. W., Zink, D. L., Guan, Z., Collado, J., Platas, G., and Pelaez, F. (2003). Isolation, structure, and HIV-1-integrase inhibitory activity of structurally diverse fungal metabolites. *Journal of Industrial Microbiology and Biotechnology* 30, 721-731.

Speakman, J., Hambly, C., Mitchell, S., and Król, E. (2008). The contribution of animal models to the study of obesity. *Laboratory animals* 42, 413-432.

Steglich, W., Fugmann, B., and Lang-Fugmann, S. (2000). "Römpp encyclopedia natural products," Georg Thieme Verlag.

Stodůlková, E., Kolařík, M., Křesinová, Z., Kuzma, M., Šulc, M., Man, P., Novák, P., Maršík, P., Landa, P., and Olšovská, J. (2009). Hydroxylated anthraquinones produced by *Geosmithia* species. *Folia microbiologica* 54, 179-187.

Stolk, A. C., and Samson, R. A. (1972). "The genus *Talaromyces*: studies on *Talaromyces* and related genera," Centraalbureau voor Schimmelcultures.

Stosz, S. K., Fravel, D. R., and Roberts, D. P. (1996). *In vitro* analysis of the role of glucose oxidase from *Talaromyces flavus* in biocontrol of the plant pathogen *Verticillium dahliae*. *Applied and environmental microbiology* 62, 3183-3186.

Supparatpinyo, K., Perriens, J., Nelson, K. E., and Sirisanthana, T. (1998). A controlled trial of itraconazole to prevent relapse of *Penicillium marneffei* infection in patients

infected with the human immunodeficiency virus. *New England Journal of Medicine* 339, 1739-1743.

Tabata, Y., Ikegami, S., Yaguchi, T., Sasaki, T., Hoshiko, S., Sakuma, S., SFFIN-YA, K., and Seto, H. (1999). Diazaphilonic acid, a new azaphilone with telomerase inhibitory activity. *The Journal of antibiotics* 52, 412-414.

Takeuchi, M., Nakajima, M., Ogita, T., Inukai, M., Kodama, K., Furuya, K., Nagaki, H., and Haneishi, T. (1989). Fosfonochlorin, a new antibiotic with spheroplast forming activity. *The Journal of antibiotics* 42, 198-205.

Tan, N., Cai, X.-L., Wang, S.-Y., Pan, J.-H., Tao, Y.-W., She, Z.-G., Zhou, S.-N., Lin, Y.-C., and Vrijmoed, L. L. (2008). A new hTopo I isomerase inhibitor produced by a mangrove endophytic fungus no. 2240. *Journal of Asian natural products research* 10, 607-610.

Thomas, T. R. A., Kavlekar, D. P., and LokaBharathi, P. A. (2010). Marine drugs from sponge-microbe association—A review. *Marine Drugs* 8, 1417-1468.

Turner, W. B. (1971). Fungal metabolites. *Journal of Pharmaceutical Sciences* 73.

Tzeng, T.-F., Lu, H.-J., Liou, S.-S., Chang, C. J., and Liu, I.-M. (2012). Emodin, a naturally occurring anthraquinone derivative, ameliorates dyslipidemia by activating AMP-activated protein kinase in high-fat-diet-fed rats. *Evidence-Based Complementary and Alternative Medicine* 2012.

Udagawa, S., and Tatsuno, T. (2003). Safety of rice grains and mycotoxins-a historical review of yellow rice mycotoxicoses. *Yakushigaku zasshi* 39, 321-342.

Unson, M., Holland, N., and Faulkner, D. (1994). A brominated secondary metabolite synthesized by the cyanobacterial symbiont of a marine sponge and accumulation of the crystalline metabolite in the sponge tissue. *Marine Biology* 119, 1-11.

Usher, K., Fromont, J., Sutton, D., and Toze, S. (2004). The biogeography and phylogeny of unicellular cyanobacterial symbionts in sponges from Australia and the Mediterranean. *Microbial ecology* 48, 167-177.

Verdaguer, H., Morilla, I., and Urruticoechea, A. (2013). Eribulin mesylate in breast cancer. *Women's Health* 9, 517-526.

Vogel, G. (2000). Zebrafish earns its stripes in genetic screens. *Science* 288, 1160-1161.

Wada, S. i., Usami, I., Umezawa, Y., Inoue, H., Ohba, S. i., Someno, T., Kawada, M., and Ikeda, D. (2010). Rubratoxin A specifically and potently inhibits protein phosphatase 2A and suppresses cancer metastasis. *Cancer science* 101, 743-750.

Wang, P.-L., Li, D.-Y., Xie, L.-R., Wu, X., Hua, H.-M., and Li, Z.-L. (2014). Two new compounds from a marine-derived fungus Penicillium oxalicum. *Natural product research* 28, 290-293.

Wang, W., Zhu, T., Tao, H., Lu, Z., Fang, Y., Gu, Q., and Zhu, W. (2007). Two new cytotoxic quinone type compounds from the halotolerant fungus *Aspergillus variecolor*. *Journal of Antibiotics* 60, 603.

Wase, N. V., and Wright, P. C. (2008). Systems biology of cyanobacterial secondary metabolite production and its role in drug discovery. *Expert opinion on drug discovery* 3, 903-929.

Wei, X., Jiang, J.-S., Feng, Z.-M., and Zhang, P.-C. (2008). Anthraquinone-benzisochromanquinone dimers from the roots of *Berchemia floribunda*. *Chemical and Pharmaceutical Bulletin* 56, 1248-1252.

Weisenborn, J. L., Kirschner, R., Cáceres, O., and Piepenbring, M. (2010). *Talaromyces indigoticus* Takada & Udagawa, the First Record for Panama and the American Continent. *Mycopathologia* 170, 203-208.

Whitley, R. J., Nahmias, A. J., Soong, S.-J., Galasso, G. G., Fleming, C. L., Alford, C. A., Connor, J., Bryson, Y., and Linnemann, C. (1980). Vidarabine therapy of neonatal herpes simplex virus infection. *Pediatrics* 66, 495-501.

Wilkinson, C. (1978). Microbial associations in sponges. I. Ecology, physiology and microbial populations of coral reef sponges. *Marine biology* 49, 161-167.

Wilkinson, C. C., and Garrone, R. R. (1980). Nutrition of marine sponges. Involvement of symbiotic bacteria in the uptake of dissolved carbon. *Nutrition in the Lower Metazoa-pages: 157-161*.

Wilkinson, C. C., Summons, R. R., and Evans, E. (1999). Nitrogen fixation in symbiotic marine sponges: ecological significance and difficulties in detection. *Memoirs of the Queensland Museum* 44, 667-673.

Wu, B., Ohlendorf, B., Oesker, V., Wiese, J., Malien, S., Schmaljohann, R., and Imhoff, J. F. (2015). Acetylcholinesterase inhibitors from a marine fungus *Talaromyces* sp. strain LF458. *Marine biotechnology* 17, 110-119.

Xu, L., Meng, W., Cao, C., Wang, J., Shan, W., and Wang, Q. (2015). Antibacterial and antifungal compounds from marine fungi. *Marine drugs* 13, 3479-3513.

Yagi, A., Makino, K., and Nishioka, I. (1977). Studies on the constituents of *Aloe saponaria* HAW. II. The structures of tetrahydroanthracene derivatives, aloesaponol III and-IV. *Chemical and Pharmaceutical Bulletin* 25, 1764-1770.

Yamazaki, M., Maebayashi, Y., and Miyaki, K. (1971). The isolation of secalonic acid A from *Aspergillus ochraceus* cultured on rice. *Chemical and Pharmaceutical Bulletin* 19, 199-201.

Yang, X., Kang, M.-C., Li, Y., Kim, E.-A., Kang, S.-M., and Jeon, Y.-J. (2014). Anti-inflammatory activity of questinol isolated from marine-derived fungus *Eurotium*

amstelodami in lipopolysaccharide-stimulated RAW 264.7 macrophages. *Journal of Microbiology and Biotechnology* 24, 1346-1353.

Yang, Y.-C., Lim, M.-Y., and Lee, H.-S. (2003). Emodin isolated from *Cassia obtusifolia* (Leguminosae) seed shows larvicidal activity against three mosquito species. *Journal of agricultural and food chemistry* 51, 7629-7631.

Yilmaz, N., Hagen, F., Meis, J. F., Houbraken, J., and Samson, R. A. (2016). Discovery of a sexual cycle in *Talaromyces amestolkiae*. *Mycologia* 108, 70-79.

Yilmaz, N., Houbraken, J., Hoekstra, E., Frisvad, J. C., Visagie, C., and Samson, R. (2012). Delimitation and characterisation of *Talaromyces purpurogenus* and related species. *Persoonia-Molecular Phylogeny and Evolution of Fungi* 29, 39-54.

Yilmaz, N., Visagie, C. M., Houbraken, J., Frisvad, J. C., and Samson, R. A. (2014). Polyphasic taxonomy of the genus *Talaromyces*. *Studies in Mycology* 78, 175-341.

Yoshida, E., Fujimoto, H., and Yamazaki, M. (1996). Isolation of three new azaphilones, luteusins C, D, and E, from an ascomycete, *talaromyces luteus*. *Chemical and pharmaceutical bulletin* 44, 284-287.

Younes, A., Yasothan, U., and Kirkpatrick, P. (2012). Brentuximab vedotin. *Nature Reviews Drug Discovery* 11, 19-20.

Yun, J. W. (2010). Possible anti-obesity therapeutics from nature–A review. *Phytochemistry* 71, 1625-1641.

Zang, Y., Genta-Jouve, G., Retailleau, P., Escargueil, A., Mann, S., Nay, B., and Prado, S. (2016). Talaroketals A and B, unusual bis (oxaphenalenone) spiro and fused ketals from the soil fungus *Talaromyces stipitatus* ATCC 10500. *Organic & biomolecular chemistry* 14, 2691-2697.

Zang, Y., Genta-Jouve, G., Sun, T. A., Li, X., Didier, B., Mann, S., Mouray, E., Larsen, A. K., Escargueil, A. E., Nay, B., and Prado, S. (2015). Unexpected talaroenamine derivatives and an undescribed polyester from the fungus *Talaromyces stipitatus* ATCC10500. *Phytochemistry* 119, 70-5.

Zhai, M.-M., Li, J., Jiang, C.-X., Shi, Y.-P., Di, D.-L., Crews, P., and Wu, Q.-X. (2016). The Bioactive Secondary Metabolites from *Talaromyces* species. *Natural products and bioprospecting* 6, 1-24.

Zhang, A.-L., Liu, L.-P., Wang, M., and Gao, J.-M. (2007). Bioactive ergosterol derivatives isolated from the fungus *Lactarius hatsudake*. *Chemistry of Natural Compounds* 43, 637-638.

Zhao, Y.-Y., Zhao, Y., Zhang, Y.-M., Lin, R.-C., and Sun, W.-J. (2009). Qualitative and quantitative analysis of the diuretic component ergone in *Polyporus umbellatus* by HPLC with fluorescence detection and HPLC-APCI-MS/MS. *Die Pharmazie-An International Journal of Pharmaceutical Sciences* 64, 366-370.

Zhou, Y., Debbab, A., Wray, V., Lin, W., Schulz, B., Trepos, R., Pile, C., Hellio, C., Proksch, P., and Aly, A. H. (2014). Marine bacterial inhibitors from the sponge-derived fungus *Aspergillus* sp. *Tetrahedron Letters* 55, 2789-2792.

Zin, W. W. M., Buttachon, S., Buaruang, J., Gales, L., Pereira, J. A., Pinto, M. M., Silva, A., and Kijjoa, A. (2015). A new meroditerpene and a new tryptoquivaline analog from the algicolous fungus *Neosartorya takakii* KUFC 7898. *Marine drugs* 13, 3776-3790.